THREE DIMENSIONAL MEASUREMENT OF TEXTURED SURFACES USING DIGITAL PHOTOGRAMMETRIC TECHNIQUES

Submitted to the University of Cape Town in fulfilment of the requirements for the Degree of Doctor of Philosophy in Engineering.

By

Julian Lloyd Smit

Department of Surveying and Geodetic Engineering

April 1997

DECLARATION

I hereby declare that this thesis is my original work and has not been submitted in any form to another university.

Julian Lloyd Smit

ABSTRACT

The deep-level gold mines on the Witwatersrand (South Africa) are located at depths of over 3,000m below surface. Mining excavations follow tabular reefs that are kilometres in extent, but only a few centimetres thick. Due to the great depths of these excavations and the large overburden of rock, immense pressure is exerted on the rock mass being excavated. In order to relieve this stress in the rock mass being mined, the rock is "pre-conditioned" by pre-fracturing the rock face with large blasts. This has the effect of pushing the critical stress load further into the rock mass, thus increasing safety at the rock face.

To better understand the rock behaviour as a result of by pre-conditioning blasts, it is desirable to quantify the deformations of the rock face. Digital photogrammetry provides an ideally suited method of monitoring these deformations, as the necessary equipment is portable and easy to use underground, where the conditions are extreme with temperatures approaching 40°C and humidity levels close to 100%. Digital photogrammetric techniques are also highly accurate, and can be used to detect relatively small three-dimensional movements.

The determination of the three-dimensional (XYZ) co-ordinates of the rock face, represented by densely spaced individual points, by means of digital photogrammetric techniques, is reported in this thesis. The novel measurement system developed comprises the following components:

- establishment of a stable reference co-ordinate system;
- image acquisition;
- camera calibration and exterior orientation calculation;
- feature extraction;
- multi-image matching and space intersection; and
- surface modelling.

The details of the techniques developed and implemented in order to generate the necessary object space co-ordinates are discussed. Sub-millimetre accuracy point determination, as required for deformation analysis was achieved and a sample of the underground test result data is presented.

The final analysis of the underground test data made it apparent that digital photogrammetry is highly suitable for the determination of digital terrain models of the rock surfaces, for subsequent deformation analysis. The relative speed of the process and the convenient size of the equipment makes the technology especially suitable to the demanding underground mining environment. The difficulties, which were experienced as a result of the highly restrictive environment, were overcome through careful planning and pre-analysis. It can thus be concluded that this approach is not only feasible, but it meets the stringent demands of the underground mining industry, as is confirmed by the high accuracy of the final surface point co-ordinates achieved.

In addition to being implemented in the underground mining industry, the measurement system developed was used for the mapping of several other textured surfaces. In particular it was used in mapping the 3.6 million-year-old hominid track-way located at Laetoli (Tanzania), the imprints of cheetah and rhinoceros for the purposes of conservation, and for the archaeological documentation of a shipwreck found off the Cape coast (South Africa). All of these applications are discussed and the results achieved presented.

ACKNOWLEDGEMENTS

I would firstly like to thank my supervisor Prof. Dr. Heinz Rüther for his support and guidance throughout my studies. It is especially his willingness to assist me in all areas of my studies that has been gratefully appreciated. Without his support and enthusiasm as a supervisor and colleague, I would never have undertaken this research.

To my friends and colleagues at the department of surveying: Dirk, Eric, Graeme, Henty, Justin, Malcolm, Mark, Mike, Nathan, Nick, Pierre, Siddique, Simon and Ulrike, thank you all for your friendship and support. I would especially like to mention Graeme van der Vlugt for his encouragement and discussion; which was greatly appreciated.

Without the support of the staff at the department of surveying, this research would have been considerably more difficult. I would in particular like to thank Val Atkinson for putting with up me for all of these years; Sue Binedell for her willingness to help; Dr. Scott Mason for his help in the later parts of this research; and Kari, Mike and Sidney for their technical assistance.

It was only with the financial support of the Mining Technology Division of the Council for Scientific and Industrial Research (CSIR) that this research project was possible. I would in particular like to thank Dr. Eddie Siebrits for his positive outlook and support of this project and Francois Malan for his assistance in gathering information for this thesis.

The financial support of the Foundation for Research and Development (FRD) for my doctoral studies has also been greatly appreciated.

TABLE OF CONTENTS

LIST OF FIGURES

LIST OF TABLES

GLOSSARY

closure	when the hangingwall and footwall make contact, that part of the stope has experienced closure;
convergence	closing of the stope normal to the plane of the excavation;
footwall	the floor of the stope;
gulley	transport tunnels used to move mined ore out of the stope;
hangingwall	overhead roof of the stope;
manway	access tunnel to the stope opening;
panel	a section of the stope being excavated; the stope is broken up into several panels which are mined separately;
ride	shear movement between the hangingwall and the footwall, along the fault;
stope	temporary opening used for ore extraction.

1 THESIS OVERVIEW

1.1 THESIS OBJECTIVES

The research work described in this thesis was initiated by the need, in the deep-level gold mining industry in South Africa, to quantify the deformations at an underground rock face resulting from blast events. Due to the constrained and hazardous nature of underground mining, a measurement system is required that is portable, robust and adaptable to changing geometric conditions. Photogrammetry provides such a measurement capability, with the additional advantage of providing a permanent photographic record, enabling further analysis of mine conditions.

As the deformations in the rock face are often small in extent, the determination of the three dimensional (XYZ) co-ordinates of the surface, represented by densely spaced individual points, is required with sub-millimetre accuracy. As digital photogrammetry has the potential to provide a dense point cloud representation of the object and highly accurate triangulation precision, it is well suited to the evaluation of the movements in the rock face to the required accuracy.

The development and subsequent underground evaluation of a digital photogrammetric system for rock engineering applications was proposed by Mining Technology, the rock engineering division of the Council for Scientific and Industrial Research (CSIR), Johannesburg, South Africa. The emphasis of the research was directed at the development of a measurement system for the analysis of the specific deformation of the "working" rock face as a result of pre-conditioning experiments. This is a non-trivial project and no easy solution was available due to the complexity of image capture and analysis, in the underground mining environment.

This thesis deals with the development and subsequent testing of methods and algorithms required for the successful implementation of a surface measurement

system in the deep-level gold mines on the Witwatersrand (South Africa). This approach to measurements in the underground mining industry has never been attempted before and represents a substantial development in quantifying rock deformation due to pressure loading.

1.2 THESIS OUTLINE

The structure of this thesis is aimed at describing the process followed in the mensuration of the rock face in the stope of a deep-level underground gold mine. It follows the development of this project from its initial stages, to the successful implementation of digital photogrammetry as a tool in monitoring deformations in this production environment.

As a means of demonstrating the flexibility of the developed measurement system, additional test of the hardware and software components of the digital photogrammetric measurement system are reported and analysis of the results achieved is presented. Intended future applications are described and recommendations for further research are made.

The design of the measurement system and its algorithms is controlled by a number of basic constraints as imposed by the physical nature of the underground mining environment and as required for accurate deformation analysis:

- The application is aimed at the measurement of a naturally textured surface, with no possibility of imposing an artificial texture;

- The photogrammetric surveys carried out are close-range in nature (typically in the order of a few metres);

- Sub-millimetre accuracies are required over the full extent of the survey area;

- The measurement system must be as fully automated as possible and should include automated target location and centring, camera calibration and exterior orientation determination, interest point detection, image matching and three dimensional object space point intersection;

- The selection of appropriate hardware needs to take into account the hazardous underground mine conditions, and especially the danger of explosions due to sparking of electronic equipment;

- The output results should be in a suitable format for further analysis using surface modelling and finite element software.

The following chapters are presented:

Chapter 2: the purpose of this research project is to quantify the deformation in the "working" rock face, to assist rock engineers in the analysis of rock behaviour in the stope. This chapter provides a background description of the conditions experienced in the deep-level underground mining environment.

Chapter 3: the principles and methods used in developing the photogrammetric measurement system used are described. It specifically provides a description of network design and the pre-analysis stages carried out, including simulation through fictitious image generation, in an effort to design the survey network most suitable to the geometric constraints present in the underground stope environment.

Chapter 4: described the procedures followed before and during image acquisition, including a description of the equipment used, survey preparations and practical considerations for image capture in the stope.

Chapter 5: documents the algorithms and methods used during the data processing stage of the system. The algorithms required for camera calibration and exterior orientation determination of the camera are outlined; the location of points of interest, which serve to represent the surface being measured, is described; and the methods used for image matching, required for the location of corresponding points of interest in conjugate images, is presented.

Chapter 6: presents the results achieved in underground testing of the system.

Chapter 7: describes additional projects that were undertaken using the developed measurement system in alternative applications of the mapping of naturally textured surfaces. These projects demonstrate the flexibility of the system for use in other close-range applications. The highly accurate results that were achieved in all cases, are presented.

Chapter 8: proposes further developments to the measurement system, in particular the extension of the developed algorithms to allow for additional applications in the underground mining industry. The use of the developed methods and algorithms for use in the photogrammetric documentation of archaeological artefacts has been initiated. A description of the aims of this project are presented.

Chapter 9: draws conclusions about the research carried out and reflects on the viability of the developed measurement system for use in the underground mining industry.

2 INTRODUCTION

2.1 PROJECT OBJECTIVES

The deep-level gold mines on the Witwatersrand (South Africa) are located at depths of more than 3,000m below surface. The gold ore is found in extensive tabular reefs, kilometres in extent, but only a few centimetres thick. Mining excavations are thus also tabular, hundreds of metres in extent, and less than 1 metre in height. The tabular shape of these excavations or panels, and the large overburden, result in extensive mining induced stress changes in the rock mass surrounding them. With each advance of the mine face, sudden changes in the rock stresses occur. This results in sudden fracturing of the exposed surfaces of the excavation, with accompanied deformation. In some mining panels, it is desirable to "pre-condition" or soften the rock mass ahead of the face by pre-fracturing it with large blasts. This has the effect of pushing the critical stress field deeper into the rock mass, alleviating some of the fracturing and hazardous deformations in the vicinity of the excavation. Safety at the rock face is thus improved, as the stress load on the rock to be excavated is decreased.

It is desirable to quantify the deformations of the face due to blasts to better understand their effect on the fracture patterns that develop. Digital photogrammetry is an ideal method to monitor these deformations. The photogrammetric equipment is portable and easy to use underground, where physical conditions are constrained and environmental conditions are extreme. Digital photogrammetric techniques are highly accurate, and can be used to detect three-dimensional changes in the sub-millimetre range. Furthermore, they can also be used to obtain a three-dimensional map of the new fractures that develop on the face due to a blast.

This thesis provides a description of the methods and algorithms developed in designing a measurement system capable of measuring a dense point cloud on the "working" rock face within the stope. The results achieved, in underground tests of

the developed system are presented, and the viability of such a system to the underground mining industry is analysed.

Before considering the design and testing of the developed measurement system, it is essential to describe the physical conditions that are experienced in the mine. Only with an understanding of this underground environment can one appreciate the complexity of the survey task at hand.

2.2 UNDERGROUND MINING ENVIRONMENT

By its very nature, the underground mining environment is particularly hazardous and physically constrained, the typical working area is not higher than 0.5m to 1m. The layout of an underground mine is necessarily more complex than that of an open pit. Deep-level excavations require safeguards to ensure that mine openings remain clear and safe for work, these include: undisturbed ore or rock left in place as pillars; ore is removed by stoping; access tunnels run away from the working face to facilitate ore transport and drainage; the stope opening is kept to a minimum to reduce the danger of rock falls from the back or roof of the stope; and artificial support by timbering, roof bolting, packwalling, or backfilling is provided wherever there is a danger of roof collapse or falling rock.

Mining of the ore from the body takes place in chambers or stopes connected via access tunnels to the drifts (horizontal galleys driven along the course of the ore vein). As mining proceeds to greater depths, in an effort to follow the ore vein, the strengths of the rock and ore decreases, hence the size of the openings that can be maintained also decreases. Internal support in stopes may be provided by artificial means, such as undisturbed ore, left as pillars, or timber support pack and hydraulic props (Dennen, 1989). Figure 2.1 depicts a typical stope environment, revealing the physical constraints common to the underground mining environment.

Figure 2.1 Image showing the physical constraints found in the stope

In deep-level, hard rock longwall mining, as is used in the South African gold mining industry, the face advances by blasting. Ore is drawn by a scraper down the stope dip into a transport gulley and from there into an ore pass. Hydraulic yielding props are used near the face, and resilient timber packs are constructed in the void behind the face. Access to the panel, which is to be mined, is gained via a manway at the top of the panel and a transport gulley at the bottom (Franklin, 1991). Figure 2.2 shows the typical layout of an underground stope, and depicts the geometric constraints imposed by such an environment.

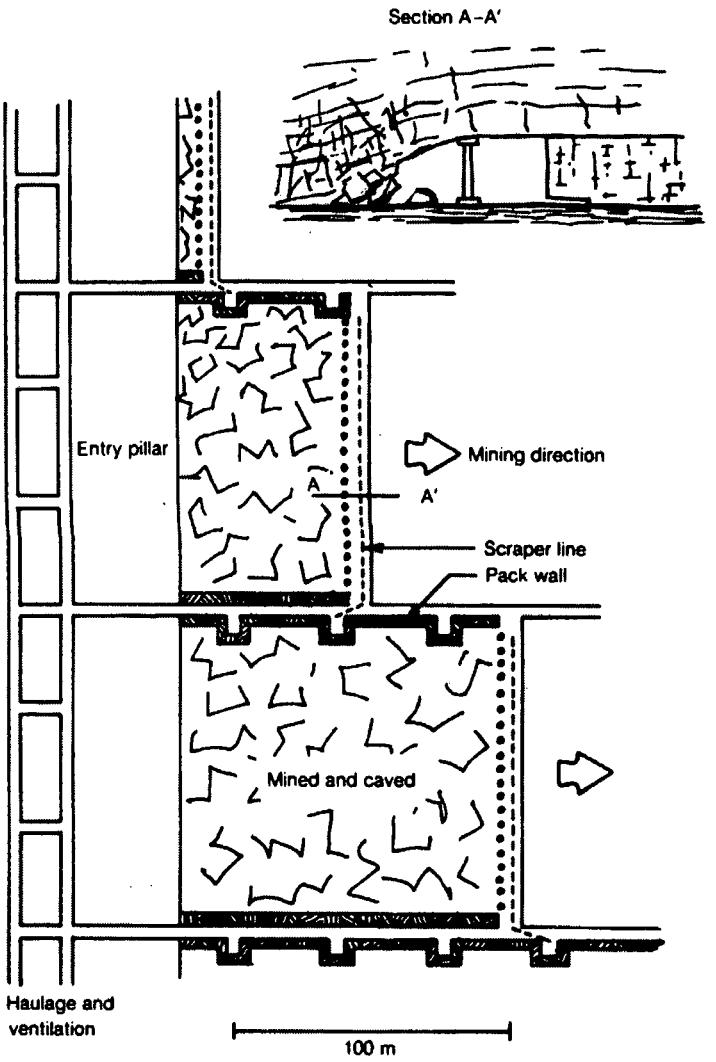

Figure 2.2 Stope Geometry and Conditions

As the excavation advances, closure of the stope opening occurs at the back wall, due to the immense pressures exerted by the overhead rock mass. The closure rates are accelerated during blast events, where sudden large closures of the stope opening take place. These blast related closures might be of the order of 10 - 20cm.

Apart from the physical space constraints imposed by the underground mining environment, additional factors such at extreme temperature and humidity levels need to be considered for the design of a measurement system. Due to the vast depths at which mining takes place, typically over 3,000m below surface, temperatures of up to 40°C are experienced in the stope. The requirement for large amounts of water in

mining operations, coupled with these high temperatures, results in humidity levels approaching 100%.

In developing a novel measurement system for use in the physically demanding and geometrically constrained environment of the underground mining industry, one is not only faced with the challenge of working in a hazardous environment, but has to design a system capable of use during normal production operations in the mine. This provides an excellent opportunity to demonstrate the versatility of digital photogrammetry as a measurement tool, capable of high accuracy measurement in extreme environments.

3 PHOTOGRAMMETRIC SURVEY OVERVIEW AND PRE-ANALYSIS

3.1 OVERVIEW OF THE PHOTOGRAMMETRIC SURVEY SYSTEMS

Photogrammetry has for many years been applied to the field of topographic mapping from aerial photography, relying on the normal case of stereophotography, i.e. camera axes that are parallel to one another. This inflexibility proved to be a limitation in the development of photogrammetry for close range applications (Fryer, 1996). The advent of analytical photogrammetry and in particular the development of multi-station analytical photogrammetry led to a new era in close range photogrammetry (Karara, 1989), with the possibility of convergent camera axes allowing for increased flexibility in photogrammetric network design.

Analytical methods are characterised by the use of the collinearity equations, which are solved for, either directly on-line in an analytical plotter or off-line in a batch process (Mikhail, 1989). The reduction of collinearity equations has taken on various forms, including the commonly used bundle adjustment (Brown, 1958) and direct linear transformation, or DLT (Abdel-Aziz and Karara, 1971). The simultaneous determination of the camera interior and exterior orientation parameters and the co-ordinates of the points of interest in object space can be solved with the use of the above mentioned formulations (McGlone, 1989).

In the past decade, advances in electronics and computer vision technologies have led to the development of digital photogrammetric methods. Based on electro-optical or video cameras, frame grabbers and computers, digital photogrammetric techniques have revolutionised close range image capture. It is not only the application in close range photogrammetry that has benefited from these electronic developments. The

field of remote sensing has gained considerably from improvements in the resolution of images captured by satellite based imaging devices (Fryer, 1996).

With a continual improvement in sensor technology, combined with computer systems becoming ever faster and storage media less expensive, there is an ever-increasing usage of digital systems (Dowman, 1996). This trend has been widely published, with applications reported in the fields of archaeology, architecture, industrial measurement and medicine among others.

It is in particular developments in industrial photogrammetry that have been revolutionised with digital systems allowing for the automation of many inspection processes. Industrial photogrammetry applies to applications in the industrial and engineering sectors (Adams, 1989) and is defined by Meyer (1973) as "application of photogrammetry in building construction, civil engineering, mining, vehicle and machine construction, metallurgy, ship building and traffic with their fundamentals and border subjects, including the phases of research, planning, production engineering, manufacture, testing, monitoring, repair and reconstruction. Objects measured by photogrammetric techniques may be solid, liquid or gaseous bodies or physical phenomena, whether stationary or moving, that allow of being photographed."

Examples of recent applications of digital photogrammetric techniques in close range industrial photogrammetry include: inspection for quality control and tooling in the aerospace industry (e.g. Schwartz, 1982; Powell, 1984; Stewart, 1975, 1979, 1986; Fraser and Mallison, 1992), periodic mensuration of marine and sub-marine propellers (Cooper, 1979 and Brown, 1981), measurement and alignment of communication antennas (e.g. Fraser, 1986, 1989, 1992b; Gustafsen, 1990), motor vehicle alignment and measurement (e.g. Haggrén, 1993; Smit *et al*, 1997), deformation of engineering structures (e.g. Fraser, 1985; Papo, 1985, Fraser and Gustafsen, 1986; Dold *et al*, 1993; Fraser and Shortis, 1995; Fraser, 1995) and the monitoring of tunnels and tunnel profiles (e.g. Ethrog and Shmutter, 1982; Anderson and Stevens, 1982; Wong, 1984).

With recent improvements in the resolution of charge coupled device (CCD) sensors, the accuracies achievable with "standard" CCD cameras is in the range of 1:10 000 to 1:30 000. Multi sensor, large area CCD cameras are now capable of relative triangulation accuracies in excess of 1:50 000 (Fraser, 1996b).

Developments in the hardware components of digital imaging systems, have created the need for algorithms capable of extracting the necessary information from the images, in order to carry out the necessary photogrammetric triangulation to determine the object point co-ordinates required. The unprocessed digital image will not necessarily be the optimum image for the desired purpose. A number of processing operations may have to be applied in order to modify the image into the desired form. These may include enhancement to improve the image sharpness and contrast, compression to decrease the amount of storage data required and classification to extract relevant image information (Dowman, 1996). The image may be filtered, to enhance or extract edge or interest point information. Interest operators for edge location have been widely investigated (e.g. Marr and Hildreth, 1980; Tabatabai and Mitchell, 1984; Canny, 1986; Förstner and Gülch, 1987).

The development of image matching algorithms, for the location of corresponding points in conjugate images, has been of vital importance to the automation of digital photogrammetry. This is also one of the most complex of digital photogrammetric tasks and has formed a major part of recent research initiatives. Image matching techniques traditionally have fallen into two categories, that of grey scale, area-based matching and feature-based matching. It is in particular the development of least squares multi-image matching algorithms by Gruen and Baltsavias (1988) that have been at the forefront of this research. In recent years, however, research has been initiated in designing matching algorithms that are more capable than conventional cross-correlation methods. These have been based on "first and second order derivative matching, relaxation methods, segmentation and graph structure matching, transform (Hough transform) matching and feature (edge) matching" (Gruen, 1996).

Although most digital photogrammetric measurement systems, in recent years, have been based on traditional analytical photogrammetric techniques, each application has specific design criteria, based on the project requirements and limitations. Based on these criteria, the choice of equipment, survey network and techniques used must be made. The rest of this chapter will focus on the design of a digital photogrammetric measurement system for the specific project at hand.

3.2 SURVEY SYSTEM DESIGN

In order to generate the three dimensional (XYZ) object space co-ordinates for the points of interest, which represent the rock face to be mapped, the following steps are taken:

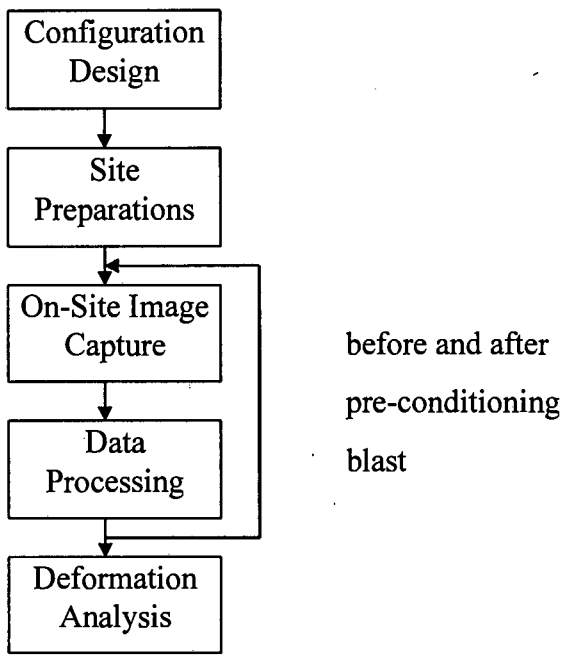

In more detail, these steps are:

- Hardware selection and design, to meet the need of the underground mining environment;

- Photogrammetric survey network design and pre-analysis, allowing for the physical space constraints in the stope, using fictitious image generation, bundle adjustments and laboratory simulation;

- The establishment of a stable reference co-ordinate system, capable of withstanding the pre-conditioning blast, to within the required accuracy;

The following steps are required both before and after the pre-conditioning blast event, in order to monitor the deformations that have occurred as a result of the blast:

- On-site image acquisition;

- Camera calibration, after the on-site survey;

- Target location and centring used in determining the interior orientation of the camera and the exterior orientation of the camera station locations, with bundle adjustments;

- Feature extraction, to select a dense image point cloud that adequately represents the surface being mapped;

- Multi-image matching, generating corresponding points of interest in multiple conjugate images;

- Space intersection to calculate the three dimensional object space co-ordinates of the points of interest; and

- Surface generation.

These procedures will be discussed in detail in the following chapters, including descriptions of the algorithms used or developed and the evaluation of the measurement system in underground mine tests.

Prior to the initiation of underground experiments, the initial design and feasibility of the system was investigated in a pre-analysis simulation of expected geometric constraints of the mine conditions. A description of network design procedures and the pre-analysis carried out follows:

3.3 NETWORK DESIGN

With the development of analytical photogrammetry came improvements in network design. The ability to include convergent images removed the restrictions of traditional stereo pairs. The result of the inclusion of extra image stations and convergence of image axes led to improvements in accuracy, as depicted in figure 3.1. The effect of convergence and extra camera stations is shown in the changes to the size and shape of the point error ellipsoids.

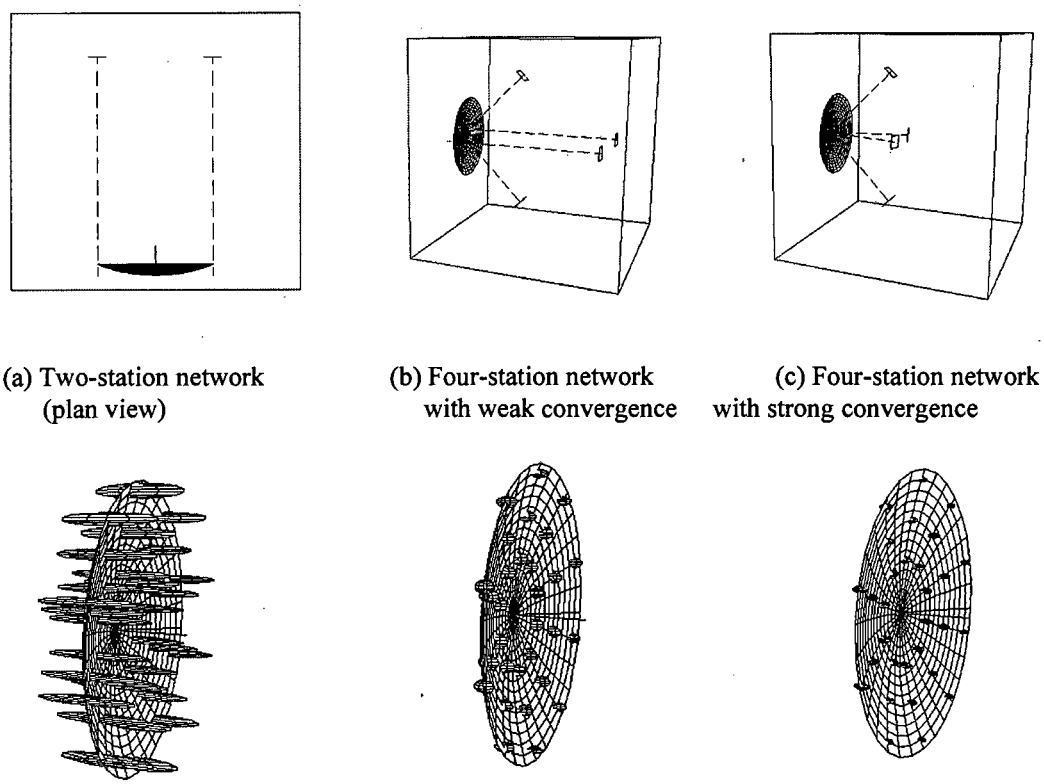

(a) Two-station network (plan view)

(b) Four-station network with weak convergence

(c) Four-station network with strong convergence

Figure 3.1 The effect of convergence and extra stations (after Mason, 1994)

Network design typically follows a "design-by-simulation" process where one starts with an optimal or "generic" network as a first approximation and then adds image stations to improve the design. The addition of image stations will not necessarily result in a broader diversity of convergence angles and will thus not necessarily provide a stronger geometry. Additional images will, however, increase precision and reliability as they add redundant observations to the network (Fraser, 1996a). The bundle method (see section 5.3.3) and appropriate sensor calibration procedures gauge the accuracy of the network (Mason, 1995a).

It is generally accepted that the design process aims to satisfy certain target conditions (e.g. precision, reliability and economy) by solving zero-, first-, second- and third-order design problems (Mason, 1994). These classifications, in relation to photogrammetric networks, can be described as:

- Zero Order Design (ZOD): defining a datum for the object point co-ordinates and exterior orientation parameters;

- First Order Design (FOD): configuring an optimal imaging geometry;

- Second Order Design (SOD): adopting a suitable measurement precision for the image co-ordinates;

- Third Order Design (TOD): network densification.

For a detailed description of these four design problems, the reader is referred to Mason (1994) and Fraser (1996a).

In designing a suitable network configuration, the physical constraints imposed by the workplace, which may limit the convergence angle of the camera stations, need to be considered when deciding on camera placements (Fraser, 1996a). The "strength" of

the configuration is a function of the image geometry, which is embodied in the factor q in the design formula given by Fraser (1984):

$$\bar{\sigma}_c = \frac{q\sigma_i S}{\sqrt{k}} \tag{3.1}$$

where $\bar{\sigma}_c$ is the average object space precision, k is the average number of photographs taken at each station, σ_i is the average image measurement co-ordinate precision, and S is the average image scale denominator, being computed as

$$S = \frac{d_v}{c} \tag{3.2}$$

Here d_V is the average camera to object distance and c is the principal distance of the camera sensor. After Mason (1995b), for a convergent network, a reasonable value for q can be expected in the range 0.4 to 0.7.

Careful consideration must paid to the constraints affecting the placement of camera stations. The constraints affecting camera station placement and hence network configuration are described by Mason (1995b):

1. *Image scale constraint*: the average precision obtainable for the photogrammetric triangulation is a function of image scale. By re-arranging equations (3.1) and (3.2), we can calculate the maximum camera-to-object distance, d_{max}, for a given accuracy tolerance (Fraser, 1996a):

$$d_{max} = \frac{\bar{\sigma}_c c\sqrt{k}}{q\sigma_i} \tag{3.3}$$

2. *Resolution constraint*: in order to obtain the desired accuracy, the object points must be imaged with optimal resolution. This has an impact on target design, image scale and image sensor selection.

3. *Workspace constraint*: structures in the workplace may restrict the placement of camera stations. This will have a bearing on image scale constraints as well as the image ray intersection geometry.
4. *Depth of field constraint*: all features on the object that are to be measured must be contained within the focal range of the camera and remain in sharp focus. The influence of lens focusing has a significant influence on the precision of image measurement (Fraser, 1996a).
5. *Incidence angle constraint*: the reliability of image measurement for planar objects decreases as the angle of incidence decreases. The minimum incidence angle is dependent on the type of feature, the feature geometry and material, as well as the illumination.
6. *Number and distribution of image points constraint*: the number of points in the image has little bearing on the precision of object point triangulation, as long as there are sufficient points in each image to solve for the exterior orientation in a bundle adjustment (Fraser, 1984). Maximising the number of points at an image station does, however, improve the internal reliability of the individual observations, through increased redundancy.
7. *Contribution to intersection angles*: the addition of an additional camera station cannot be assessed individually, but must be evaluated in terms of its contribution to the overall triangulation precision.
8. *Field of view*: it is beneficial to have the maximum number of object targets contained within the field of view at each camera station. This has the effect of simplifying the network design, enhancing economy and achieving a stronger imaging geometry.
9. *Visibility*: objects in the workplace may obscure visibility at certain image stations resulting in occlusions. This will have the effect of reducing triangulation precision for the occluded features.

The combined influence of constraints (1) to (5), (8) and (9) is depicted in figure 3.2, where the region for possible camera placement is shown for a simple planar object.

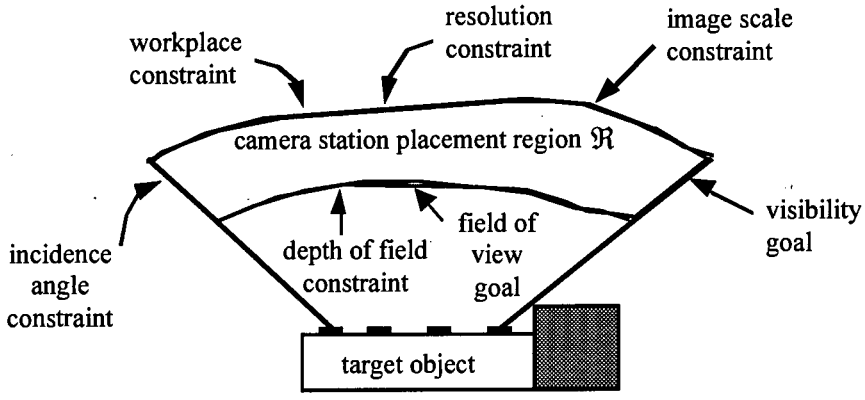

Figure 3.2 The influence of camera station placement constraints, in two dimensions (after Mason, 1995b)

Another factor, which requires consideration in network design, is that of reliability. An optimal configuration must enable the detection of gross observational errors (internal reliability) and the calculation of the influence of undetected gross errors on the final parameter values (external reliability) in the photogrammetric triangulation (Fraser, 1996a). In order to increase internal reliability we need to increase redundancy through the addition of image stations. It is assumed that high internal reliability coupled with optimal precision will lead to high external reliability (Fraser, 1996a).

The design-by-simulation process is essentially a trial and error process relying on expertise and user intervention. It follows a logical procedure based strategy as depicted in figure 3.3 (Fraser, 1996a).

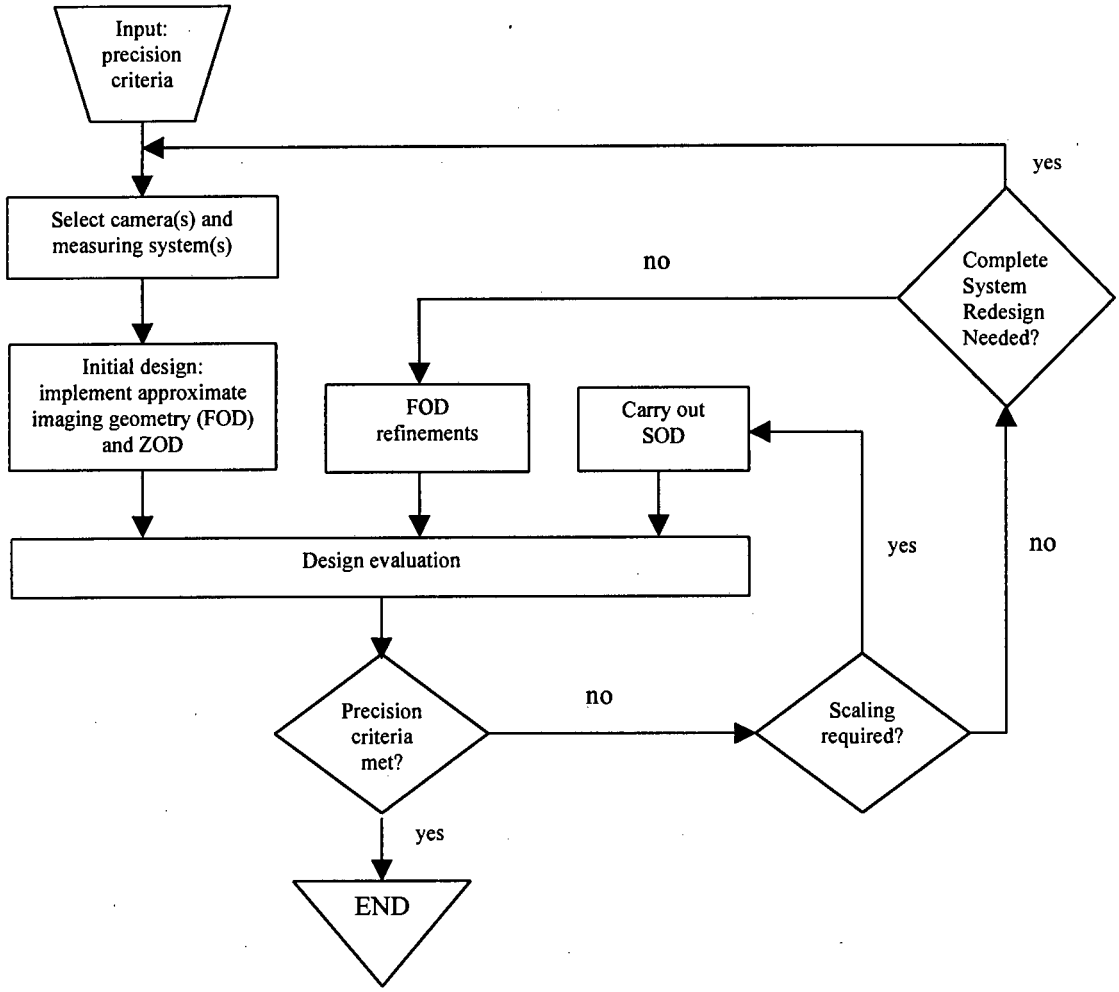

Figure 3.3 Flowchart for network design-by-simulation (after Fraser, 1994)

The most common solution to design-by-simulation involves FOD issues, while including considerations for photographic constraints such as field of view, depth of field and incidence angle (Fraser, 1996a). Additional consideration must be given to the choice of imaging device, targeting and lighting.

Recent investigations have been aimed at expert systems (ES), where computer software aids to simulate the problem solving for FOD (e.g. Mason, 1994, 1995a, 1995b). Although this is not likely to replace human expertise to the extent of full automation, ES can act as an aid to network design (Fraser, 1996a).

3.4 PRE-ANALYSIS

As a result of the space constraints imposed in the stope, with limited access and physical instability, the design and testing of the survey network to be used is severely restricted. In order to achieve the required sub-millimetre accuracy, over the period of time in which the rock face is to be monitored, a stable reference co-ordinate system needs to be established. It is particularly important that the reference frames used to define the co-ordinate system are not disturbed during the blast event, when the majority of the deformations occurring within the stope take place.

Pre-constructed reference frames, consisting of steel tubes and a steel back plate (as seen in figure 3.4), with attached circular retro-reflective targets are used to define the local co-ordinate system to be used in the stope. In the given underground mining situation, the maximum reference frame size tolerated is 0.5m x 0.5m x 0.2m.

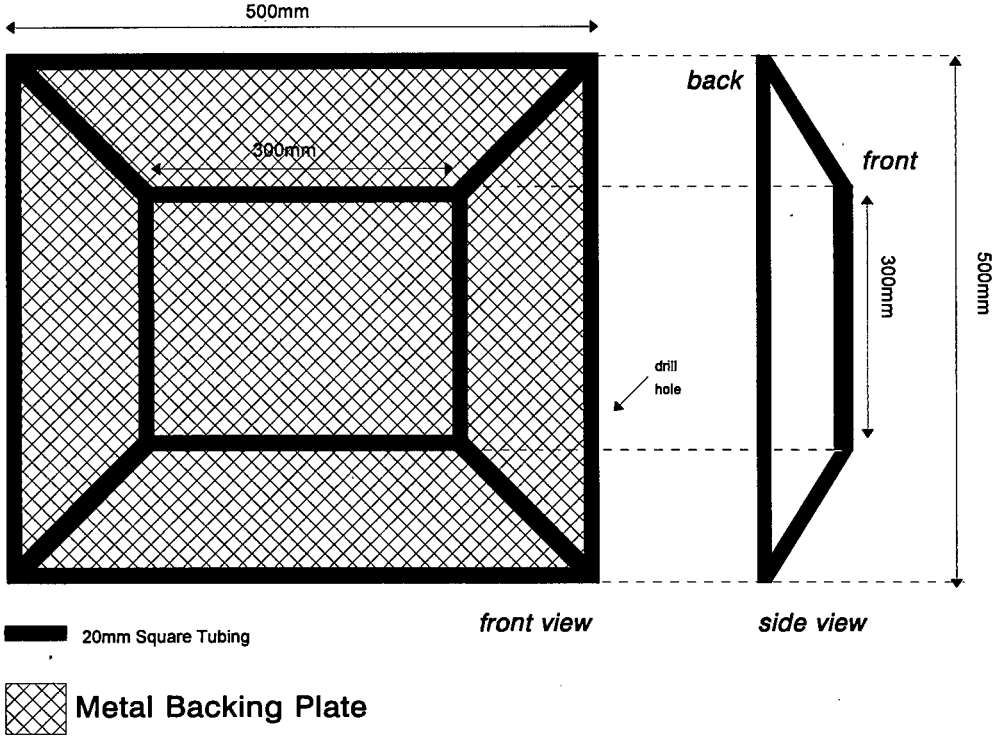

Figure 3.4 Co-ordinate reference frame design

As a result of the force generated by the blast, sudden and substantial deformation occurs within the stope. This deformation consists not only of the movement of the rock face itself, but includes closure of the hangingwall parallel to the plane of the excavation (in the vertical plane) and lateral movement, or ride, of the footwall. Of these movements, the vertical closure of the stope is the most substantial and may have a magnitude of up to 10 - 20cm.

The only surfaces in the stope capable of withstanding the blast, to within the desired accuracy, over a short period of time, are those found on the timber support packs at the back of the stope opening. This poses a substantial problem as it makes it necessary to place the co-ordinate reference frame, attached to a pack, at right angles to the rock face being measured. The resultant poor geometry, as depicted in figure 3.5 below, creates a considerable problem in the solution of the survey network design.

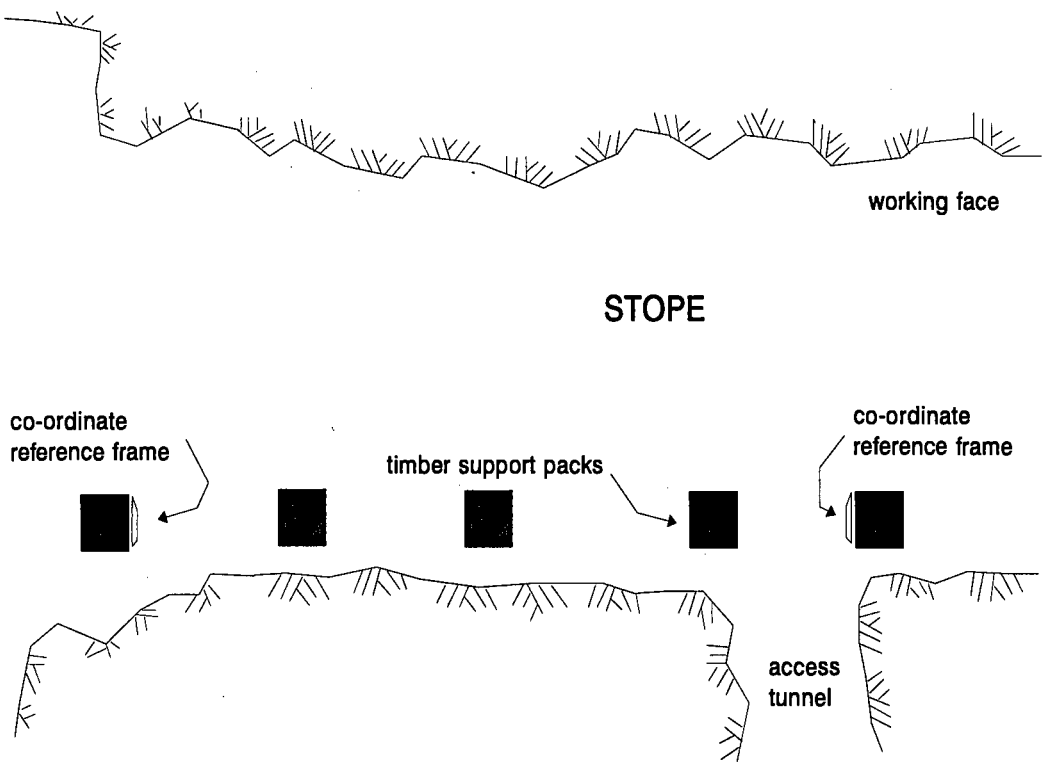

Figure 3.5 Stope Layout

In order to compensate for the divergent imagery, a complex configuration of camera positions and co-ordinate control points is required for the establishment of accurate point co-ordinates on the rock face itself. The design and testing of the network used, required numerous design stages before arriving at a viable solution. Various approaches were investigated in arriving at a practical and accurate solution to the network design; a description of the efforts made follows, starting with a coupled camera approach, to the final single camera approach with multi-perspective set-ups.

In order to detect any movement in the co-ordinate system throughout the duration of the photogrammetric survey, a second co-ordinate reference frame is attached to a support pack at the furthest extreme of the deformation area to be measured, as is shown in figure 3.6. Image capture is then extended to include this second reference frame.

Although the two reference frames will only be "tied" photogrammetrically, they will provide a means detecting any relative movement between the reference frames and thus deformation of the co-ordinate system as a result of the pre-conditioning blast. The second frame also provides a means of checking the scale at the end of the survey network. The two frame design does not make it possible to determine if one, or both, of the frames has moved, or if only one frame has moved, which one of the frames suffered from the deformation. It merely provides a limited check for systematic errors that have occurred to the co-ordinate system as a result of the pre-conditioning blast. A check for absolute movements of the co-ordinate system is only possible by taking time consuming theodolite observations, from stable positions outside of the stope (such as the mine survey points located in the manway or gulley which join the stope to the transport gulley). This method would, however, require a very complex observation procedure to provide the required sub-millimetre accuracy, and it is likely that such accuracy would be impossible to obtain under such conditions.

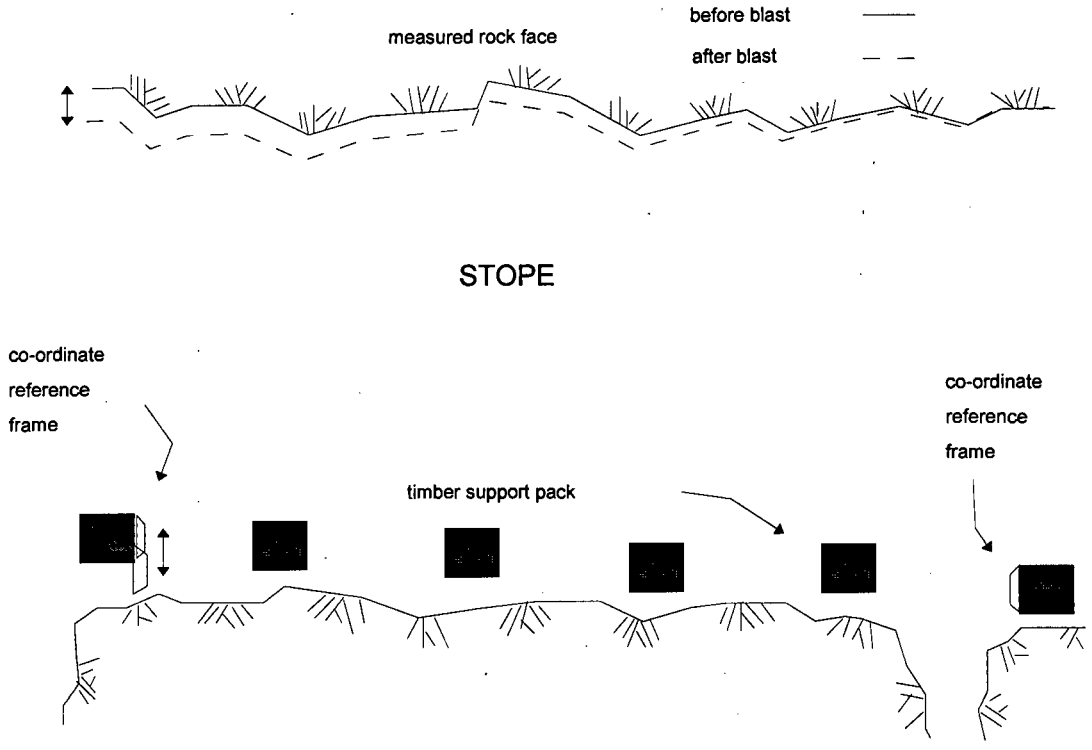

Figure 3.6 The use of a second reference frame to detect co-ordinate system movement

Before considering the development of the photogrammetric survey network design, it is necessary to discuss the simulation process, with the use of fictitious images, a process that is an integral part of testing the proposed network designs.

3.4.1 NETWORK SIMULATION

In carrying out a pre-analysis of the proposed photogrammetric survey network, fictitious images were used to simulate the proposed network configuration. The solution of the bundle adjustment, based on the fictitious images, is a reliable indication of the accuracy potential of the network configuration design. It is only the *a priori* σ_0 of the adjustment that provides a scaling factor for the actual images.

Hence, pre-analysis based on fictitious images will adequately model the proposed network design that is to be used in reality.

The mathematical model used in the fictitious image generation is based on the formulation by Brown (1985). With reference to figure 3.7, we choose angles A_0,E_0 to define the direction of the fictitious camera. It is then assumed that angles A_i,E_i (i=1,2,...,n) denote the observation angles at the given station.

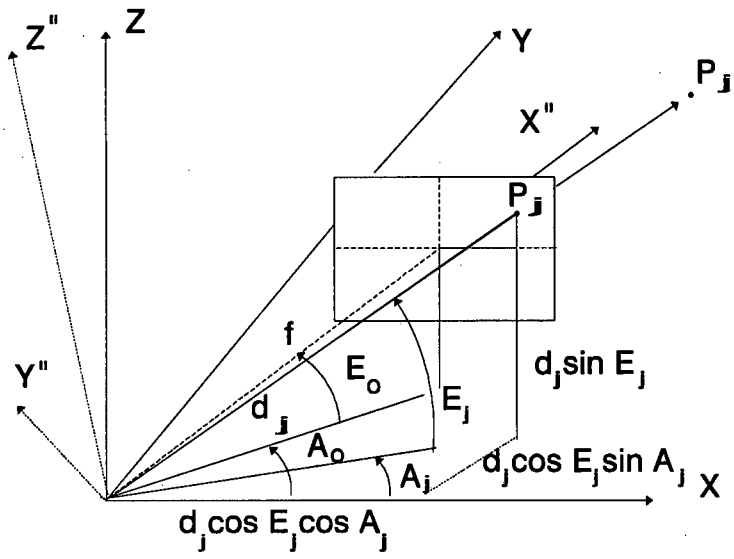

Figure 3.7 Image space co-ordinate system

Having specified A_0 and E_0 for the given station, it follows to evaluate the fictitious image co-ordinates for each of the observation rays, with defining directions A_i and E_i. This requires a transformation from the object space co-ordinate system (XYZ) into the image co-ordinate system (x,y,*c*). Without derivation, this allows us to obtain the fictitious image co-ordinates, with *c* as the focal length of the fictitious camera:

$$x_j = c\frac{m_j}{q_j}$$
$$y_j = c\frac{n_j}{q_j} \qquad \textbf{(3.4)}$$

where,

$$m_j = \cos E_j \sin(A_0 - A_j) \tag{3.5}$$

$$n_j = -\sin E_0 \cos E_j \cos(A_0 - A_j) + \cos E_0 \sin E_j \tag{3.6}$$

$$q_j = \cos E_0 \cos E_j \cos(A_0 - A_j) + \sin E_0 \sin E_j \tag{3.7}$$

where,

A_j is the horizontal angle of the image point ray, counted from the positive X-axis to the object point P_j increasing from X to Y;

E_j the elevation angle of the image point ray, counted from the positive XY plane to point P_j increasing from the XY plane towards the positive Z-axis;

A_0 the azimuth to the approximate centre of the object as seen from the perspective centre of the camera station; and

E_0 the elevation angle to the approximate centre of the object.

The horizontal angle, A_0, and elevation, E_0, are chosen so that the image centre coincides approximately with the centre of the object as seen from the perspective centre of the camera station. This reduces the angular spread of observation which, according to Brown (1985), has the effect of lowering the correlation between the derived *x* and *y* image co-ordinates. Thus the bundle adjustment, having no provision for the consideration of correlated errors may produce nearly optimal results for the fictitious images.

In the pre-analysis of the photogrammetric network, the calculated image co-ordinates are assigned random errors, which are scaled according to the expected standard deviations of the actual image co-ordinate measurement (in this case, the determination of circular target centres, as discussed in section 5.1). The random

errors are calculated by means of computer generated, normally distributed random numbers, as described by Rüther (1989).

It is assumed that observations are subject to normally or near normally distributed uncorrelated random errors. Computers typically have random number generators, which produce uniformly distributed pseudo random values. Hence a transformation is required to convert these values into normally distributed values.

It can be shown that *N(0,1)* normally distributed random numbers can be approximated by,

$$s_i' = (\sum_{j=1}^{k} r_j - \frac{k}{2})\sqrt{\frac{12}{k}} \tag{3.8}$$

where k≈6 provides an adequate solution.

This approximation can be further improved by,

$$s_i = s_i' - \frac{1}{20k}(3s_i' - s_i'^3) \tag{3.9}$$

For the purpose of pre-analysis of the proposed photogrammetric network, a standard deviation of 0.001mm was used. This is equivalent to approximately 1/10 of a pixel on the image and is an average accuracy achieved for circular target image co-ordinate determination.

The development and testing of the network configuration was carried out using two methods of image capture. Firstly, the use of two CCD cameras, mechanically coupled to one another in a stereo approach and secondly the use of a single CCD camera in a multi-perspective approach. These methods will each be described in turn in the following sections.

3.4.2 COUPLED CCD-VIDEO CAMERA

An initial proposal, based on assumptions concerning the layout of support structures within the stope, was to have a mechanically coupled set of two CCD video cameras, one camera viewing the reference control frame, attached to a support pack, in the rear section of the stope, and the other viewing the rock face to be mapped. These CCD cameras were to be connected, for image capture, to an image processing card, housed in a docking station linked to a notebook computer.

The initial assumptions made about the geometry of the stope are that there is a stope height (footwall to hangingwall opening) of 1-1.5m, providing good visibility throughout; that the distance from the rock face to the support packs, at the back of the stope, is 3m or more and that there is a 1.5m separation between the support packs. These dimensions, provided by rock engineers as typical of stope conditions, are depicted in figure 3.8 below.

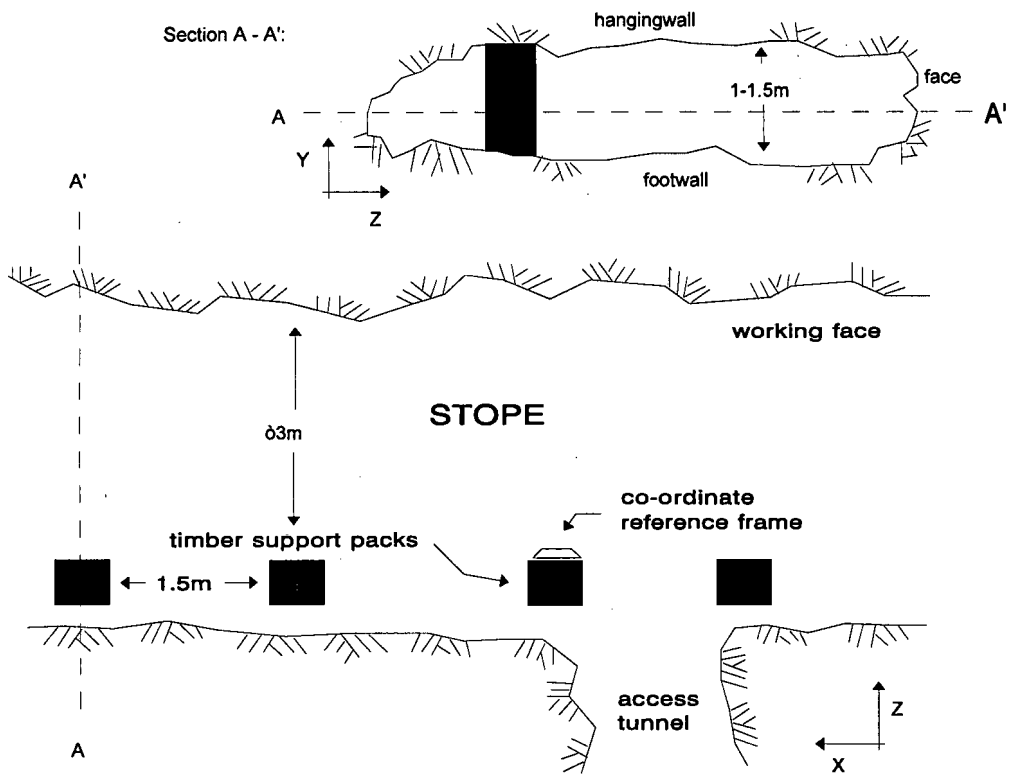

Figure 3.8 Initial assumptions about the stope geometry

In order to maintain a base:distance ratio of 1:6 for sequential camera set-ups, to optimise both the image perspective and geometry, a camera base separation of 0.5m is required for the given situation. With the CCD cameras used, ITC - TM458 CCD video cameras with 1/2" CCD sensors, it was decided to use a 6mm lens for the camera to view the rock face, providing a field of view of approximately 59°, for the camera viewing the reference control frame, an 8mm lens, providing a 45° field of view was chosen. By adopting this lens combination, the necessary overlap is obtained between the stereo models of the rock face, while ensuring that the maximum extent of the image is occupied by co-ordinate control points on the support pack. This is depicted in figure 3.9, where the relation between the coupled cameras, the reference control frame and the rock face is shown.

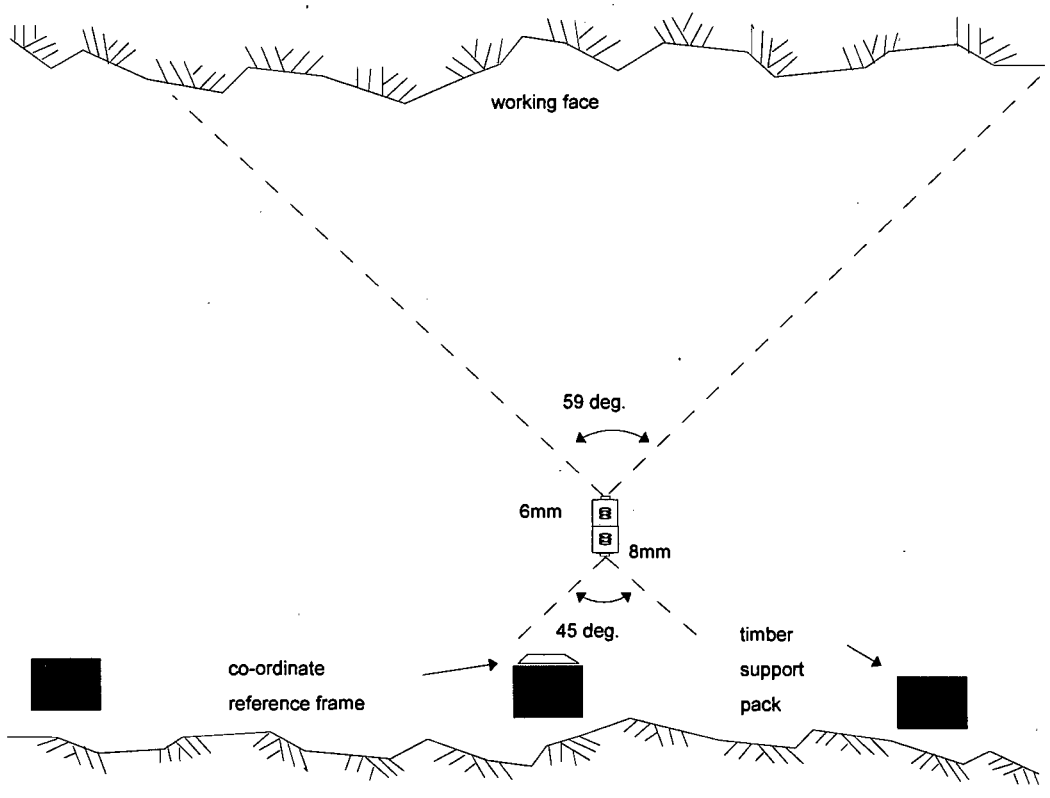

Figure 3.9 Camera set-up to suit stope geometry

The two cameras are mechanically secured to one another and their relative positions and orientations are calibrated using a calibration control field. The functional design of the proposed photogrammetric survey required two sets of connected cameras, one

at either end of the stereo base. Each of these sets of cameras requires co-ordinate reference, as provided by the control frame. The relative positions of the cameras, co-ordinate reference frames and the rock face are depicted in figure 3.10. From the diagram, it can be noted that the position and orientation of cameras (c1-a) and (c1-b) can be determined by means of a space resection from the reference co-ordinates found on the control frame attached to the support pack. The position and orientation of cameras (c2-a) and (c2-b) are then determined by applying the pre-calibrated link transformation parameters between the coupled cameras.

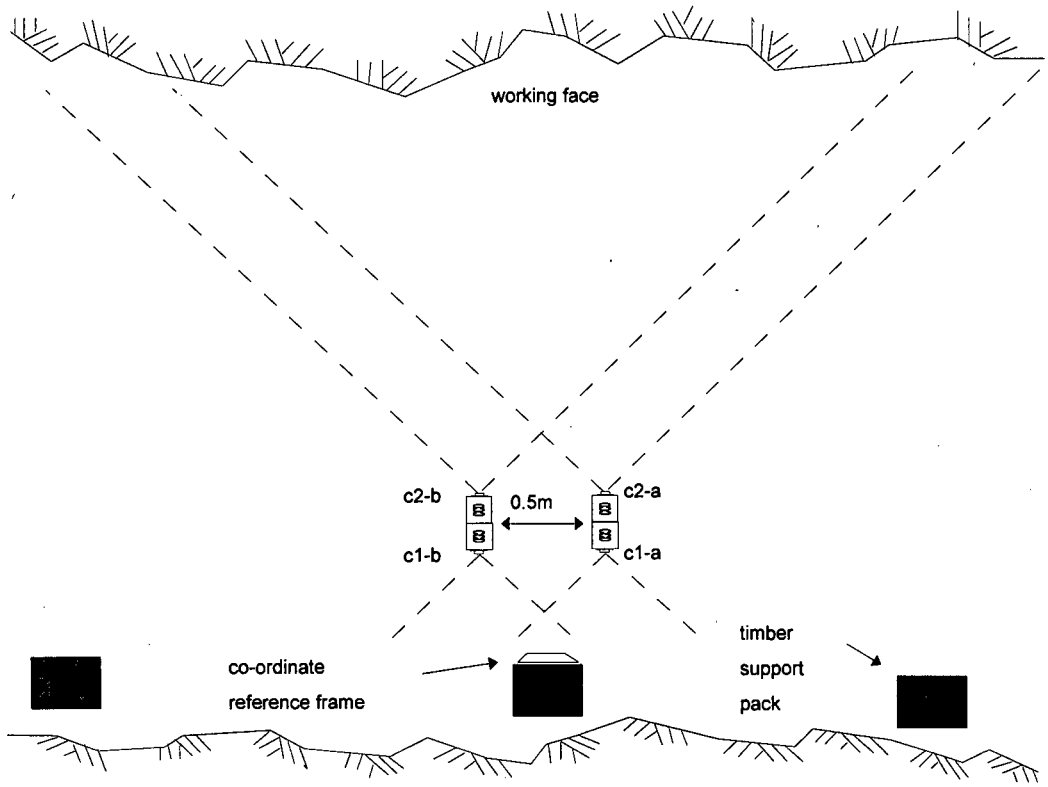

Figure 3.10 Stereo linked camera set-up

As deformations of the rock face are required to sub-millimetre accuracy, image capture must occur as soon before and after the blast as is possible, ensuring minimal movement in the positions of the reference control frames, as a result of stope closure resulting from the blast. In calculating deformations caused by the blast, it is assumed that any errors in the calculation of the link parameters, between the coupled cameras, will be small and remain unchanged, thus having no effect on the calculation of

relative movements of the rock face. This relies on the premise that the mechanical link between the coupled cameras remains unmoved.

After laboratory tests, it was noted that inaccuracies in the parameters linking the coupled cameras and difficulties experienced in calculating the bundle adjustment, resulted in precision estimates exceeding the required 1mm tolerance level. It was also found that the physical environment of the stope is substantially more constrained than the initial assumptions made. It was thus no longer possible to use this coupled camera configuration.

After testing an alternative, single camera, multi-perspective approach, it was found that for the stope environment, the accuracies achieved with the coupled camera approach could be improved upon. It was thus decided to continue the development of the measurement system using a single camera configuration. The coupled camera system could, however, be advantageous in other applications in the underground mining industry, for example in measuring the progress and boring pattern of tunnelling machines, where the physical constraints of the mine are in the lateral plane. Here, coupled cameras could provide the solution to extending the co-ordinate system, defined by co-ordinate reference frames, onto the rock face, where little lateral movement is possible.

3.4.3 SINGLE CAMERA, MULTI-PERSPECTIVE APPROACH

This alternative approach to the network configuration problem uses images that are captured in a strip, analogous to an aerial photography flight strip along the rock face, as depicted in figure 3.11, starting and ending with reference co-ordinate control points on either end of the rock face. This solution allows for choice of imaging devices, two of which were investigated: a CCD-video camera, coupled to a frame grabber and a notebook PC and the Kodak DCS420 digital camera.

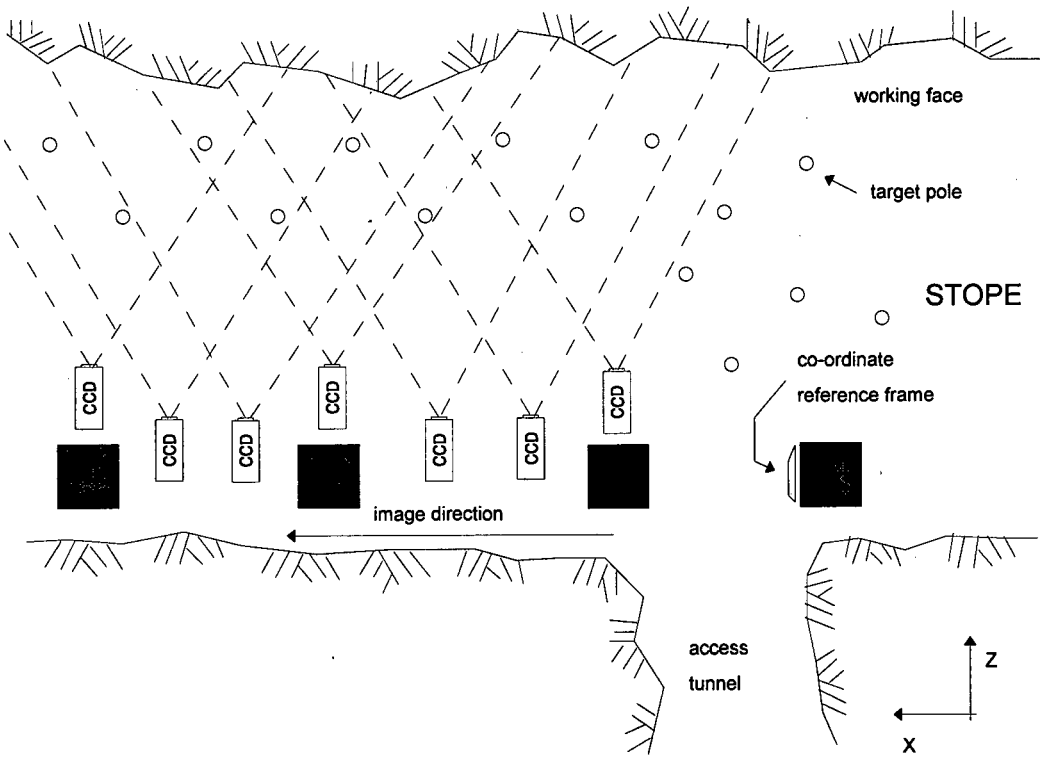

Figure 3.11 Image strip along the rock face

The network design, in the region of the reference co-ordinate frames, is largely dictated by the constrained geometry in the stope and the geometrically unfavourable position of the support packs. As a result, a set of camera positions following a circular curved path, as depicted in figure 3.12, is required to transfer co-ordinate control from the reference frame to the target points on the rock face.

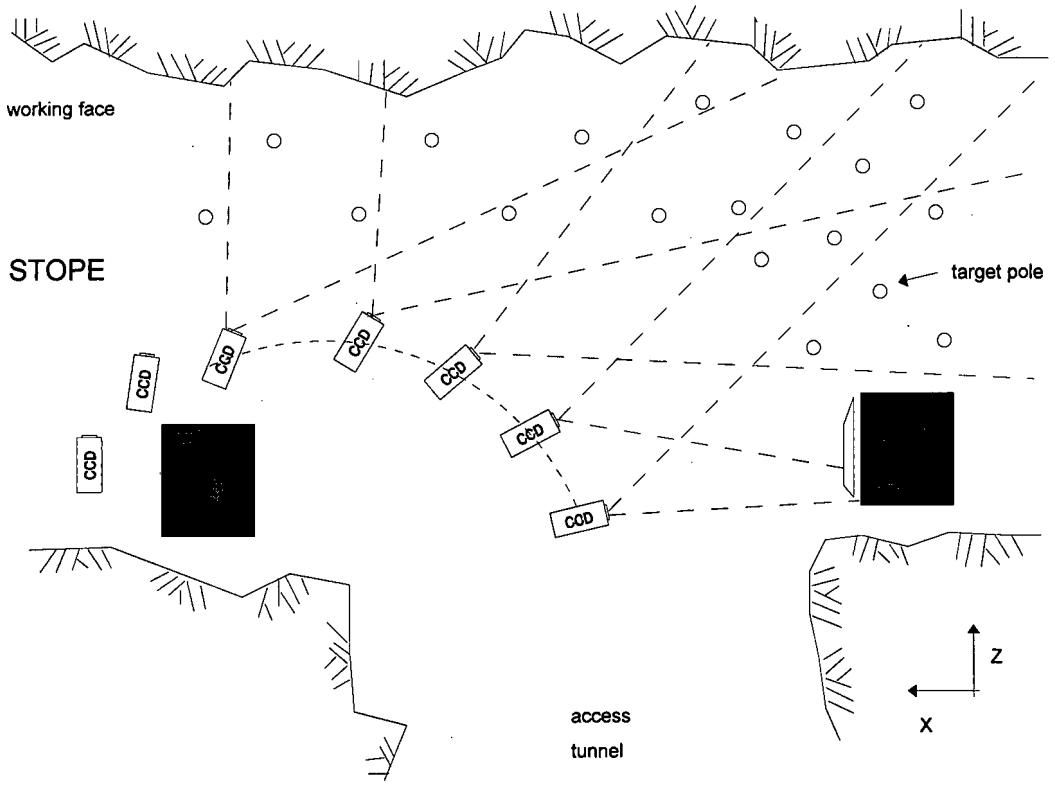

Figure 3.12 Circular path required for image positions in the region of the reference frame (plan view)

The addition of multiple image perspectives at each camera station, with convergent imagery at two height levels, provides an increased redundancy, improving the geometry for exterior orientation determination and ultimately, image matching. These additional images, required for the transfer of co-ordinates from the frame to the rock face, are of particular importance in the region of the reference co-ordinate frames, where divergence of the image axes is found. Images in this region are not only required at two height levels, but also with varying lateral perspectives, to strengthen a geometrically weak network.

Target points, located on the rock face and placed on poles positioned throughout the stope (between the rock face and the camera locations), are used as tie points, required for the successful calculation of a bundle adjustment of the photogrammetric survey network. The second co-ordinate reference frame required at the end of the panel to mapped, provides a means of checking that the scale of the co-ordinate system has not

changed, and also allows for the detection of relative movement of the co-ordinate system. Thus, systematic errors in the maintenance of the co-ordinate system can be detected.

Initial attempts to transfer the co-ordinate system from the reference frame to the rock face, without the use of multi-perspective imagery, resulted in poor object space co-ordinate accuracies on the rock face. A bundle adjustment, constrained by the co-ordinates of one of the reference frames, carried out in a simulation, with fictitious images (see sect. 3.4.1), provided the following accuracies for the object space co-ordinates calculated, where the Y and Z are lateral axes and X is the depth axis:

RMS σX (mm)	RMS σY (mm)	RMS σZ (mm)
3.12	1.86	0.82

Table 3.1 Bundle adjustment precision - divergent imagery

Where the root-mean-squared (RMS) standard deviations are calculated as,

$$RMS\sigma = \sqrt{\frac{\sum \sigma^2}{n}} \tag{3.10}$$

for n sample points.

It was decided to improve the network geometry of the system by capturing two sets of images at each camera set-up, one at a low elevation and one at a high elevation, both viewing the same image area, as is depicted in figure 3.13 below.

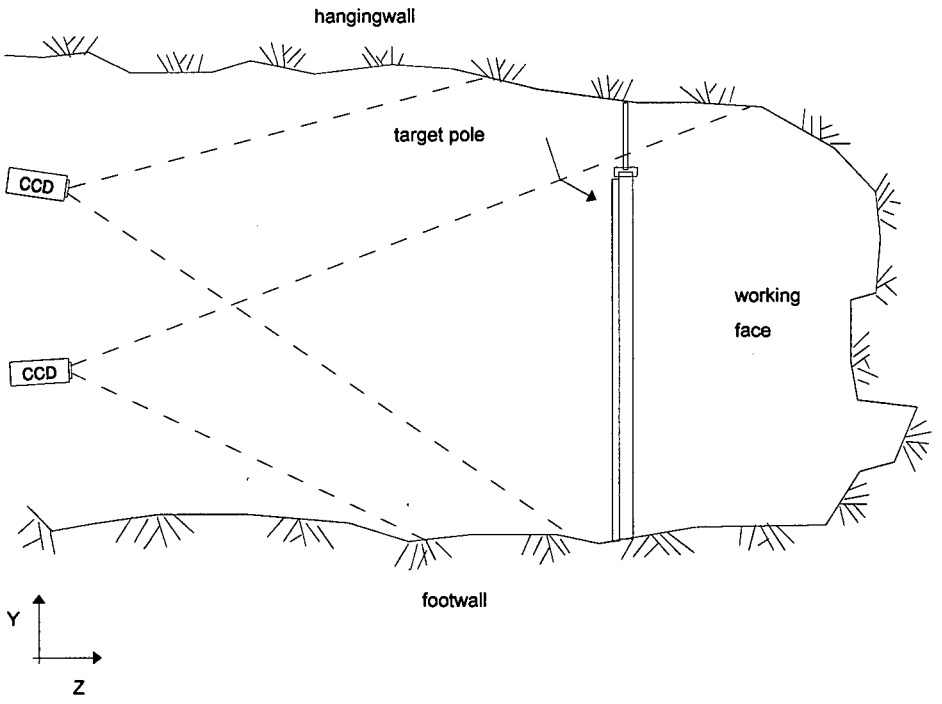

Figure 3.13 Image convergence from two height levels (vertical section)

Again the simulation of the network design was carried out using fictitious images, with two height levels at each camera set-up. The results of a bundle adjustment, constrained by the reference frame co-ordinates at one end of the panel, revealed a substantial improvement in the object space co-ordinate accuracies obtained for the points on the rock face. This is shown in table 3.2 below:

RMS σX (mm)	RMS σY (mm)	RMS σZ (mm)
0.97	0.77	0.40

Table 3.2 Bundle adjustment precision - two height level imagery

In order to further improve the network geometry and increase redundancies in the region of the co-ordinate reference frames, an additional set of images at each camera set-up is included. These "backward facing" images, as depicted in figure 3.14, view the object area captured at the previous camera station, thereby providing a link over a

number of images, with multiple perspectives of the same scene from different camera stations.

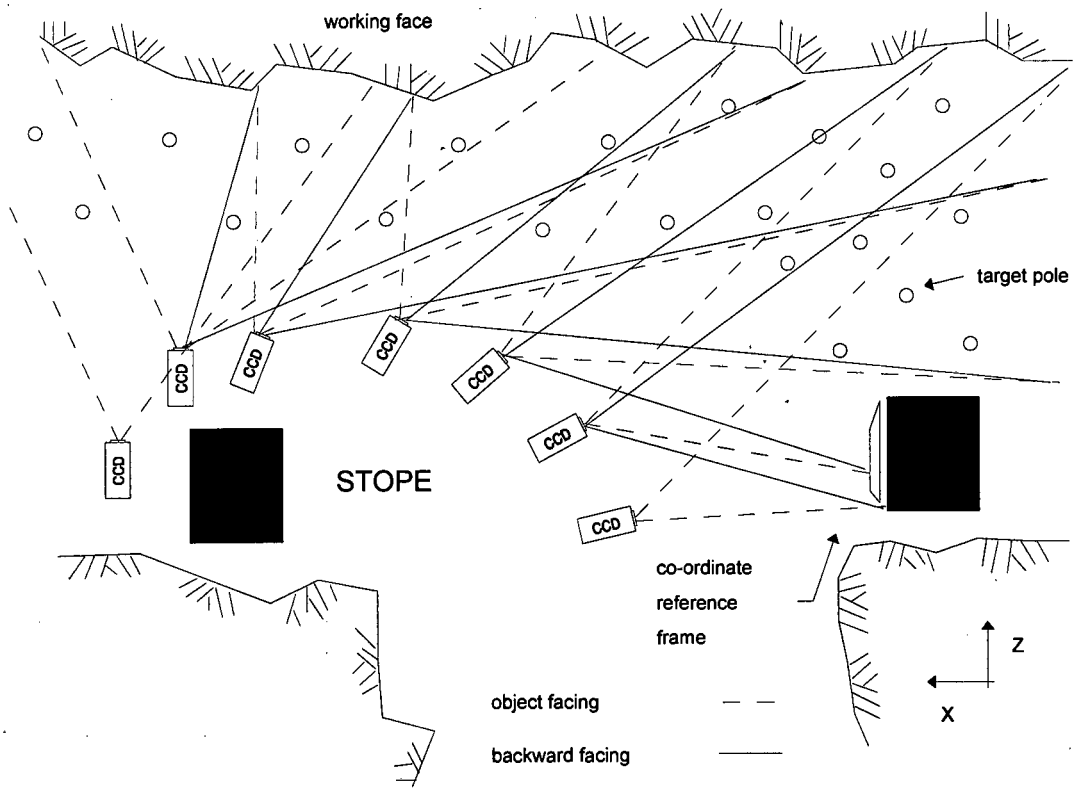

Figure 3.14 Object- and backward-facing imagery

The resulting constrained bundle adjustment indicates that the addition of "backward facing" imagery has a positive effect on the resultant object space co-ordinates of points on the rock face. The improved object space co-ordinate accuracies, and in particular the accuracy in depth of 0.60mm, can be noted in table 3.3 below:

RMS σX (mm)	RMS σY (mm)	RMS σZ (mm)
0.60	0.45	0.23

Table 3.3 Bundle adjustment precision with additional "backward facing" imagery

Initial simulations were based on a target pole separation of 0.5m. This provided a desirable network solution, but had the effect of target poles obscuring a fairly

substantial part of the rock face to be mapped. It was thus decided to increase the target pole separation to 0.75m, in an effort to reduce the obscured rock area. The results of the simulation with this configuration showed no significant decrease in the accuracy of the object space co-ordinates calculated. This is seen in table 3.4 below, with the depth accuracy 0.70mm being within the desired sub-millimetre range.

RMS σX (mm)	RMS σY (mm)	RMS σZ (mm)
0.70	0.51	0.25

Table 3.4 Bundle adjustment precision - 0.75m target pole separation

In order to confirm the simulation, the network design was tested in a laboratory reconstruction of the adopted configuration, requiring the reproduction of physical mine conditions, and in particular the geometric constraints found in the stope. In doing this, the initial assumptions about the stope conditions, as depicted in figure 3.8 above were used for the laboratory set-up. Camera stations, co-ordinate reference frame positions and target point locations were placed in accordance with the adopted survey network design.

Image capture for this test was carried out using a monochrome CCD video camera, linked to an image processing card, producing a 512 x 512 pixel image (this imaging system is more fully described in section 4.1). Based on the analysis and subsequent bundle adjustment of the captured images, it was confirmed that the proposed network design is feasible, and should provide the desired accuracy and functional flexibility required in the underground mining environment. The precision of the bundle adjustment carried out on the laboratory test images, as seen in table 3.5, confirm the adequacy of the camera positions and target pole locations in the adopted network configuration. It can be seen that a depth accuracy of 0.71mm is close to the fictitious simulation result of 0.70mm and within the sub-millimetre requirement for object point determination.

RMS σX (mm)	RMS σY (mm)	RMS σZ (mm)
0.71	0.57	0.30

Table 3.5 Bundle adjustment precision - laboratory tests

4 IMAGE ACQUISITION

When considering the acquisition of the images for the survey, once again particular attention must be paid to the nature of the underground mining environment. It is for this reason that the choice of imaging equipment to be used is so vital. Once the selection of appropriate equipment has been made, preparations for the on-site survey, including reference frame co-ordination and target pole construction, need to be carried out.

4.1 IMAGING EQUIPMENT

When designing a measurement system for the underground mining industry, one is once again limited by the extreme conditions in the stope. Of particular importance is the ability of the equipment to withstand high temperatures (often approaching 40°C) and humidity levels close to 100%. The imaging equipment should also be free from electrical sparking in its operation, in order to prevent the possibility of explosions due to the potential presence of flammable gasses in the stope. In addition the equipment used must be portable and rugged, to be able to withstand transport in and out of the mine.

The design and testing of this project was based on two image capture systems, providing a low cost CCD video camera based system and a system based on the Kodak DCS420 digital camera. The merits of each of these alternatives will be discussed.

The technical specifications of the CCD video camera based imaging device are as follows:

- ITC-TM458 Monochrome CCD video camera, comprising:
  ½" interline transfer CCD

7.95mm x 6.45mm image area

795(H) x 596(V) picture elements

- Matrox PIP512b image processing card, with:

  512(H) x 512(V) pixel A/D conversion.

In practise, the image processing card is attached to a notebook computer, with the use of a docking station. The addition of an external monitor is required for viewing the video output from the CCD camera during image acquisition, to enable accurate camera positioning.

Initial in situ tests revealed that this system, although viable, comprised too many components, which decreased portability and made image capture more cumbersome, with cables being required for image transfer from the camera to the image processing card, and for power to the camera, monitor and computer. In addition, this system requires an external source of lighting, as no flash unit can be used. During mine tests a malfunction of the notebook computer's monitor occurred due to the high degree of humidity. Figure 4.1 depicts the image capture system as used in the first underground mine tests and highlights the problems associated with the large number of components required.

Figure 4.1 CCD-Video image capture system

The Kodak DCS420 digital still camera provides a higher cost alternative, but with substantial benefits to ease of use in the stope. The Kodak DCS420 with its 1524x1012 pixel CCD chip provides the ideal solution to image capture within the stope; it is portable, reasonably rugged and capable of storing sufficient images to accurately map the rock face of interest. In addition the DCS420, based on a traditional Nikon SLR camera body, is capable of providing its own lighting by means of a flash unit.

An aspect of note with the DCS420, as with most digital still cameras, is that the image area occupied by the CCD chip is less than half of that covered by conventional 35mm film, in a traditional SLR camera. This results in only half of the image area viewed through the camera viewfinder being imaged. As a consequence, the choice of lens required must take into account a 2.6x factor reduction in the size of the field of view. Bearing this in mind the use of a 14mm wide-angle lens was required in order to capture a suitable area of the object surface. Thus, a 1:1 ratio between camera distance

Figure 4.1 CCD-Video image capture system

The Kodak DCS420 digital still camera provides a higher cost alternative, but with substantial benefits to ease of use in the stope. The Kodak DCS420 with its 1524x1012 pixel CCD chip provides the ideal solution to image capture within the stope; it is portable, reasonably rugged and capable of storing sufficient images to accurately map the rock face of interest. In addition the DCS420, based on a traditional Nikon SLR camera body, is capable of providing its own lighting by means of a flash unit.

An aspect of note with the DCS420, as with most digital still cameras, is that the image area occupied by the CCD chip is less than half of that covered by conventional 35mm film, in a traditional SLR camera. This results in only half of the image area viewed through the camera viewfinder being imaged. As a consequence, the choice of lens required must take into account a 2.6x factor reduction in the size of the field of view. Bearing this in mind the use of a 14mm wide-angle lens was required in order to capture a suitable area of the object surface. Thus, a 1:1 ratio between camera distance

from the rock face and lateral extent of rock face viewed (along face), as required in the photogrammetric survey network design, is maintained.

The technical specifications of the imaging equipment used are as follows:

- Kodak DCS420m digital camera, featuring:
  - Traditional SLR operation
  - Mono CCD sensor
  - 14mm x 9.3mm image area
  - 1524(H) x 1012(V) picture elements
  - PCMCIA-ATA Type III removable hard drive for image storage

- Nikon SB-26 Speedlight; hot shoe flash unit

- Sigma 14mm f/3.5 AF lens

While this camera has proven highly reliable in the extreme conditions of the stope environment, it must be noted that the PCMCIA hard drives, used to store the images captured, proved less robust, and special care must be taken when handling them. It is suspected that the high temperatures experienced within the stope can be detrimental to the sustained operation of these storage devices.

In considering the accuracy potential of the Kodak DCS420 camera and its suitability to highly accurate digital photogrammetric measurement, attention must be paid to the inherent limitations in the camera design. Of particular interest is instability in the CCD chip mounting, as reported by Gruen (1995). It was found that the CCD chip of the DCS200, which is of equivalent construction to the DCS420, is attached to the camera body only on one side. This can lead to movement in the vertical sensor direction as a result of temperature changes, the force of gravity and movement of the camera itself. Although this phenomenon will have an effect on the achievable accuracy potential of the DCS420, such possible sensor movements are well below the required sub-millimetre accuracy for the rock face measurements.

The Kodak DCS420 digital camera, although the obvious choice for image capture, due to its ease of use, portability and high resolution, is the more expensive of the two options investigated. On the other hand, the imaging system comprising CCD video camera, docking station and notebook computer, although still viable, is cumbersome and subject to more difficulties in operating. The advantages of the DCS420 clearly outweigh those of the CCD system, and it was decided to base the further development and testing of this measurement system entirely on image capture by means of the Kodak DCS420m digital camera.

4.2 SITE PREPARATIONS

Before proceeding with image capture underground, it is necessary to carry out some preparatory operations to ensure that image capture in the stope is efficient and accurate. The reference frame required for co-ordinate control must be prepared, and target poles necessary for photogrammetric tie points must be constructed.

4.2.1 CO-ORDINATION OF REFERENCE CONTROL FRAMES

In order to establish the co-ordinate reference system used for deformation analysis in the stope, it is necessary to construct a control frame, which contains targets of known co-ordinates. The frame, as depicted in figure 3.4 above, should consist of a steel tubing frame and a steel back plate. As previously mentioned, due to the space limitations within the stope, the frame should not exceed 0.5m x 0.5m x 0.2m in dimension. Target points consisting of circular, retro-reflective discs (8mm in diameter) are attached to the frame to provide reference points for the co-ordinate system.

Before the reference frame can be used in the stope, the target points on the frame must be co-ordinated, in a local "frame" co-ordinate system. This follows the same process as is used in camera calibration (see section 5.2), except that for the purpose of image scale, at least two highly accurate distance measurements between extreme target centres are included in a free network bundle adjustment, to calculate the co-ordinates of the target point centres. These distances are typically measured with a large Vernier's calliper and should include perpendicular measurements in both lateral directions.

The determination of the co-ordinates of the target centres requires the following procedures:

- distance measurement
- image capture
- target centring
- target identification
- free bundle adjustment

The details of the calculation stages will be discussed in chapter 5. Table 4.1 shows typical accuracies achieved in object space for target centre co-ordinate determination, using this process. These are well within the required sub-millimetre accuracy for the reference co-ordinate system determination.

RMS σX (mm)	RMS σY (mm)	RMS σZ (mm)
0.04	0.04	0.19

Table 4.1 Reference frame co-ordinate accuracies

4.2.2 TARGET POLE CONSTRUCTION

Knowledge of camera position and orientation is required for all camera stations, a process which requires a combination of known control points and *tie* points as a means of extending the co-ordinate system from the reference control frame through the image sequence on the rock face to the second control frame. Tie points, in the form of circular, retro-reflective targets on telescopic target poles, are used to carry out the transfer of co-ordinates from one camera station to the next along the rock face. Figure 4.2 depicts the use of the target poles as a means of transferring co-ordinates from one image station to the next.

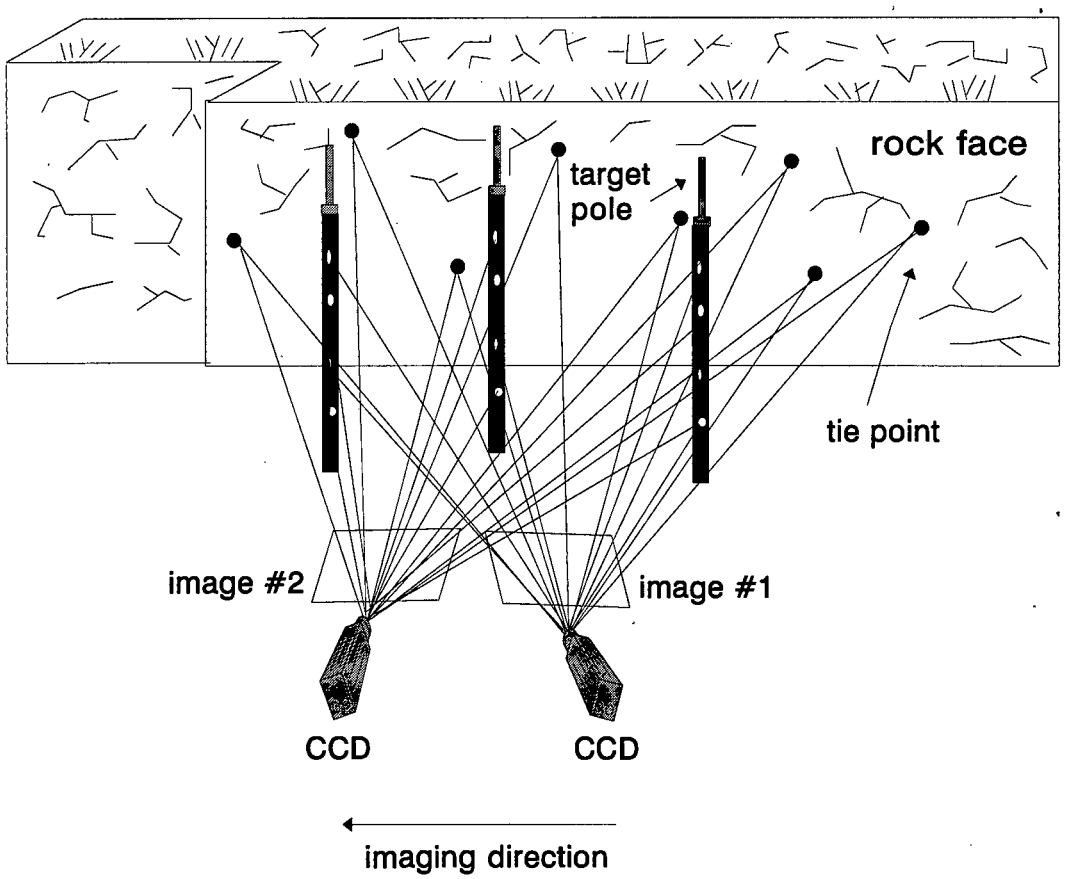

Figure 4.2 Target poles required for tie points between image sets

Although no exact positioning is possible, the target poles should be placed in accordance with the adopted network design, as far as possible.

For ease of use and portability, the target poles must be light. It was thus decided to construct them out of PVC tubing painted black to provide maximum contrast for the attached retro-reflective targets. The retro-reflective discs used to mark the target points on the poles vary in diameter between 8mm and 15mm, thus allowing for a means of distinguishing individual targets from one another. To allow for differing stope openings, i.e. the opening between the footwall and hangingwall, telescopic poles are required to enable successful positioning of the poles in the stope. Figure 4.3 shows the construction of the target poles used in underground mine experiments.

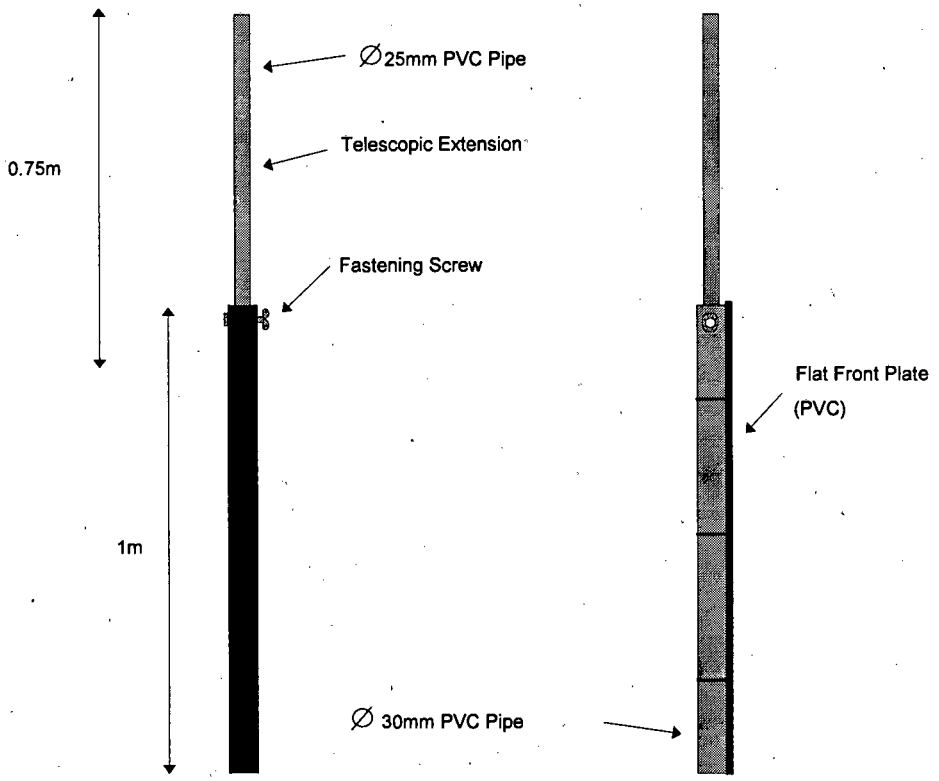

Figure 4.3 Target pole construction

4.3 IMAGE CAPTURE

Once in the stope, the reference co-ordinate system must be established and the camera prepared for use, before image capture may commence.

4.3.1 REFERENCE CO-ORDINATE SYSTEM

As previously described, the only structures in the stope capable of withstanding the pre-conditioning blast to within the required accuracy, are the wooden support packs located at the back of the stope opening. A suitable support pack, one at either end of the panel to be measured, must be selected as support structures for the two reference frames, which are used to define the local co-ordinate system in the stope.

The selection of suitable support packs should take into account the geometry of the stope and, in particular, access to suitable positions for image capture as required by the network of camera positions and control point locations previously described (see chapter 3). These support packs are the ones located closest to the manways or gulleys found at the ends of the panel to be surveyed.

Once suitable support packs have been identified, the reference frames must be securely attached with several nails driven through pre-drilled holes in the frame into the wooden beams, out of which the support pack are constructed.

4.3.2 CAMERA PREPARATION

As the environment in the stope is hot and humid, the camera equipment requires time to acclimatise. In order to reduce the risk of electrical shorting due to moisture, the camera must be loaded with a PCMCIA hard drive, for data storage, before entering the mine. Practical experience has shown that all of the equipment should be exposed

to the environment in the stope for at least half an hour before image capture to allow for the extremely high levels of humidity experienced in the stope. This is of particular importance for the lens which must be kept clean and free from condensation during image capture.

4.3.3 CONFIGURATION OF CONTROL AND CAMERA POSITIONS AND IMAGE CAPTURE

In order to achieve the required sub-millimetre accuracy for points on the rock face, a large number of redundant observations for each point are required. These redundant observations come about through multiple images, from different perspectives, of the same scene. While setting up the network of target poles and camera stations, an effort must be made to adhere to the network design proposed and tested in the pre-analysis (see chapter 3). In practise it must be noted that no fixed network design can be maintained. Ever changing stope conditions require that the network design be modified to suit present conditions, including hazardous sections in the stope, where for safety reasons, no physical contact with the rock face or overhead hangingwall may be made. Thus, image capture must be a flexible process relying not only on the adopted photogrammetric survey network, but on intuition gained from photogrammetric survey experience and underground testing. It is, however, essential to ensure that sufficient overlap between conjugate images is maintained (60% overlap or more is suggested). This is of particular importance in the region around the reference frames, where divergence in the imagery predominates.

Image capture commences with the reference frame at one extreme of the rock face to be measured, with imagery at two height levels and both conventional object facing and backward facing imagery being required. Once the image plane is parallel to the rock face, it is only required that object facing images at two height levels are captured, while maintaining sufficient lateral overlap between neighbouring image

sets. In closing on the second reference frame, at the end of the rock face to be measured, the use of object facing and forward facing imagery is once again required.

5 DATA PROCESSING

Once the images have been captured, both before and after the pre-conditioning blast events, they need to be processed in order to extract the relevant co-ordinates required for analysis. This includes camera calibration, the determination of camera positions in the stope co-ordinate system, as defined by one of the two reference frames, the extraction of relevant features on the rock face and the matching of those features in conjugate images to calculate their three dimensional (XYZ) object space co-ordinates. These data processing stages are outlined in the flowchart below:

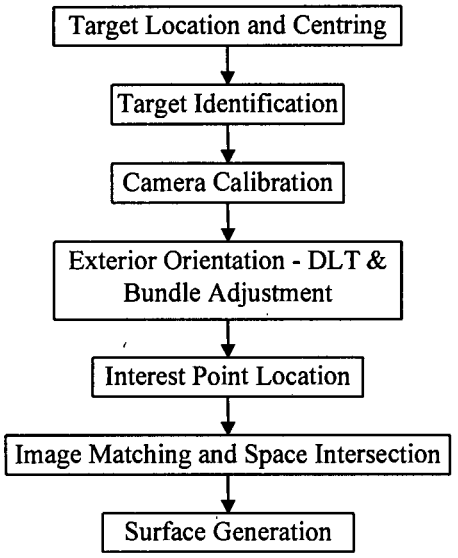

Figure 5.1 Flowchart of data processing

Before considering the data processing, it is important to define the relationship between object space and image co-ordinate systems as depicted in figure 5.2 below. The object space co-ordinate system is a left-handed 3D Cartesian co-ordinate system whose origin is defined by the co-ordinates of points on the reference frame, as determined earlier. The image co-ordinate system is a 3D right-handed Cartesian co-ordinate system with the x and y-axes being in the image plane and the z-axis being aligned towards the perspective centre (McGlone, 1989).

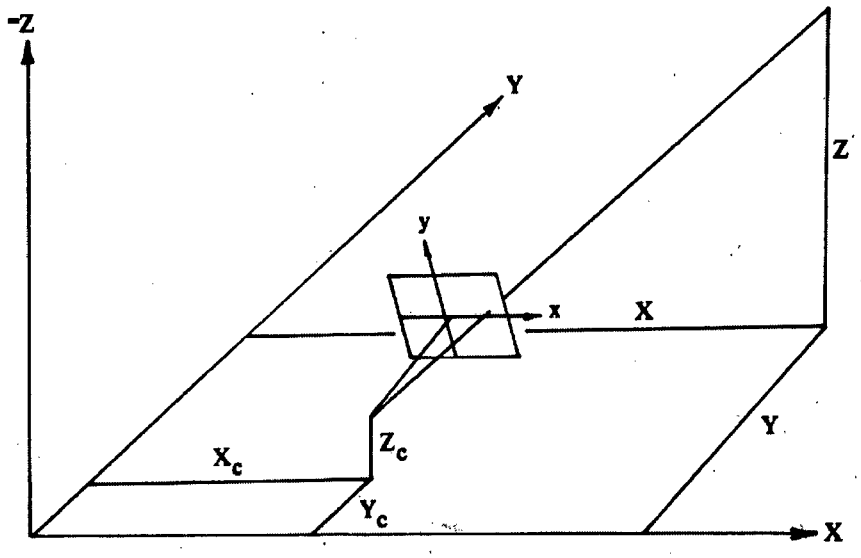

Figure 5.2 Object space (XYZ) and image (xy) co-ordinate systems

The angular relationship between the image and object space co-ordinate systems is described by a 3x3 orthogonal rotation matrix. One system is the definition of the orientation matrix by sequential rotations around the X, Y and Z axes, in that order.

$$R = R_{XYZ} = R_{\omega} R_{\kappa} R_{\phi} \tag{5.1}$$

or

$$R = \begin{bmatrix} r_{11} & r_{12} & r_{13} \\ r_{21} & r_{22} & r_{23} \\ r_{31} & r_{32} & r_{33} \end{bmatrix} \tag{5.2}$$

with

$$\begin{aligned} r_{11} &= \cos\kappa \cos\phi \\ r_{12} &= -\cos\kappa \sin\phi \\ r_{13} &= \sin\kappa \\ r_{21} &= \sin\omega \sin\kappa \cos\phi + \cos\omega \sin\phi \\ r_{22} &= \cos\omega \cos\phi - \sin\omega \sin\kappa \sin\phi \\ r_{23} &= -\sin\omega \cos\kappa \\ r_{31} &= \sin\omega \sin\phi - \cos\omega \sin\kappa \cos\phi \\ r_{32} &= \cos\omega \sin\kappa \sin\phi + \sin\omega \cos\phi \\ r_{33} &= \cos\omega \cos\kappa \end{aligned} \tag{5.3}$$

This angular relationship is applied in the collinearity equations (see 5.3.1) when formulating the relationship between image space to object space, through the imaging process.

Another consideration in working with digital images is the pixel format of this image data. Image measurements are often expressed in terms of pixels or fractions thereof, however, all of the equations relating to the geometry of image and object space, co-ordinates are required in metric units and related to the perspective centre of the image plane. The relationship between *image* and *pixel* co-ordinate systems is depicted in figure 5.3 below.

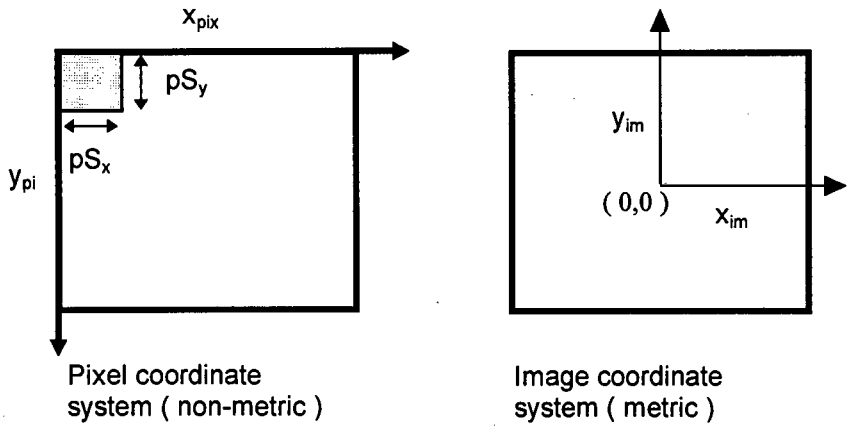

Figure 5.3 Image and pixel co-ordinate systems

Due to metric units being required for the geometric calculations relating image space to object space, we need to be able to transform between pixel co-ordinates and metric image co-ordinates. The conversion from *pixel* to *image* co-ordinates is given in equations (5.4) below.

$$x_{im} = \left[x_{pix} - \frac{(num_x - 1)}{2} \right] pS_x$$
$$y_{im} = \left[\frac{(num_y - 1)}{2} - y_{pix} \right] pS_y \qquad \textbf{(5.4)}$$

where, x_{im}, y_{im} are the image co-ordinates of the point,

x_{pix}, y_{pix} the pixel co-ordinates of the point,

num_x the number of horizontal pixels in the image,

num_y the number of vertical pixels in the image, and

pS_x, pS_y the pixel cell sizes in the x and y directions.

It must be noted that different conventions are used in the pixel co-ordinate system. The origin of the co-ordinate system varies from (0,0) to (0.5,0.5) and (1,1) for the centre of the top-left pixel. All of the algorithms programmed during this research use the origin of the pixel co-ordinate system as (0,0) for the centre of the top-left pixel.

5.1 TARGET LOCATION, CENTRING AND IDENTIFICATION

The retro-reflective targets used to provide the co-ordinate control need to be located in the images before they can be used as observations in the adjustment calculations for interior and exterior orientation determination.

As the targets consist of white circles on a black background, they may be easily located by a thresholding process, which separates the targets from the background, in the image. The centres of these circles may then be calculated by a simple *weighted centre of gravity* calculation, using the pixel grey levels, in a window around the target (as defined by thresholding), as a weight. Such an area based centring routine is commonly used, as reported in Trinder (1989), Xue (1992) and van der Vlugt (1995) and is recommended by van der Vlugt as being one of the most efficient and accurate techniques.

The algorithm is formulated for a white target on a black background (an alternative formulation is required for the reverse situation), with equations (5.5) and (5.6) being derived from moments:

$$x_0 = \frac{\sum_{i=1}^{n}\sum_{j=1}^{m} g_{ij} x_i}{\sum_{i=1}^{n}\sum_{j=1}^{m} g_{ij}} \tag{5.5}$$

$$y_0 = \frac{\sum_{i=1}^{n}\sum_{j=1}^{m} g_{ij} y_j}{\sum_{i=1}^{n}\sum_{j=1}^{m} g_{ij}} \tag{5.6}$$

where g_{ij} is the grey value located in row i and column j of the digital image.

Once the target centres have been located, they need to be identified; i.e. association of targets with corresponding numbers in the control co-ordinate list. This semi-automated process, as described by van der Vlugt (1995), requires the manual identification of an initial eight targets, after which an automated identification process relying on a direct linear transformation (DLT) resection calculation locates the remaining control co-ordinates.

After locating all of the known target points in the image, the provisional exterior orientation parameters are calculated in a DLT resection using all of the identified target points. This is necessary to provide good provisional values to the least squares bundle adjustment, which follows. Additional target points, the tie points, which are not yet co-ordinated, must then be manually identified and their provisional co-ordinates calculated using a DLT intersection algorithm.

5.2 CAMERA CALIBRATION

Throughout the process of image capture, the camera must remain at a fixed focal length. This is vital to the analysis of the image data after image capture, as no in situ camera calibration can be carried out in the mine, due to the lack of suitable reference control points within the stope.

The determination of the interior orientation parameters is treated here as a separate process after image capture in the stope. The camera is focused at the rock face, before image capture, and the focusing ring is taped fast onto the lens body to prevent movement during transport and image capture. Images for camera calibration are subsequently captured using a laboratory control field with highly accurate targets.

In camera calibration it is typical to employ the bundle adjustment to solve for the geometric parameters of the camera (principal distance "*c*" and principal point co-ordinates "x_p, y_p") seen in figure 5.4. It is also necessary to solve for some of the systematic errors present in the measurement system. Typically included are parameters for *radial lens distortion*, *decentering distortion*, *focal plane unflatness* and *focal plane distortion*.

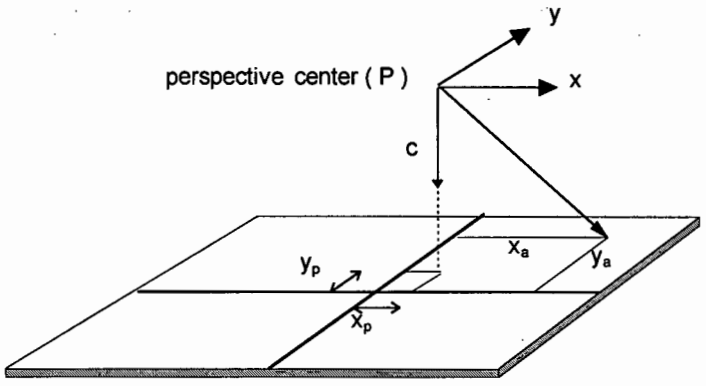

Figure 5.4 Interior orientation elements, with a positive image plane

5.2.1 RADIAL LENS DISTORTION

Symmetric radial lens distortion in analytical photogrammetry is commonly represented as a polynomial series of odd powered terms, as a consequence of the nature of Seidel aberrations (Fraser, 1992a):

$$dr = k_1 r + k_2 r^5 + k_3 r^7 + ... \tag{5.7}$$

where, k_i are termed the coefficients of radial lens distortion, and

r the radial distance from the principal point, i.e.

$$r^2 = (x - x_p)^2 + (y - y_p)^2 = \bar{x}^2 + \bar{y}^2 \tag{5.8}$$

where, x, y are image co-ordinates of the interest point, and

x_p, y_p the principal point co-ordinates.

From eqn. (5.7) the necessary radial distortion corrections for the x and y image co-ordinates follow as

$$\begin{aligned} dx_r &= (k_1 r^3 + k_2 r^5 + k_3 r^7 + ...)\bar{x} \\ dy_r &= (k_1 r^3 + k_2 r^5 + k_3 r^7 + ...)\bar{y} \end{aligned} \tag{5.9}$$

For the majority of normal-angle, non-photogrammetric lenses employed in today's metric and non-metric close-range cameras, the third-order term (k_1) is sufficient to account for the distortions. According to Fryer (1986), telephoto or "zoom" lenses exhibit a low degree of radial lens distortion, and it was found that for a 35-70mm Canon FD zoom lens that the k_3 term is insignificant. For wide-angle lenses, higher order terms (rarely above the seventh-order) are often required to adequately model radial lens distortions. As the image area captured by the DCS420 occupies the centre of the area covered by 35mm film, for which the lens system is designed, only the

third-order term (k_1) is required for lens distortion calculation, even though the 14mm lens used has substantial distortion at its extremities.

The distortion profile "*dr*" associated with a particular principal distance value "*c*", is termed the *Gaussian distortion profile* (Fraser, 1992a). The Gaussian profile of radial lens distortion is shown in figure 5.5 below for the 14mm lens used with the Kodak DCS420 digital camera:

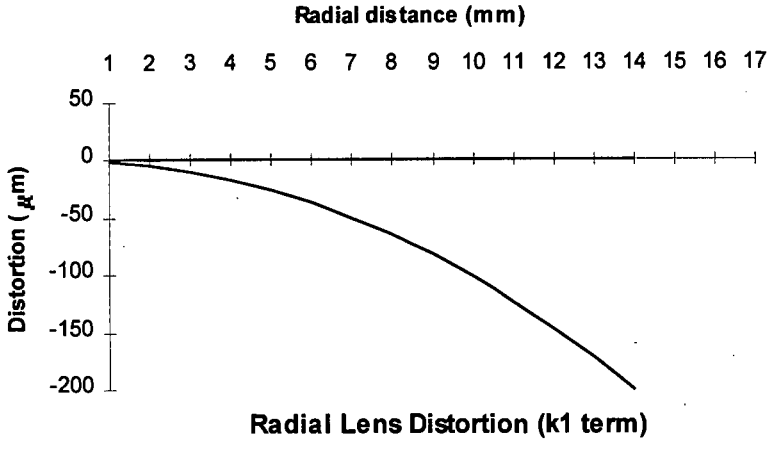

Figure 5.5 Radial Lens Distortion Profile

5.2.2 DECENTERING DISTORTION

Decentering distortion is caused by the misalignment of the elements of the lens system (Fryer, 1988) and has a metric impact on analytical restitution. The misalignment of lens components causes both radial and tangential image displacements (Fraser, 1992a). The distortions resulting from this misalignment can be modelled by correction equations, as given by Brown (1966):

$$\begin{aligned} dx_d &= P_1(r^2 + 2\bar{x}^2) + 2P_2\bar{x}\bar{y} \\ dy_d &= P_2(r^2 + 2\bar{y}^2) + 2P_1\bar{x}\bar{y} \end{aligned} \qquad \textbf{(5.10)}$$

Most high "quality" lenses exhibit a low degree of decentering distortion, typically not exceeding a few tens of micrometers at the extremities of the image format, and often much less (Fraser, 1992a). Decentering distortion also varies with focus (Fryer and Brown, 1986), as does radial lens distortion, but the resulting image co-ordinate deformations are typically small and their effect is ignored in most photogrammetric applications (Fraser, 1992a).

Although it is not obvious from eqn's. (5.10), the terms of decentering distortion, P_1 and P_2, exhibit a high degree of projective correlation with the principal point offsets x_p and y_p. This has the practical consequence that to a large degree, the effect of decentering distortion can be taken up by a shift in the principal point position. This projective compensation may have the effect that calibration indicates a lens that is free from decentering distortion (Fraser, 1992a).

5.2.3 FOCAL PLANE UNFLATNESS

A major limiting factor in the obtainable accuracy of photogrammetric triangulation is the influence of symmetric image co-ordinate errors as a result of focal plane (or film) unflatness. This is especially the case with non-metric cameras, as are commonly used in close range digital photogrammetry. Wide angle lenses exhibit a higher degree of "out-of-plane" deformation than long focal length, narrow lenses (Fraser, 1992a).

Most CCD arrays exhibit a high degree of planarity, resulting in small deviations as a consequence of unflatness of the imaging sensor. A practical consideration, however, is that for "video" CCD cameras, the CCD chip should be allowed adequate time to reach a working temperature, before image capture proceeds. About 15 minutes has proved sufficient to allow the CCD chip to obtain its "working" temperature, thereby preventing untimely "bowing" or "popping" of the focal plane during image capture. As the Kodak DCS range of digital cameras capture images by means of a traditional SLR camera mechanism, no variation in planarity occurs as the CCD chip operates from ambient temperature and image capture is in short bursts.

5.2.4 FOCAL PLANE DISTORTION

Focal plane distortion differs from focal plane unflatness in that it takes place within the plane of the image. In film-cameras, in-plane distortion can arise from the processing and subsequent storage of the film (Fraser, 1992a). With CCD arrays, the high integrity of the pixel elements would normally guarantee that distortion is not a problem, and indeed it appears not to be for digital "still" cameras (such as the Kodak DCS range of digital cameras). Distortions do, however, arise with analogue "video" CCD cameras, where A/D conversion takes place in a frame grabber, external to the camera. Pixel clock non-synchronisation and poor video transmission result in line jitter and non-linearities within the scale of the horizontal or x-axis of the image (Fraser, 1992a).

These distortions can be sufficiently modelled with the introduction of a scale factor "S_x" along the x-axis of the image, and a shear factor "a" for pixel irregularities (rarely used with modern CCD arrays) after van der Vlugt (1995).

$$\begin{aligned} dx_f &= \bar{y}a + \bar{x}S_x \\ dy_f &= \bar{x}a \end{aligned} \qquad \textbf{(5.11)}$$

Although focal plane distortions were not considered when capturing images with the Kodak DCS420 digital camera, for the development of this project, they must still be taken into account when using the lower cost "video" CCD image capture system, which employs external A/D conversion.

5.2.5 PRACTICAL CONSIDERATIONS OF CAMERA CALIBRATION

Practical camera calibration tests, using an object space control field of known ("fixed") XYZ co-ordinates, provided highly accurate results for the interior orientation parameters of the cameras being calibrated for this project. Figures 5.6 and 5.7 show the camera positions adopted for calibration and the object space control field points respectively. Nine images were captured at three different height levels and three different horizontal positions, as can be seen in figure 5.6. The control field in all cases should occupy the maximum extent of the image frame, so as to adequately model distortions at the edges of the image, where their effect is most pronounced.

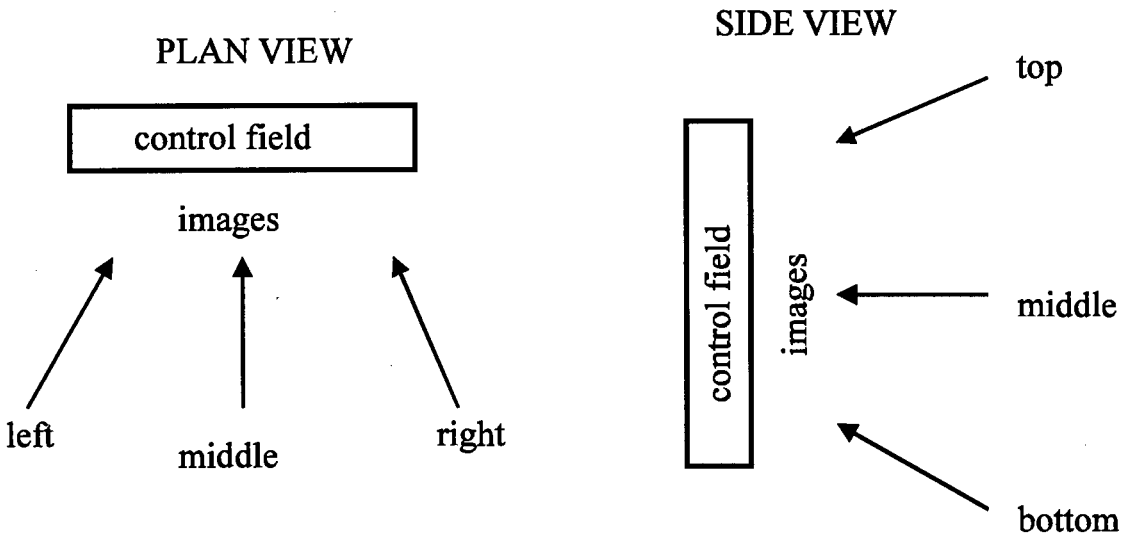

Figure 5.6 Adopted camera positions for calibration

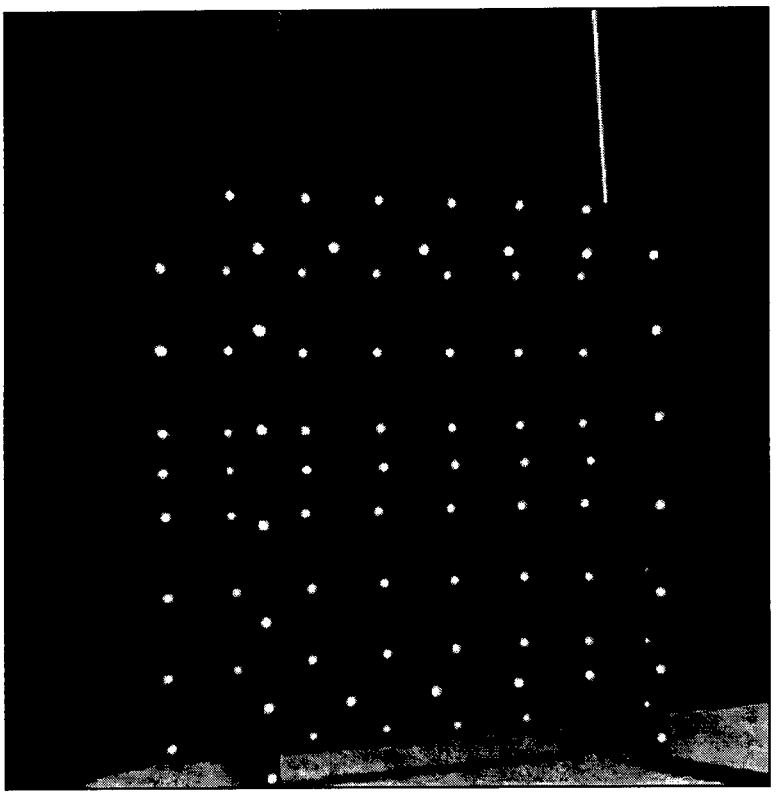

Figure 5.7 Control field for calibration

In order to fill the maximum extent of the image with control points, one often is not at the most appropriate focal setting, as the focal length is pre-set for image capture in the stope. This does not, however, pose a problem, as the calculated (weighted centre-of-gravity) target centres (see section 5.1) will remain the same, even with slightly blurred images.

As previously mentioned, before commencing with image capture, the focusing ring of the lens (for non-metric cameras) must be taped down. For this reason, it is often more practical to calibrate the camera at the end of the photogrammetric survey, as the focal length will then be fixed to the position most appropriate for project conditions. One must bear in mind that the calibration parameters are determined under present stope conditions will not be valid for different conditions. Changes in focusing and aperture setting may change the values of the additional parameters (Beyer, 1990).

Some general characteristics of test-range calibration, after Fraser (1992a), that are pertinent to close-range photogrammetric networks are as follows:

- Due to projective coupling of interior orientation parameters with the exterior orientation parameters, it is essential that the control point field used for calibration be well distributed in three dimensions. This will allow for the recovery of the interior orientation elements x_p, y_p and c with less influence from the exterior orientation parameters.

- The inclusion of camera stations with varying image scales (without changing the focal setting) and multiple camera roll angles greatly enhances the determinability of x_p, y_p and c by decreasing their correlation with the exterior orientation parameters.

- As was previously mentioned, the first term of radial lens distortion k_1 should account for radial deformations in most commonly used non-photogrammetric lenses.

- "The decentering distortion parameters P_1 and P_2 typically exhibit a high degree of projective coupling with both x_p and y_p, and the elements of exterior orientation. The use of multiple camera stations and a diversity of camera roll angles enhance the determinability of these parameters" (Fraser, 1992a). The high correlation between P_1, P_2 and x_p, y_p can be expected to remain even when such measures are taken.

- With a high density of image points there will be better determination of the calibration parameters. This statement applies to all terms of interior orientation, but is most pertinent to scale ratio S_x, shear term a and the parameters of radial and decentering distortion.

5.3 EXTERIOR ORIENTATION

Before features on the rock surface can be measured, it is necessary to determine the location and orientation of the camera set-ups in object space, as defined by the reference frame co-ordinate system. This process of *exterior orientation*, requires the location and centring of the circular, retro-reflective targets in the image; identification of these targets as previously described; direct linear transformation (DLT) resection, to determine provisional exterior orientation for the camera set-up; and finally a bundle adjustment of the entire photogrammetric survey network. Each of these stages will be investigated in turn.

5.3.1 THE COLLINEARITY EQUATIONS

Having described the object and image space co-ordinate systems, and the angular relationship between them (see figure 5.2), we can now describe the imaging process (McGlone, 1989). The image vector, a, expressed in the image co-ordinate system, is

$$a = \begin{bmatrix} x - x_p \\ y - y_p \\ c \end{bmatrix} \tag{5.12}$$

where, x, y are the *image* co-ordinates of the interest point,

x_p, y_p the principal point co-ordinates, and

c the principal distance.

The vector, A, from the perspective centre to the interest point, expressed in the object space co-ordinate system, is

$$A = \begin{bmatrix} X - X_c \\ Y - Y_c \\ Z - Z_c \end{bmatrix} \tag{5.13}$$

where, X, Y, Z are the *object space* co-ordinates of the interest point, and

X_C, Y_C, Z_C the *object space* co-ordinates of the perspective centre.

The imaging process requires that the image and object rays are collinear, thus we multiply the object space vector by the rotation matrix, R, to bring it into the same co-ordinate system. An unknown scale factor, k, is then included, giving

$$a = kRA$$

$$\begin{bmatrix} x - x_p \\ y - y_p \\ c \end{bmatrix} = kR \begin{bmatrix} X - X_c \\ Y - Y_c \\ Z - Z_c \end{bmatrix} \tag{5.14}$$

This produces three equations that describe the relationship between object and image co-ordinate systems. Since the scale factor, k, is of no interest in itself, dividing the 1st and 2nd equations by the 3rd and rearranging to yield an explicit form can eliminate it. Including distortion parameters as applied (opposed to the theoretical formulation given earlier), this leads to the most commonly used form of the *collinearity equations*:

$$x = x_p - dx + c\frac{r_{11}(X - X_c) + r_{12}(Y - Y_c) + r_{13}(Z - Z_c)}{r_{31}(X - X_c) + r_{32}(Y - Y_c) + r_{33}(Z - Z_c)}$$

$$y = y_p - dy + c\frac{r_{21}(X - X_c) + r_{22}(Y - Y_c) + r_{23}(Z - Z_c)}{r_{31}(X - X_c) + r_{32}(Y - Y_c) + r_{33}(Z - Z_c)} \tag{5.15}$$

where, x, y are *image* co-ordinates of the interest point,

x_p, y_p principal point co-ordinates,

dx, dy distortion parameters,

c the principal distance,

X, Y, Z the *object space* co-ordinates of the interest point,

X_c, Y_c, Z_c the perspective centre co-ordinates, and

$r_{11}...r_{33}$ the rotation matrix elements.

and

$$dx = \bar{x}k_1r^2 + P_1(r^2 + 2\bar{x}^2) + 2P_2\bar{x}\bar{y}$$
$$dy = \bar{y}k_1r^2 + 2P_1\bar{x}\bar{y} + P_2(r^2 + 2\bar{y}^2) \quad \textbf{(5.16)}$$

where, k_1 is the first term of radial lens distortion, and

P_1, P_2 terms of decentering distortion.

and

$$\bar{x} = x - x_p$$
$$\bar{y} = y - y_p \quad \textbf{(5.17)}$$
$$r = \sqrt{\bar{x}^2 + \bar{y}^2}$$

5.3.2 DIRECT LINEAR TRANSFORMATION

One formulation of the analytical orientation problem, of relating the object space co-ordinate system to the image co-ordinate system, is the Direct Linear Transformation, or DLT, as originally proposed by Abdel-Aziz and Karara (1971). The main advantage of this method is that it can be solved without the need for initial

approximations for the parameters. After algebraic manipulation of the collinearity equations (5.15), the following formulation can be obtained

$$x - dx = \frac{L_1 X + L_2 Y + L_3 Z + L_4}{L_9 X + L_{10} Y + L_{11} + 1}$$
$$y - dy = \frac{L_5 X + L_6 Y + L_7 Z + L_8}{L_9 X + L_{10} Y + L_{11} + 1} \quad \textbf{(5.18)}$$

where, x, y are the *image* co-ordinates of the interest point, and
dx, dy the distortion parameters,

with the DLT parameters

$$\begin{aligned}
L_1 &= (x_p r_{31} - c r_{11})/L \\
L_2 &= (x_p r_{32} - c r_{12})/L \\
L_3 &= (x_p r_{33} - c r_{13})/L \\
L_4 &= x_p + c(r_{11} X_c + r_{12} Y_c + r_{13} Z_c)/L \\
L_5 &= (y_p r_{31} - c r_{21})/L \\
L_6 &= (y_p r_{32} - c r_{22})/L \\
L_7 &= (y_p r_{33} - c r_{23})/L \\
L_8 &= y_p + c(r_{21} X_c + r_{22} Y_c + r_{23} Z_c)/L \\
L_9 &= r_{31}/L \\
L_{10} &= r_{32}/L \\
L_{11} &= r_{33}/L \\
L &= -(r_{31} X_c + r_{32} Y_c + r_{33} Z_c)
\end{aligned} \quad \textbf{(5.19)}$$

where, x_p, y_p are the principal point co-ordinates,
c the principal distance,
X_C, Y_C, Z_C the perspective centre co-ordinates, and
$r_{11} \ldots r_{33}$ the rotation matrix elements.

Either a direct method or an iterative one can solve for the resulting equations.

These 11 DLT parameters can be interpreted in terms of the interior and exterior orientation parameters. The camera parameters are defined according to the following algebraic solution, according to McGlone (1989):

$$
\begin{aligned}
\lambda &= -1/\sqrt{(L_9^2 + L_{10}^2 + L_{11}^2)} \\
x_p &= (L_1 * L_9 + L_2 * L_{10} + L_3 * L_{11})\lambda^2 \\
y_p &= (L_5 * L_9 + L_6 * L_{10} + L_7 * L_{11})\lambda^2 \\
c_x &= \sqrt{\left[(L_1^2 + L_2^2 + L_3^2)\lambda^2 - x_p^2\right]} \\
c_y &= \sqrt{\left[(L_5^2 + L_6^2 + L_7^2)\lambda^2 - y_p^2\right]} \\
c &= (c_x + c_y)^2 \\
\phi &= \sin^{-1}(L_9 * \lambda) \\
\omega &= \tan^{-1}(-L_{10} / L_{11}) \\
r_{11} &= \lambda\,(x_p * L_9 - L_1) / c_x \\
\kappa &= \cos^{-1}(r_{11}) / \cos\phi
\end{aligned}
\qquad \textbf{(5.20)}
$$

and

$$
\begin{bmatrix} X_c \\ Y_c \\ Z_c \end{bmatrix} = \begin{bmatrix} L_1 & L_2 & L_3 \\ L_5 & L_6 & L_7 \\ L_9 & L_{10} & L_{11} \end{bmatrix}^{-1} \begin{bmatrix} L_4 \\ L_8 \\ 1 \end{bmatrix} \qquad \textbf{(5.21)}
$$

where,

c_x and c_y are the principal distances in the x and y image directions.

5.3.3 BUNDLE ADJUSTMENT

In an alternative solution to the exterior orientation problem, the collinearity equations can be written for each image point, in all of the images captured, and the equations

combined into a simultaneous solution for the unknown parameters. This is referred to as the *bundle adjustment*, after Brown (1958).

The observation equations for a least squares bundle adjustment may be obtained by linearising the collinearity equations (5.15) through a Taylor's series expansion (Brown, 1958, van der Vlugt, 1995). The observation equations then form part of a standard parametric least squares formulation:

$$v = Ax - l \tag{5.22}$$

where the corrections to the parameters can be computed from

$$x = N^{-1}c \tag{5.23}$$

in which N is the normal equation matrix given by

$$N = A^T PA \tag{5.24}$$

and

$$c = A^T Pl \tag{5.25}$$

where, A is the design matrix containing the coefficients of the unknowns,

P is the weight matrix,

l is the discrepancy vector,

v is the residual vector, and

x is the solution vector.

5.3.4 PRACTICAL CONSIDERATIONS IN DETERMINING EXTERIOR ORIENTATION IN THE STOPE

In calculating the exterior orientation of the camera positions in the stope conditions, it is advisable to hold the interior orientation parameters of the camera fixed in the adjustment, these parameters having being separately determined in a camera calibration, as previously described (see section 5.2). No self-calibration is possible, due to a lack of suitable reference control points in the stope.

The field of co-ordinate control points must fill the maximum extent of the surface to be measured and ideally should contain variation in depth. At least six control points are required in each image to obtain a unique solution for the DLT calculation. These points should be well distributed throughout the image, i.e. they should not all occupy one region of the image area covered (which may result in numerical instability in the adjustment). It is not essential, however, to have control points spread throughout the stope. Well defined control points at the beginning and end of the surface to be measured will suffice, with "tie" points being used for intermediate images, see figure 5.8 below. These "tie" points should be well defined in all of the images; ideally targets should be used to mark these points on the rock surface (e.g. circular retro-reflective targets) as well as on intermediate target poles placed in front of the rock face.

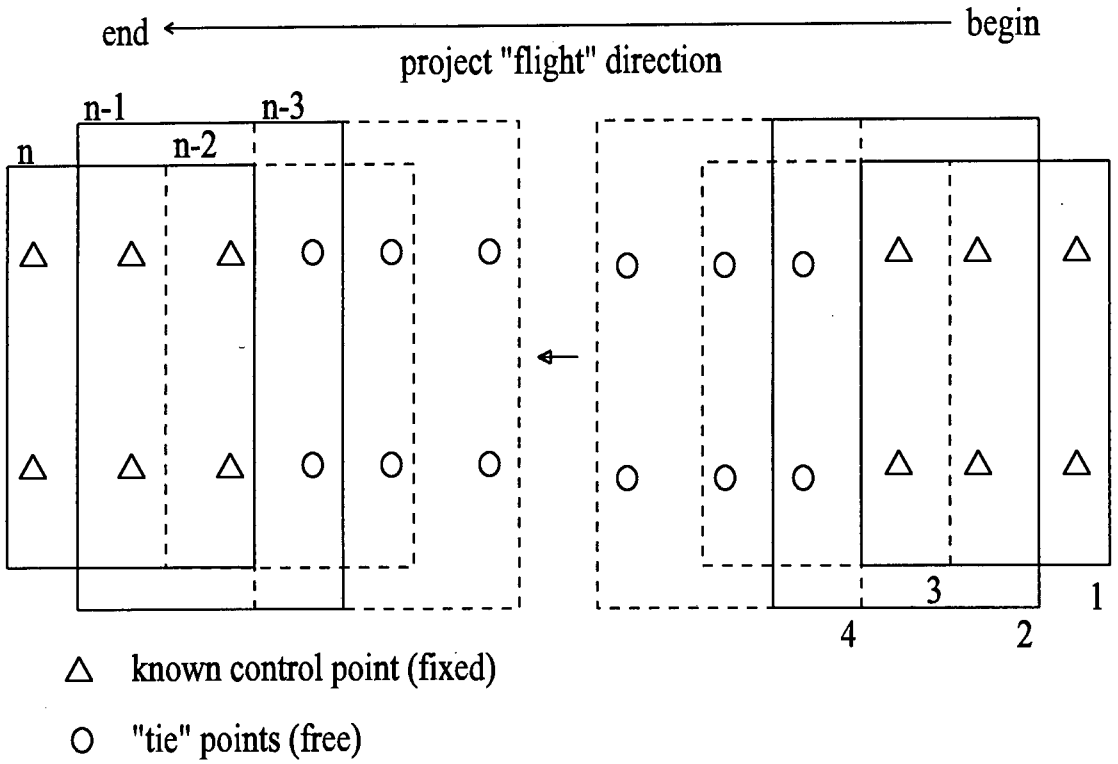

Figure 5.8 Control points and "tie" points

In underground mine tests carried out by the author, the calculation of exterior orientation parameters has been approached as a two stage "*folding-out*, *folding-in*" process (Smit, 1996), as depicted in figure 5.9 below:

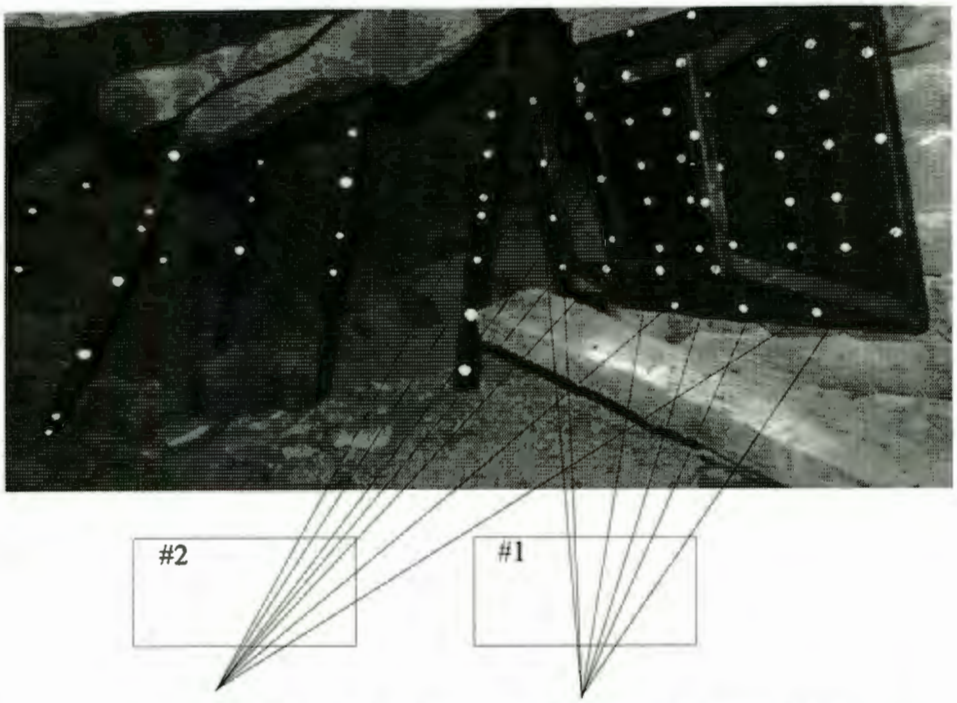

Figure 5.9 Folding-out, folding-in process

Firstly, the 11 DLT parameters are calculated in a DLT *resection*, using the initial few images containing "known" control points (for example images 1, 2 and 3 in figure 5.8, above). In the second stage, the object space co-ordinates of "tie" points visible in the same images are calculated in a DLT *intersection* algorithm (for example the "tie"

points visible in both images 2 and 3 in figure 5.8). This process is continued for all of the images captures, using the calculated "tie" points as control for the next set of images. Ending on a field of "known" control points completes the project. In practice, however, it proved necessary at this preparatory stage to carry out sub-block bundle adjustments due to excessive error propagation.

Finally, a bundle adjustment of the entire project is carried out. This is done as a "constrained" network adjustment, with the calibrated interior orientation parameters and the co-ordinates of the "known" control points on the first frame held fixed. The bundle adjustment produces highly accurate object space co-ordinates for the *unknown* "tie" points and calculates the desired exterior orientation parameters of the camera stations, in one simultaneous calculation.

5.4 FEATURE EXTRACTION

Points of interest on the rock face, represented by changes in texture in the images, are used to provide a dense distribution of features defining the surface of the rock face being surveyed. These points first need to be extracted from one image, in a stereo set, before they can be matched in conjugate images, to enable the calculation of their object space co-ordinates.

An even and dense distribution of points is required to accurately represent the surface being mapped. Various interest operators for the extraction of the points of interest are available, providing both single pixel and sub-pixel levels of point location. The selection of an appropriate interest operator is largely dependent on image characteristics, with factors such as resolution, image sharpness and homogeneity of the image texture being integral to the selection criteria.

During the course of this research, three commonly used interest operators were investigated, each with its own distinct characteristics, to provide a selection of

algorithms to meet all image requirements found in the underground mining environment. Each of the interest operators investigated will be described, followed by a discussion of the merits of each.

5.4.1 CANNY FILTER

Whenever a grey-level intensity change occurs, there will be a corresponding peak in the first directional derivative of intensity. In fact, we may define intensity change in this way, so that the task of detecting these changes can be reduced to finding the maxima of the first directional derivative of the grey-level intensity (Marr, 1980).

In deciding on the filter that is to be used, two considerations that must be taken into account. Firstly, the optimal filter should reduce the range of grey scales over which the intensity change takes place. The filter's spectrum should therefore be smooth and roughly band-limited in the frequency domain. Secondly, a high degree of spatial localisation in detecting the edge is required. Thus, the edge location should be calculated from a smooth average of nearby points, rather than any kind of average from widely scattered points (Marr, 1980). The one function that provides an optimal trade-off, between the conflicting requirements of the frequency and spatial domains, is the *Gaussian* function. This is used as the basis for an interest operator developed by Canny (1986).

Thus, as described by Canny (1986) we seek the maxima in

$$f(x,y) = D^1[G(r) * I(x,y)] \qquad \textbf{(5.26)}$$

where, $I(x,y)$ is the image,

$*$ the convolution operator, and

$G(r)$ the *Gaussian* operator.

By the derivative rule for convolutions,

$$f(x,y) = D^1G * I(x,y) \tag{5.27}$$

We can write the operator D^1G as G', giving the operator and its first derivative in one dimension,

$$G(x) = \frac{x}{\sigma\sqrt{2\pi}} e^{\frac{-x^2}{2\sigma^2}}$$
$$G'(x) = \frac{-x}{\sigma^2} G(x) \tag{5.28}$$

where, σ the shaping parameters of the *Gaussian* function, and

x the one dimensional pixel location.

The function $G(x)$ and its first derivative $G'(x)$ is seen in figure 5.10 below.

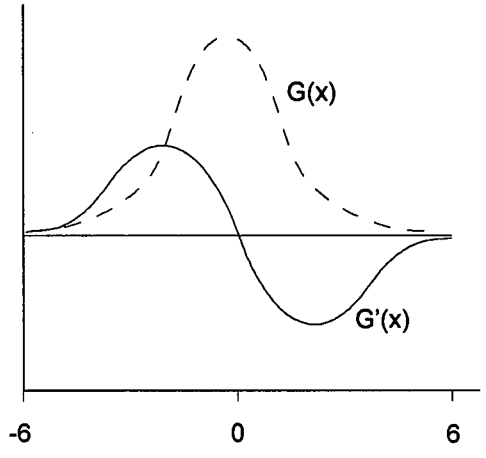

Figure 5.10 The first derivative of the Gaussian function

Depending on the magnitude of the shaping parameter, σ, the size of the kernel sampled from equation (5.28) will vary. The size of the kernel being calculated as the next odd number above $3 * 2\sqrt{2} * \sigma$; an increase in σ will result in an increase in the

size of the kernel, with the discrete values contained within the kernel being sampled from the continuous function *G'(x)* at different positions. As the size of σ is increased so the amount of *Gaussian* smoothing, an integral part of the *Canny* filter due to its *Gaussian* origin, is increased (van der Merwe, 1995). This will have an effect on the amount of edges located, with increased smoothing resulting in the loss of high frequency signal components, including a reduction in multiplicative noise (Ekstrom, 1984). For the purposes of the research carried out for this thesis, a σ value of 1.5 was chosen, corresponding to a kernel width of 13 pixels.

The discrete kernel is convolved with the image in both image directions. The resulting intensity profiles, of the edge gradients, are searched for maxima (and minima) which correspond to edge locations. The edge direction is then calculated by using the vector of the edge strengths at the point of the maxima, as depicted in figure 5.11 below.

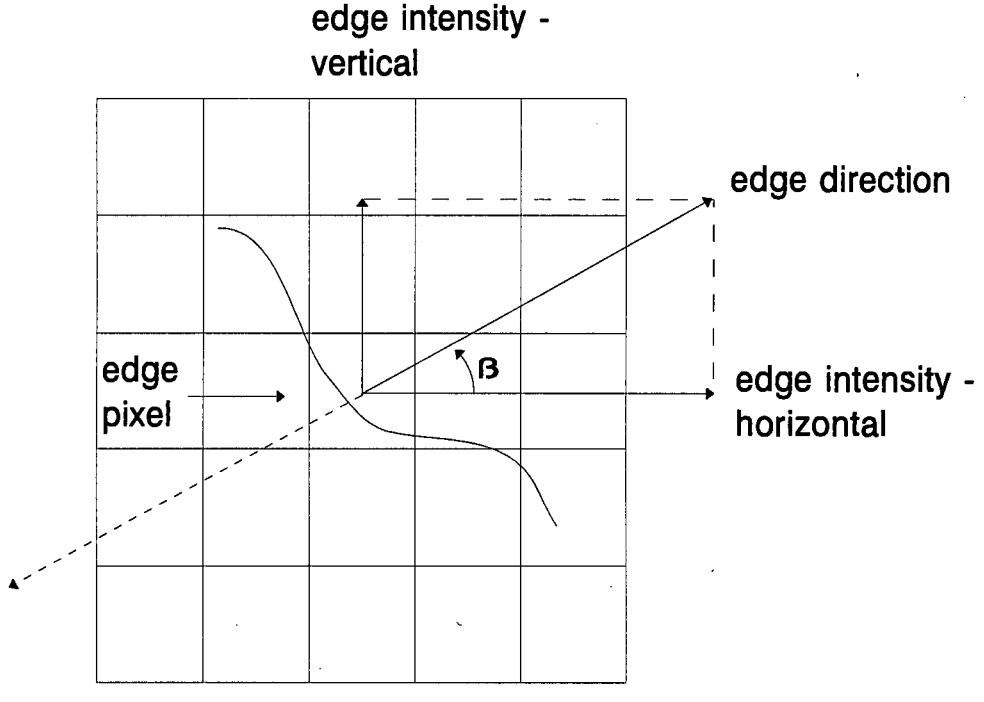

Figure 5.11 Edge direction based on the vector of the edge strengths

This provides edge locations to single pixel accuracy, with sub-pixel locations to be subsequently determined using the method of moment preserving (see 5.4.5 below).

5.4.2 SOBEL FILTER

Similar in concept to the *Canny* filter, the *Sobel* filter is more sensitive to noise. Using a 3x3 area to compute the gradient at the pixel of interest in two edge directions, the *Sobel* operator weights the pixels closest to the centre to provide smoothing, decreasing its sensitivity to noise in the image (Gonzalez, 1987). The operator, as described by Ekstrom (1984) and Gonzalez (1987) among others, takes the form

-1	0	1
-2	0	2
-1	0	1

-1	-2	-1
0	0	0
1	2	1

Figure 5.12 The masks used to calculate G_y' and G_x' at the interest point

for computing the pixel grey level gradients G_y' and G_x' at the centre point of a 3x3 region. Seen graphically in figure 5.13 below, the *Sobel* operator is convolved with the image to produce a gradient image in both horizontal and vertical image directions, where

$$f(x,y) = G' * I(x,y) \tag{5.29}$$

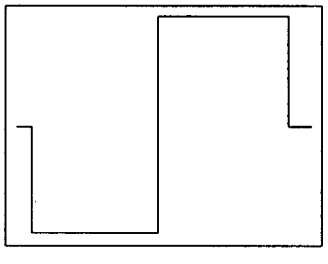

Figure 5.13 The Sobel operator

These gradient images' intensity profiles are searched for maxima (and minima) which correspond to the edge locations. Again, edge directions are obtained by calculating the edge vector derived from the horizontal and vertical edge intensity profiles at the point where the maxima occurs (see figure 5.11 above). Sub-pixel edge locations are once more determined using the method of preservation of moments (see 5.4.5 below).

5.4.3 MAXIMUM GRADIENT FILTER

In contrast to the previous two interest operators, the maximum gradient filter does not convolve a kernel with the image. The maximum gradient in a 3x3 neighbourhood around the interest pixel is located, as follows:

$$gradient = \frac{grey_j - grey_i}{2} \tag{5.30}$$

where, $i = 1, 2, 3, 4$ and

$j = 9, 8, 7, 6$

for the gradients calculated in four image directions as seen in figure 5.14.

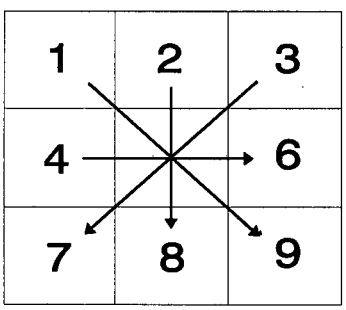

Figure 5.14 Gradient directions used

The direction in which the maximum gradient occurs is used as the edge direction, at the pixel of interest, for subsequent sub-pixel edge location, as described in section 5.4.5 below.

5.4.4 PRACTICAL CONSIDERATIONS IN INTEREST POINT DETECTION

In deciding which single pixel interest operator to use, the quality of the image (i.e. image sharpness) and the amount of edges desired must be taken into account. Where the image quality is poor it may be necessary to enhance the image with a high-pass filter to increase image sharpness before edge extraction.

Some practical aspects of the single pixel interest operators described above, are listed below:

- The *Canny* operator, due to its Gaussian origins, has the effect of low-pass filtering of the edge components of the image. This results in only the high-contrast edge components being detected with noise being filtered out as high frequency image information.

- The *Sobel* operator has little filtering effect and locates high frequency as well as low-frequency edges equally well. Hence the noise components of the image may also be shown as edge detail. As a consequence the *Sobel* filter locates more edges than the *Canny* filter, but also includes more non-edge detail.

- The maximum gradient edge operator essentially locates an edge at every pixel, some of these are weak and are removed in a user-defined thresholding process. This method of edge location produces the most number of edges and is often useful in modelling surfaces of little local contrast.

The computer programs coded for all of the interest operator algorithms allow the user to select an edge intensity threshold above which edge detail will be accepted, as depicted in figure 5.15. In selecting a threshold level, attention must be paid to maintaining a well distributed point cloud with which the surface is to be represented.

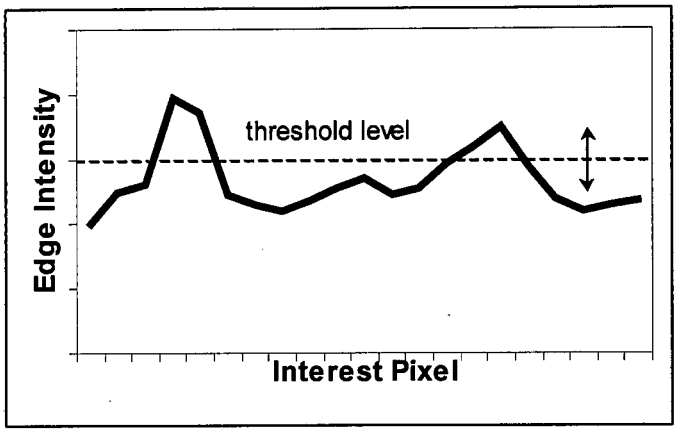

Figure 5.15 Edge intensity threshold

As the point density obtained using the interest operators discussed tends to be high in regions of high local contrast, it is necessary to thin the data before image matching. This is done by suppression of the local non-maxima by setting the edge gradient to zero at a local non-maxima (Förstner, 1987).

Here the size of the neighbourhood, within which the edge has to be a relative maxima, has to be specified. The smallest possible window size of 3 x 3 will yield selected windows whose centres are separated by at least one pixel. More thinning of the local non-maxima can be achieved by increasing the size of the window. For the purpose of interest point thinning of the rock face images, a 10 x 10 window was selected for local non-maxima suppression.

The filter operates by excluding interest points, on which the window is centred, which have lower edge intensity than other interest points contained within the window. Thus, if the gradient magnitude of the centre pixel compared to the gradient of any of its neighbouring pixels, contained within the defined window, is lower, then

the centre pixel gradient is set to zero and the window is moved to the next relative maxima (Föstner, 1987). This is done over the entire gradient image, thus only the points with the highest edge intensity will remain, providing a representative point cloud of the surface to be mapped.

The results of the interest operators are used as a basis for sub-pixel edge location using the, method of preservation of moments. A discussion of this technique follows.

5.4.5 SUB-PIXEL EDGE LOCATION BY THE METHOD OF MOMENT PRESERVING

The above three edge location methods are able to locate edges to single pixel accuracy as well as providing edge directions. The method of preservation of moments, as described by Tabatabai (1984) and Mikhail (1984), is subsequently used to locate the edge positions to sub-pixel accuracy.

A sample scan line across a step edge in the absence of noise is characterised by a set of grey values x_i's, i = 1, 2, ..., n, that are either monotonically non-decreasing or non-increasing. On the other hand, an ideal edge is a sequence of one brightness value h_1, followed by a sequence of another brightness value h_2 (see figure 5.16, below).

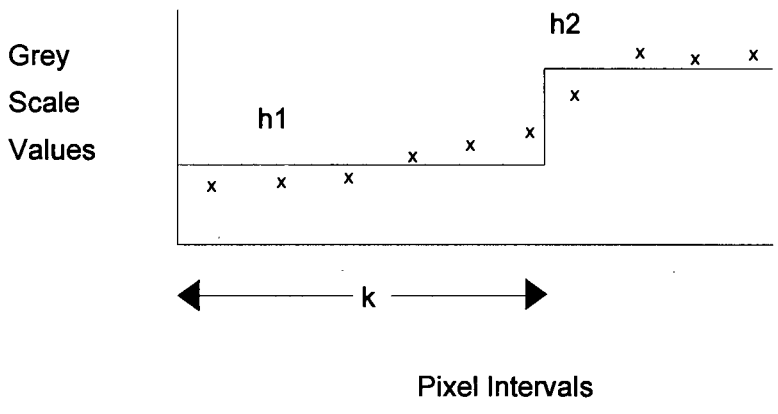

Figure 5.16 Ideal edge step

Here an operator is defined that, when applied to empirically obtained edge data, locates an ideal step edge, such that the first three sample moments of the input data sequence, defined as

$$\overline{m_i} = \frac{1}{n}\sum_{j=1}^{n} x^i{}_j \tag{5.31}$$

for $i = 1, 2, 3$ are preserved.

Letting k denote the number of h_1 values from the beginning of the sample to the ideal edge, there are three equations to solve for the unknowns h_1, h_2 and k (Davis, 1988):

$$\overline{m_1} = \frac{kh_1 + (n-k)h_2}{n} \tag{5.32}$$

$$\overline{m_2} = \frac{kh_1^2 + (n-k)h_2^2}{n} \tag{5.33}$$

$$\overline{m_3} = \frac{kh_1^3 + (n-k)h_2^3}{n} \tag{5.34}$$

The edge of the first pixel is located at $j = 1/2$ and subsequent pixels have a spacing of one. We are then able to obtain a sub-pixel measurement k of edge location. The solution is

$$k = \frac{1}{2}n\left(1 - \frac{c}{\sqrt{4+c^2}}\right) \tag{5.35}$$

where

$$c = \frac{3\overline{m_1}\,\overline{m_2} - 2\overline{m_1}^3 - \overline{m_3}}{\sigma^3} \tag{5.36}$$

and

$$\sigma = \sqrt{\overline{m_2} - \overline{m_1}^2} \tag{5.37}$$

$$h_1 = \overline{m_1} + \beta\sigma \tag{5.38}$$

$$h_2 = \overline{m_1} - \frac{\sigma}{\beta} \tag{5.39}$$

where

$$\beta = \sqrt{\frac{k}{n-k}} \tag{5.40}$$

Sub-pixel edge location using this method was employed in the location of the points of interest to represent the rock face being measured.

5.5 IMAGE MATCHING

The most time consuming and indeed complex of digital photogrammetric tasks is that of image matching. This is the process of locating corresponding points of interest in conjugate images for the purpose of three dimensional point position location in object space.

In order to minimise the need for extensive *a priori* knowledge of the points to be matched, the image matching process used follows two distinct, yet linked algorithms. Firstly, the use of epipolar geometry of the conjugate images and cross-correlation of the *reference* and *search* patches, in the *reference* and *target* images respectively, as described by Wong (1986), is employed to locate the initial approximation of the corresponding search position for the point of interest, as well as providing initial estimates for the affine transformation parameters between conjugate image patches. These approximations are then used in a least squares multi-image matching algorithm with imposed geometric constraints, in the form of the collinearity equations, as presented by Gruen and Baltsavias (1988).

5.5.1 EPIPOLAR GEOMETRY

In order to find corresponding points in conjugate images with no *a priori* knowledge of the *search* patch positions in the *target* images, *epipolar geometry* and cross-correlation are used to locate the initial match position of corresponding points in conjugate image scenes. Before considering its function in image matching, it is necessary to define the epipolar "line"; being the line of intersection between the image plane and the plane passing through the object point and the perspective centres of the two images. Figure 5.17 below shows the basic principle of epipolar geometry and the epipolar "line":

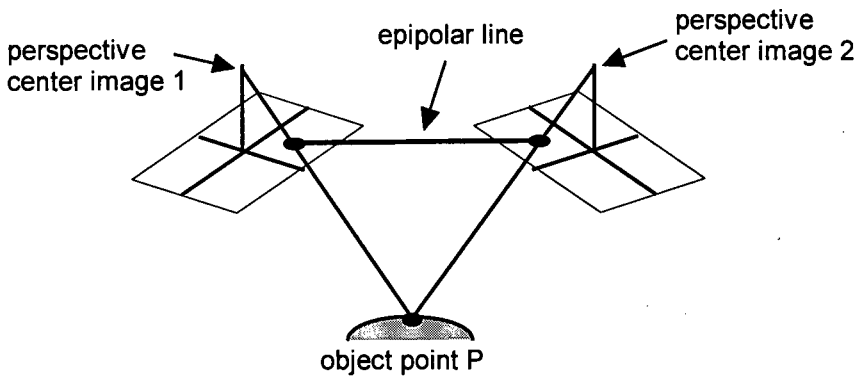

Figure 5.17 Epipolar geometry

From projective geometry the relationship between the *target* image and the object can be described in terms of the collinearity equations (5.15).

Pre-selecting Z-values at regular intervals within the constraint of the epipolar line makes it possible to evaluate a series of X and Y object space co-ordinates of candidates, potentially corresponding to the point of interest, as depicted in figure 5.18 below. Image distortions are taken into account in this computation.

In order to avoid over or under sampling, due to differing image scales and geometries, the point sample interval is chosen as a maximum step of 1 pixel in image

space (in the *target* images), with the Z-search range along the epipolar "line" being limited by prior estimation of the object depth. Interpretation of a single pixel interval in image space into a change in depth (Z) is given in equation (5.41) as provided by van der Vlugt (1995). This computation is updated after *search* patch sampling, in all of the *target* images, at each incremental step along Z-search range. The next depth increment ΔZ_{i+1}, computed after the ith sample is given by:

$$\Delta Z_{i+1} = \frac{\Delta Z \Delta s_0}{\Delta s_i} \tag{5.41}$$

where, ΔZ_i is the depth increment at sample i,

Δs_0 the required largest image step = 1,

Δs_i the largest image step amongst the search images at sample i.

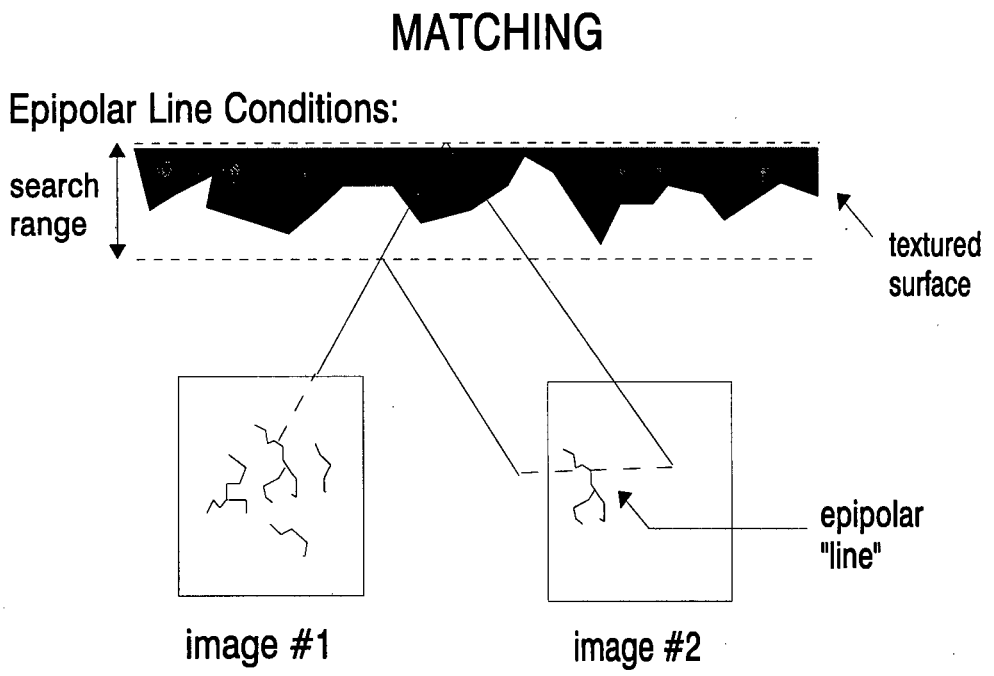

Figure 5.18 Multi-image correlation with epipolar line geometry

The X/Y co-ordinates are evaluated from the collinearity equations (5.15) in the form:

$$\begin{bmatrix} \Delta Xr_{31} - cr_{11} & \Delta Xr_{32} - cr_{12} \\ \Delta Yr_{31} - cr_{21} & \Delta Yr_{32} - cr_{22} \end{bmatrix} \begin{bmatrix} Y \\ Y \end{bmatrix} = \begin{bmatrix} RHS_1 \\ RHS_2 \end{bmatrix} \tag{5.42}$$

hence

$$\begin{bmatrix} X \\ Y \end{bmatrix} = \begin{bmatrix} \Delta Xr_{31} - cr_{11} & \Delta Xr_{32} - cr_{12} \\ \Delta Yr_{31} - cr_{21} & \Delta Yr_{32} - cr_{22} \end{bmatrix}^{-1} \begin{bmatrix} RHS_1 \\ RHS_2 \end{bmatrix} \tag{5.43}$$

where

$$\begin{aligned} \Delta X &= x - x_p + dx \\ \Delta Y &= y - y_p + dy \end{aligned} \tag{5.44}$$

and

$$\begin{aligned} RHS_1 = &-(\Delta Xr_{33} - cr_{13})Z + (\Delta Xr_{31} - cr_{11})X_c + \\ &+(\Delta Xr_{32} - cr_{12})Y_c + (\Delta Xr_{33} - cr_{13})Z_c \end{aligned} \tag{5.45}$$

$$\begin{aligned} RHS_2 = &-(\Delta Yr_{33} - cr_{23})Z + (\Delta Yr_{31} - cr_{21})X_c + \\ &+(\Delta Yr_{32} - cr_{22})Y_c + (\Delta Yr_{33} - cr_{23})Z_c \end{aligned} \tag{5.46}$$

In the next step, the image co-ordinates of the candidates in the conjugate *search* image(s) are calculated using the collinearity equations (5.15).

A patch surrounding the image position of each of the candidates along the epipolar line is used to determine the normalised cross-correlation (R_{XY}) between the *reference* image and the respective *target* image(s). This cross-correlation function is given by Wong (1986), with summation over all patch pixel:

$$R_{XY} = \frac{\sum (g_r - \overline{g_r})(g_s - \overline{g_s})}{\sqrt{\sum (g_r - \overline{g_r})^2} \sqrt{\sum (g_s - \overline{g_s})^2}} \tag{5.47}$$

where, g_r and g_t represent the grey-scale values on the *reference* and *search* patches respectively, and

$\overline{g_r}$ and $\overline{g_s}$ the average grey-scale values for the *reference* and *search* patches respectively.

This process is executed for the full extent of the Z (depth) search range obtaining cross-correlation values for all of the search images for each of the depth increments, i.

The maximum cross-correlation, i.e. the value closest to 1, is chosen as corresponding to the most likely match for the point of interest in the *target* image(s). This criteria for the selection of the correct match may not always produce the correct answer as the correct match may correspond to a local correlation maximum, instead of the absolute maximum. A number of factors may influence the cross-correlation results; as mentioned by van der Vlugt (1995), these include:

- the use of only two images,
- errors in the camera parameters,
- unmodelled or inappropriate *search* patch shaping,
- inappropriate patch size,
- image resolution,
- occlusions in certain *target* images,
- search step increment, and
- repetitive features in the image *search* space which are similar to the *reference* patch.

In an effort to avoid false matches, only search patches whose correlation is larger than a user-defined threshold are considered in the selection of the match point. The minimum accepted cross-correlation for matching of the rock face images was set at 0.75, a value which provided a low occurrence of spurious results during testing. The number of search images, at each depth increment, whose patch correlation is above the threshold also have an influence on the decision, with more images carrying a

higher weighting. Redefining the limited depth range over which the cross-correlation search is carried out also helps to reduce the risk of spurious results, especially in regions with repetitive features. Decreasing the original range by a user-defined scale factor and moving the depth range centre in accordance with previously matched points can do this. Equations (5.48) show the calculation stages in this process. It is recommended that this option only be carried out when mapping continuous surfaces, as sudden changes in object height could result in the search range falling beyond the interest point location.

$$Z_a = Z_n - \left[\frac{R}{2 * rf}\right]$$
$$Z_b = Z_n + \left[\frac{R}{2 * rf}\right] \qquad \textbf{(5.48)}$$

where, Z_a is the start of the modified depth range,

Z_b the end of the modified depth range,

Z_n the Z (depth) value of the last successfully matched point,

R the original depth range, and

rf the scale factor by which the original range is to be modified.

In considering the magnitude of the scale factor *rf* to be used, the homogeneity of the surface must be taken into account. For surfaces where there are no sudden elevation changes the scale factor can be high, however, where more undulation in the surface terrain occurs, the scale factor should be low. Due to the irregular nature of the rock face surface being mapped for this project application, no scale factor was applied.

In addition to locating corresponding points in conjugate images, the epipolar geometry can be used to calculate the shaping parameters between the conjugate image patches. According to van der Vlugt (1995), there are two factors which cause the initially square *search* patch to take on a distorted shape in the *target* image. These are:

- the position and orientation of the *target* image(s) with respect to the *reference* image, and
- the different heights of the surface elements imaged within the *reference* patch.

The *search* patch(es) can be shaped *a priori* to model the known effects of the camera geometry. The surface shape is generally not known and hence the second effect cannot be modelled.

The method of determining the patch shaping parameters involves the use of two additional patch pixel positions in the unshaped patch; the top left and right pixels are chosen. These pixels are then transformed using the collinearity equations, as previously described. The use of these two pixels in conjunction with the centre patch pixel allows for the calculation of the shaping parameters. Van der Vlugt (1995) describes this process with the use of figure 5.19 below.

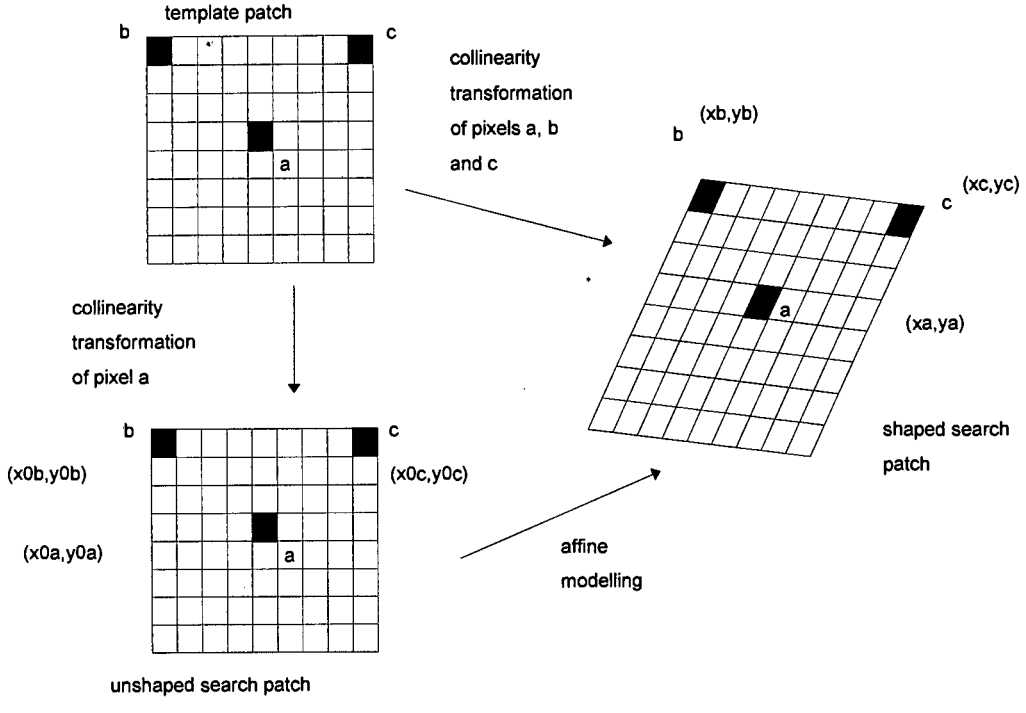

Figure 5.19 Computation of the affine shaping parameters

With reference to figure 5.19, the shaping parameters of an individual search patch may be calculated by transforming the three reference pixels (a, b and c) into the search image using a common Z (depth) ordinate for each pixel. The shaped position of each pixel that results from this, is given by (x_a, y_a), (x_b, y_b) and (x_c, y_c). The associated unshaped positions are (x_a^0, y_a^0), (x_b^0, y_b^0) and (x_c^0, y_c^0), where

$$\begin{aligned}(x_a^0, y_a^0) &= (x_a, y_a) \\ (x_b^0, y_b^0) &= (x_a - r, y_a - r) \\ (x_c^0, y_c^0) &= (x_a + r, y_a - r)\end{aligned} \tag{5.49}$$

and

$$r = (psize - 1)/2 \tag{5.50}$$

where *psize* is the size of the *reference* patch, being square and odd in number.

The affine shaping parameters are then calculated in the following manner:

$$\begin{bmatrix} a_{11} \\ a_{12} \\ a_{21} \\ b_{11} \\ b_{12} \\ b_{21} \end{bmatrix} = \begin{bmatrix} 1 & x_a^0 & y_a^0 & 0 & 0 & 0 \\ 0 & 0 & 0 & 1 & x_a^0 & y_a^0 \\ 1 & x_b^0 & y_b^0 & 0 & 0 & 0 \\ 0 & 0 & 0 & 1 & x_b^0 & y_b^0 \\ 1 & x_c^0 & y_c^0 & 0 & 0 & 0 \\ 0 & 0 & 0 & 1 & x_c^0 & y_c^0 \end{bmatrix}^{-1} \begin{bmatrix} x_a \\ y_a \\ x_b \\ y_b \\ x_c \\ y_c \end{bmatrix} \tag{5.51}$$

The unshaped search patches are then transformed using the above calculated affine shaping parameters and the transformed sub-pixel search patch grid is resampled using a bi-linear interpolation algorithm, as depicted in figure 5.20 and equation (5.52) to compute the grey values of the patch positions.

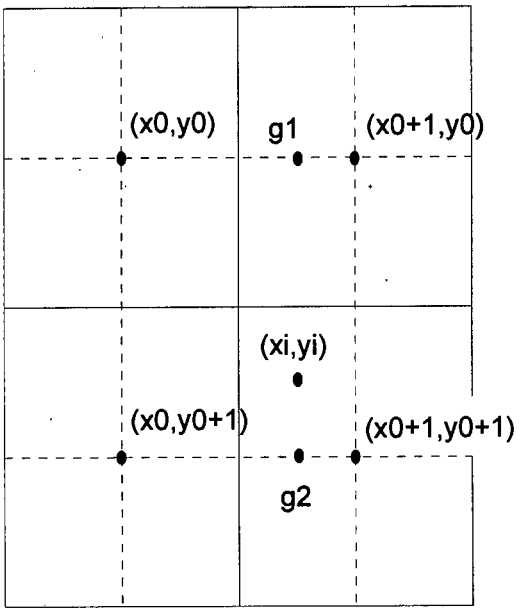

Figure 5.20 Bilinear interpolation

with respect to figure 5.20,

$$g_1 = g(x_0, y_0) + \big(g(x_0 + 1, y_0) - g(x_0, y_0)\big)(x_i - x_0)$$

$$g_2 = g(x_0, y_0 + 1) + \big(g(x_0 + 1, y_0 + 1) - g(x_0, y_0 + 1)\big)(x_i - x_0) \qquad \textbf{(5.52)}$$

$$g(x_i, y_i) = g_1 + (g_2 - g_1)(y_i - y_0)$$

These match positions and patch shaping parameters are then used, as starting point provisional values, for the least squares, grey-scale area-based matching algorithm, to obtain a final match position, as discussed in the following section.

5.5.2 GEOMETRICALLY CONSTRAINED MULTI-PHOTO MATCHING

The adaptive least-squares correlation, combining grey-level matching with geometric constraints, as presented by Gruen and Baltsavias (1988), is applied for *X*, *Y*, *Z* object co-ordinate determination.

The observation equations consist of two parts: *grey-level* matching and imposed *geometrical constraints*. The two parts are related through shift parameters of the image patches. The constraints are the *collinearity conditions*. Here a multi-image approach is used, whereby the grey-level matching equations are formulated such that they allow for simultaneous, local image shaping, for the inclusion of additional geometric constraints as well as for discrete corrections, which are required because of the deviation of the actual sensor geometry from the theoretical model. *Radiometric corrections* are applied to the search patches prior to the adjustment, using Wallis filtering, as described by Baltsavias (1991):

$$g^c(x,y) = \left[g(x,y) - m_g\right]\left(s_f / s_g\right) + m_f \tag{5.53}$$

where,

$g^c(x,y)$	is the radiometrically corrected *search* patch grey level,
$g(x,y)$	the original *search* patch grey level,
m_f	the mean of the *reference* patch grey levels,
s_f	the standard deviation of the *reference* patch grey levels,
m_g	the mean of the *search* patch grey levels, and
s_g	the standard deviation of the *search* patch grey levels.

Assume that there is a sequence of $n+1$ conjugate images of an object. The object is defined in a 3D cartesian co-ordinate system (X, Y, Z) and the images in a 3D cartesian co-ordinate system (x, y, c=0). The images are discrete 2D approximations of continuous functions. One image function $f(x,y)$, the $(n+1)^{th}$ image, serves as the *reference* image, and the remaining n images $g_1(x,y)$, ..., $g_n(x,y)$ as the *target* image(s) (Gruen and Baltsavias, 1988). For an ideal match of corresponding points we have

$$f(x,y) = g_i(x,y), i = 1,\ldots,n \tag{5.54}$$

Taking into consideration noise and assuming that template noise is independent of the picture noise, equation (5.54) becomes

$$f(x,y) - e_i(x,y) = g_i(x,y) \tag{5.55}$$

where $e_i(x,y)$ is a true error vector.

Equation (5.54) can be considered a non-linear observation equation which models the observation vector $f(x,y)$ with functions $g_i(x,y)$ whose locations in the pictures $1,....,n$ need to be determined. The location is described by Δx_i, Δy_i shifts with respect to an approximate position of each function $g_i^0(x,y)$.

To account for systematic image deformations caused by differing perspective views, so as to achieve a better match, additional geometric transformation parameters are included to allow for image "shaping".

Each function $g_i^0(x,y)$ forms a grid of grey-values and is located in a larger search region $w_i(x,y)$. The image shaping is achieved by transforming the x_0, y_0 co-ordinates of $g_i^0(x,y)$ and resampling in $w_i(x,y)$. The geometrical transformation can be modelled by the affine transformation (six parameter) (Gruen and Baltsavias, 1988).

Because equation (5.55) is non-linear, it is linearised according to

$$f(x,y) - e_i(x,y) = g_i^0(x,y) + \frac{\partial g_i^0(x,y)}{\partial x_i} dx_i + \frac{\partial g_i^0(x,y)}{\partial y_i} dy_i \tag{5.56}$$

with the notations

$$g_{x_i} = \frac{\partial g_i^{\,0}(x,y)}{\partial x_i}$$
$$g_{y_i} = \frac{\partial g_i^{\,0}(x,y)}{\partial y_i} \qquad (5.57)$$

where g_{x_i} and g_{y_i} are the patch gradients in x and y image directions, equation (5.56) becomes

$$\begin{aligned} f(x,y) - e_i(x,y) = g_i^{\,0}(x,y) + g_{x_i} da_{11_i} + g_{x_i} x_0 da_{12_i} + \\ + g_{x_i} y_0 da_{21_i} + g_{y_i} db_{11_i} + g_{y_i} x_0 db_{12_i} + \\ + g_{y_i} y_0 db_{21_i} \end{aligned} \qquad (5.58)$$

with

$$\begin{aligned} x_i^{\,T} &= \left(da_{11} \quad da_{12} \quad da_{21} \quad db_{11} \quad db_{12} \quad db_{21}\right) \\ l_i &= f(x,y) - g_i^{\,0}(x,y) \\ A_i &= \left(g_x \quad g_x x_0 \quad g_x y_0 \quad g_y \quad g_y x_0 \quad g_y y_0\right)_i \end{aligned} \qquad (5.59)$$

Equation (5.58) results in

$$-e_i(x,y) = A_i x_i - l_i; \quad P_i \qquad (5.60)$$

P_i...weight co-efficient matrix of l_i

Equations (5.60) form a system of n sets of grey-level correlation equations (for each of the n *target* images), with each set consisting of $n_1 n_2$ correlation equations (n_1,n_2...dimensions of each pixel patch used for the match).

If the image formation process followed the law of perspective projection, a set of $n+1$ collinearity conditions can be formulated for each imaged object point p as

$$\vec{x}_{pk} = \frac{1}{\lambda_{pk}} R_k (\vec{X}_p - \vec{X}_{0k}) \tag{5.61}$$

with $k = 0, 1, 2, ..., n$

p = object point index

$$\vec{x}_{pk} = \begin{bmatrix} x_p \\ y_p \\ c \end{bmatrix}$$

where x_{pk}, y_{pk} are the image co-ordinates of the point p in the scene (k), reduced to the principal point, and

c_k the principal distance of sensor of scene (k).

$R_k = (r_1..r_2..r_3)_k$ is the rotation matrix of scene (k), as previously defined.

$$\vec{X}_p = \begin{bmatrix} X \\ Y \\ Z \end{bmatrix}_p$$

$\vec{X}_p$ = vector of object point co-ordinates of point p

$$\vec{X}_{0k} = \begin{bmatrix} X_0 \\ Y_0 \\ Z_0 \end{bmatrix}_k$$

$\vec{X}_{0k}$ = vector of object co-ordinates of the perspective centres of scene (k)

λ_{pk} = scale factor for point p imaged in scene (k).

The x, y components of equation (5.61) are

$$x_{pk} = c_k \frac{r_{1k}(\vec{X}_p - \vec{X}_{0k})}{r_{3k}(\vec{X}_p - \vec{X}_{0k})} \equiv -F_k^x \tag{5.62}$$

$$y_{pk} = c_k \frac{r_{2k}(\vec{X}_p - \vec{X}_{0k})}{r_{3k}(\vec{X}_p - \vec{X}_{0k})} \equiv -F_k^y \tag{5.63}$$

For simplification, the point index p is ignored in the following.

With

$$\begin{aligned} x_k &= x_k^0 + \Delta x_k \\ y_k &= y_k^0 + \Delta y_k \end{aligned} \tag{5.64}$$

where Δx_k, Δy_k are the shift parameters in equation (5.60), and
Δx_0, $\Delta y_0 = 0$ (for the template), equations (5.62) and (5.63) become

$$\Delta x_k + F_k^x + x_k^0 = 0 \tag{5.65}$$

$$\Delta y_k + F_k^y + y_k^0 = 0 \tag{5.66}$$

It is assumed that the exterior orientation parameters of each sensor k $(X_0, Y_0, Z_0, \omega, \kappa, \phi)_k$ with $k=1,...,n+1$ are given and the interior orientation parameters of the sensors $(x_p, y_p$ ... principal point co-ordinates, c ... principal distance$)_k$ are pre-determined as well. Then the parameters to be estimated in equations (5.65) and (5.66) are the shift values Δx_k, Δy_k and the co-ordinates of the object point X, Y, Z. Equations (5.65) and (5.66) with respect to the object co-ordinates X, Y, Z result in

$$\Delta x_k + \frac{\partial F_k^x}{\partial X} dX + \frac{\partial F_k^x}{\partial Y} dY + \frac{\partial F_k^x}{\partial Z} dZ + F_k^{x(0)} + x_k^0 = 0 \qquad \textbf{(5.67)}$$

$$\Delta y_k + \frac{\partial F_k^y}{\partial X} dX + \frac{\partial F_k^y}{\partial Y} dY + \frac{\partial F_k^y}{\partial Z} dZ + F_k^{y(0)} + y_k^0 = 0 \qquad \textbf{(5.68)}$$

with

$$t_k = \begin{bmatrix} F^{x(0)} + x^0 + \Delta x_s \\ F^{y(0)} + y^0 + \Delta y_s \end{bmatrix}_k \qquad \textbf{(5.69)}$$

x = vector of all parameters, and

B_k = design matrix of the co-efficients of the parameters for scene (k),

where, Δx_s, Δy_s are terms for possible systematic image distortion,

the extended equations (5.67) and (5.68) yield

$$B_k x + t_k = 0; k = 0,\ldots,n \qquad \textbf{(5.70)}$$

Equations (5.60) and (5.70) are connected by means of the shift parameters Δx_k, Δy_k that appear in both equations.

The equations (5.70) are not treated as functional constraints but as a set of observation equations. In this case, equations (5.70) become

$$-e_t = Bx + t; \quad P_t \qquad \textbf{(5.71)}$$

P_t ... weight co-efficient matrix of t

with

$$e_t \approx N(0,\sigma_0^2 Q_{tt}); \qquad Q_{tt} = P_t^{-1}$$

The least-squares solution for the joint system equations (5.60) and equations (5.71) gives

$$\hat{x} = (A^T PA + B^T P_t B)^{-1}(A^T Pl - B^T P_t t) \qquad \textbf{(5.72)}$$

Providing a simultaneous solution for the corresponding image points in conjugate *target* images and object space co-ordinates for the interest point.

The weight matrices P, P_t are used as diagonal matrices. With the solution vector $\hat{x}$ we get

$v = A\hat{x} - l$	residual vector for grey-level observations,
$v_t = B\hat{x} + t$	residual vector for collinearity constraint observations, and

$$\hat{\sigma}_0^2 = \frac{v^T Pv + v_t{}^T P_t v_t}{r} \quad \text{variance factor,} \qquad \textbf{(5.73)}$$

where,

$r = n_o - u$	redundancy,
n_o	number of observations, and
u	number of parameters.

With,

$$n_o = M n + m\,(n+1)$$

$$u = np\ n + 3$$

where, M is the number of pixels in each patch,

n+1 the number of camera stations,

m the number of collinearity observation equations per image patch = 2, and

np the number of geometric transformations per patch (the maximum of six for the full affine transformation is used for this project).

Because of the non-linearity of the joint system, the final solution is obtained iteratively, whereby approximate values for the non-linear parameters (six transformation parameters for each picture patch, object co-ordinates of point p) are required. As previously described, these approximations are supplied by the epipolar "matching" algorithm. The iterations stop if each element of the solution vector $\hat{x}$ in equation (5.72) falls below a user defined threshold.

5.5.3 IMAGE MATCHING - DISCUSSION

During the investigation into the use of the multi-image least squares matching algorithm, the limitation, with respect to large rotations, of the images with respect to one another, was revealed. If the *target* image(s) are rotated, by large angles, with respect to the *reference* image then the least squares matching algorithm cannot estimate the shear parameters of the affine transformation and hence the solution cannot converge.

In most cases, this is easily avoided by capturing images that do not have large rotations in the image plane. This is, however, not always possible, with field conditions and equipment restrictions sometimes enforcing unsuitable camera geometry for image capture. Such a case was found in a research project aimed at the tracking and identification of individuals in a population of cheetah (as describe in chapter 7). Image capture was initially carried out with ±90° rotations, between the

various perspective views. This resulted in the non-determinability of the shear parameters of the affine transformation in image matching. Hence, no successful image matching was possible with the existing software and no surface model could be generated.

Two possible solutions to this problem are posed (e-mail communication with E.P.Baltsavias, ETH, Zürich). The first lies in the method of resampling the image patches in the *target* image(s) used for matching. The second solution uses an approximation for the angular difference, between the *reference* and *target* image, in the least squares matching algorithm. These methods are proposed as further research into the practical application of image matching and will be briefly outlined in the following sections.

5.5.3.1 Resampling a rotated patch

In concept, this would proceed as follows:

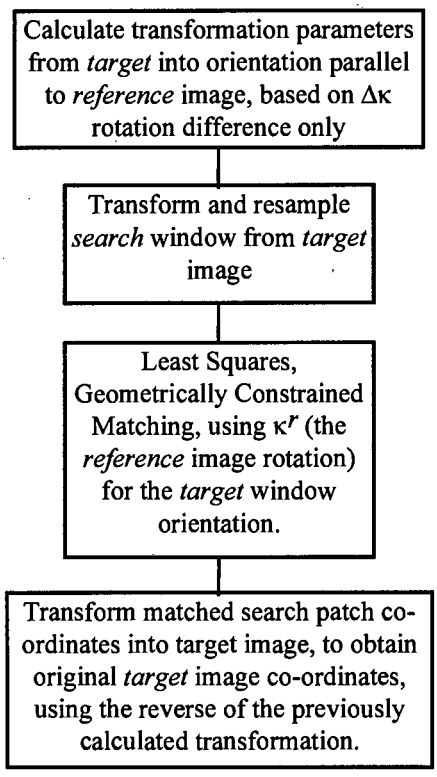

Figure 5.21 Resampling of a rotated patch

Search windows are generated by transforming and resampling rotated patches from the *target* images. The transformation is calculated using Δκ, the angular difference in rotation about the Z-axis between the *reference* image and the *target* image.

$$\Delta\kappa = \kappa_i^t - \kappa^r \tag{5.74}$$

where, κ^r is the rotation about the Z-axis for the *reference* image, and

κ^t_i the rotation about the Z-axis for the *target* image, for the *i*th *target* image number.

The process of transforming and resampling the *search* window from the target image is depicted in figure 5.22, and shows how the *search* window is rotated by $\Delta\kappa$ to be aligned with κ^r, of the *reference* image, from κ^t_i, of the *target* image.

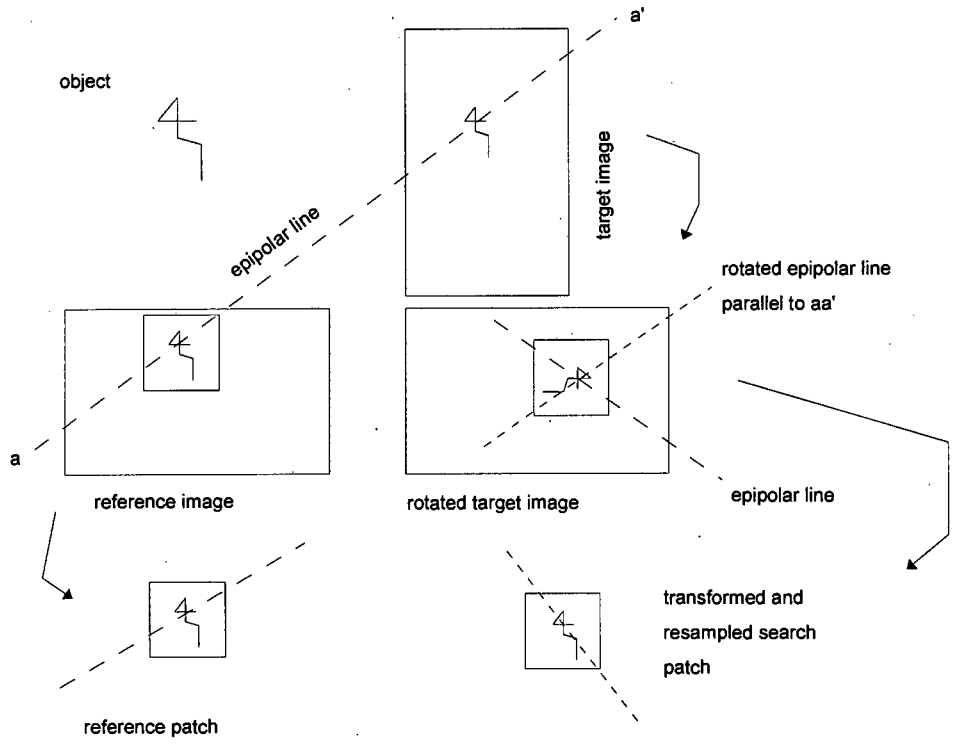

Figure 5.22 Transformation and resampling of *search* window

Then use $\kappa^s_i = \kappa^r$, for the *search* patch orientation, in least squares image matching with geometric constraints, as previously described. Although the object space co-ordinates calculated in this simultaneous adjustment will be correct, the image co-ordinates of the corresponding point in the *target* image will be in the transformed co-ordinate system. In order to calculate the image co-ordinates in the original target image, the reverse transformation from *target* image to *reference* image must be applied.

The additional interpolation of the *search* patch(es), due to this resampling, should have a minor effect on the accuracy, and could even be beneficial in noisy images, similar to low pass filtering of the image.

5.5.3.2 Approximation for rotation in matching:

In this proposed solution, the *search* patch is sampled from the *target* image in the normal manner (as applied in least squares image matching). The angular difference $\Delta\kappa$ in rotation about the Z-axis between the *reference* image and the *target* image, is introduced as an approximation for the rotation in the image matching routine, by means of the two shear parameters of the affine transformation. It must be noted that the angle $\Delta\kappa$ refers to a rotation in the local pixel co-ordinate system of the *search* patch (with its origin at the patch centre).

In applying the geometric constraints of the image matching algorithm, it must be noted that the transformation from the local pixel co-ordinate system, of the *search* patch, to the *target* image co-ordinate system has changed. The transformation must now take into account the angular difference $\Delta\kappa$ between the local pixel and global image co-ordinate systems for the *search* patch in the *target* image.

After image matching, the matched pixel position must be appropriately rotated in order to get the matched image co-ordinates into the *target* image co-ordinate system. For example, if the approximation for the angular difference $\Delta\kappa$ is 90°, then x_l in the local *search* patch co-ordinate system is y in the global *target* image system, and similarly for y_l.

5.6 SPACE INTERSECTION

In addition to providing geometric constraints to the least squares matching, the collinearity equations provided the calculation of the three dimensional (XYZ) object space co-ordinates of the interest point being matched. Thus, the result of the image matching algorithm is not just the corresponding image co-ordinates of interest points in conjugate images, but also a dense point cloud of three dimensional, object space, co-ordinates of successfully matched interest points.

This three dimensional point cloud can then be processed, by digital terrain modelling (DTM), to provide a regular grid representation, or a triangle irregular network (TIN), of the mapped data in a format more suitable for further processing. Additional processing includes surface modelling, volume calculation and deformation analysis.

6 ANALYSIS OF RESULTS

The output of the digital photogrammetric process is a dense point cloud of 3D (XYZ) co-ordinates which represent the rock face under investigation. This data needs to be represented in a way suited to further analysis. Various visualisation methods were investigated and a sample of the data obtained from the underground mine test is presented.

In order to generate a representation of the mapped surface, the three dimensional point cloud produced by image matching needs to be represented by a regular grid of interpolated points (DTM) or a TIN. Commercially available surface generation software was used for this purpose. With a wide range of interpolation methods and display options, including contour maps, three dimensional mesh perspective plots and profile sections, all of the basic visualisation needs were met.

6.1 EVALUATION OF UNDERGROUND TESTS

The final evaluation of the measurement system was carried out at Blyvooruitsig mine on the Witwatersrand (South Africa), at a depth of approximately 2170m below surface. Stope conditions were poor, with pronounced closure and a roof height of less than 1m. Temperature and humidity were at very high levels and production mining was taking place in the adjacent panel.

Image capture proceeded smoothly, with approximately 1.5 hours before and 1 hour after the pre-conditioning blast being required to set up the co-ordinate control field and intermediate target poles, and capture the required images.

Processing of the results proved to be a more arduous task than initially anticipated, with identification of the target points proving the most cumbersome of processes. A proposed solution to this problem is given in the recommendations (see chapter 9),

involving clearer marking of individual target points on the rock face. Once completed, the exterior orientation of the cameras provided excellent results, with positional accuracy of less than 1mm in all cases, as seen in table 6.1 below. The depth axis being in the X-direction.

RMS σX_c (mm)	RMS σY_c (mm)	RMS σZ_c (mm)
0.69	0.56	0.55

Table 6.1 Exterior orientation precision

The subsequent interest point location and image matching proceeded well, proving a complete success with interest point positioning accuracy better than the required 1mm in object space (XYZ) in all cases. This is shown in table 6.2, with the root-mean-squared standard deviation of the matched point intersections being better than 0.5mm in depth and 0.1mm lateral to the plane of the rock face.

RMS σX (mm)	RMS σY (mm)	RMS σZ (mm)
0.45	0.06	0.01

Table 6.2 Interest point precision

Figures 6.1 to 6.5 below, provide examples of the final output of the surface re-construction of the rock face. This data will be used in finite element analysis and computer aided design software used by rock engineers, at the Mining Technology Division of the Council for Scientific and Industrial Research (Johannesburg), to calculate and predict volume changes in the rock face due to pre-conditioning blasts. These images were produced using the commercially available surface generation software Surfer™ from Golden Software Inc..

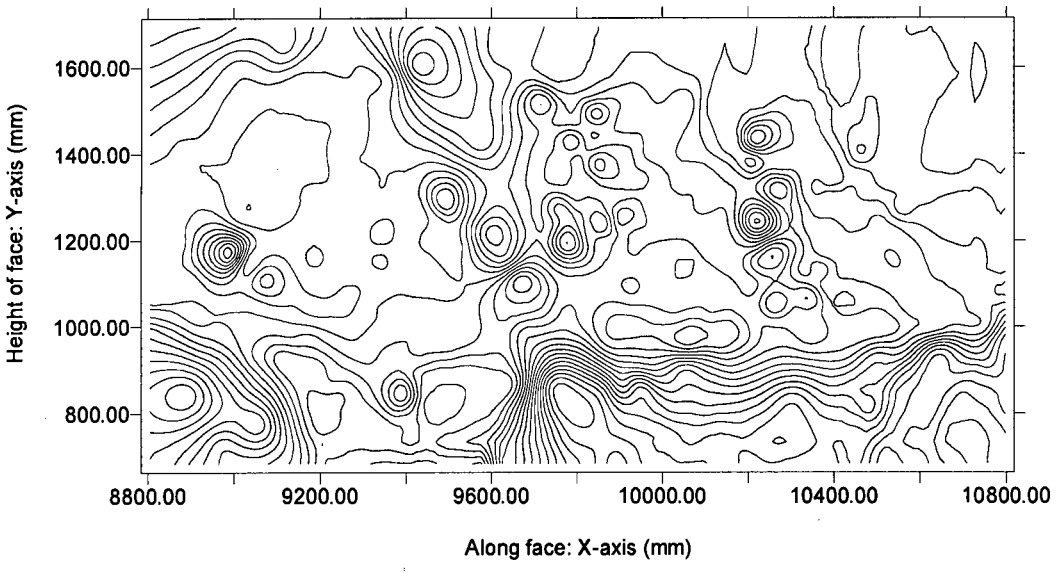

Figure 6.1 Contour plot the rock face

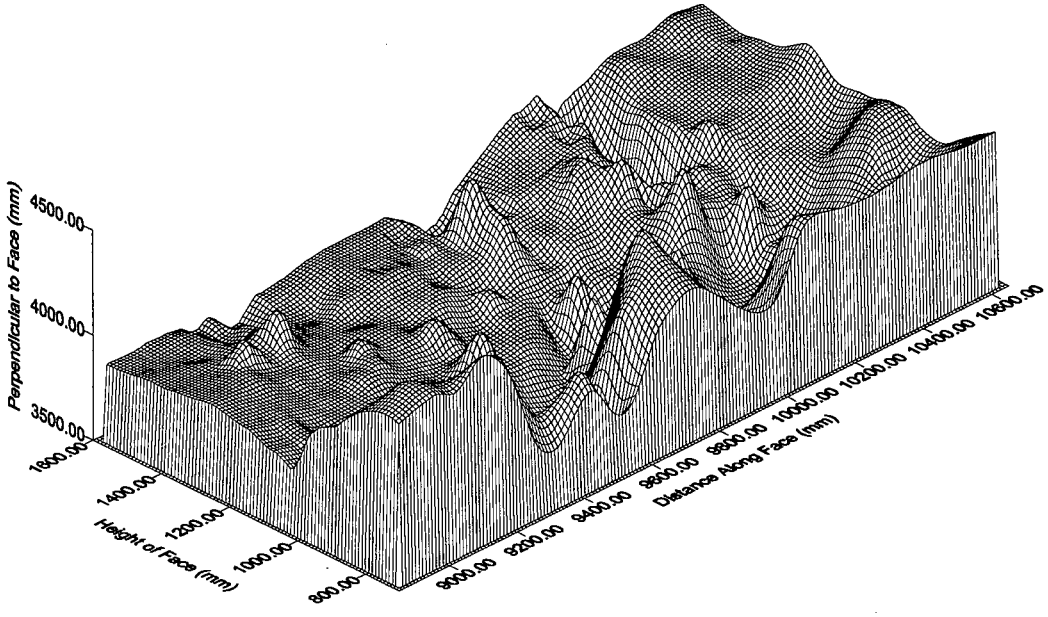

Figure 6.2 Three dimensional mesh perspective plot of the rock face - before blast

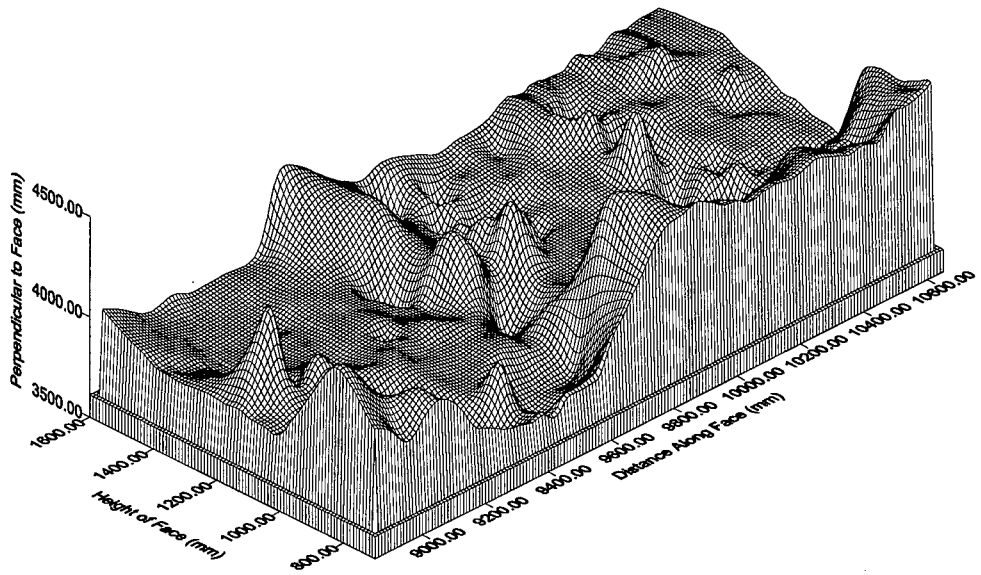

Figure 6.3 Three dimensional mesh perspective plot of the rock face - after blast

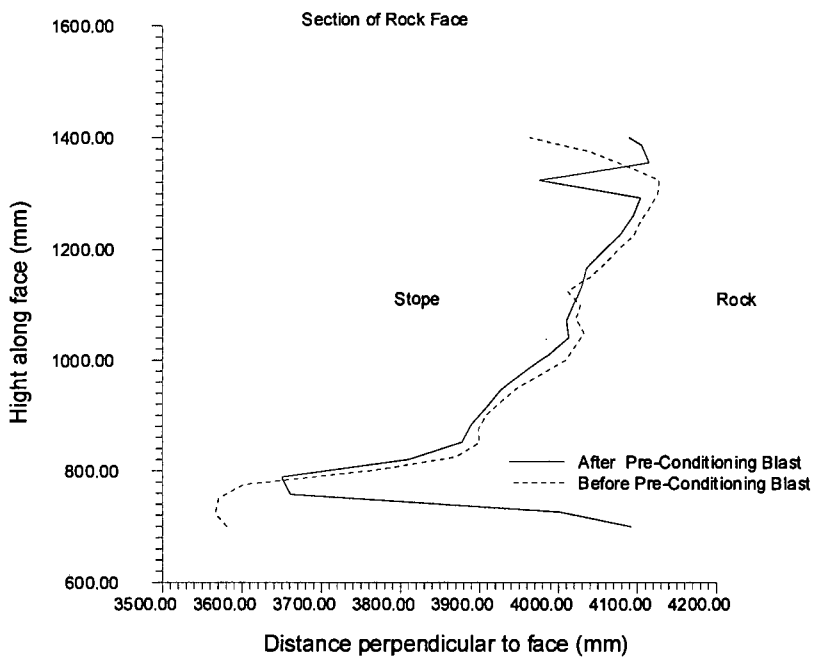

Figure 6.4 Section of the rock face before and after the pre-conditioning blast

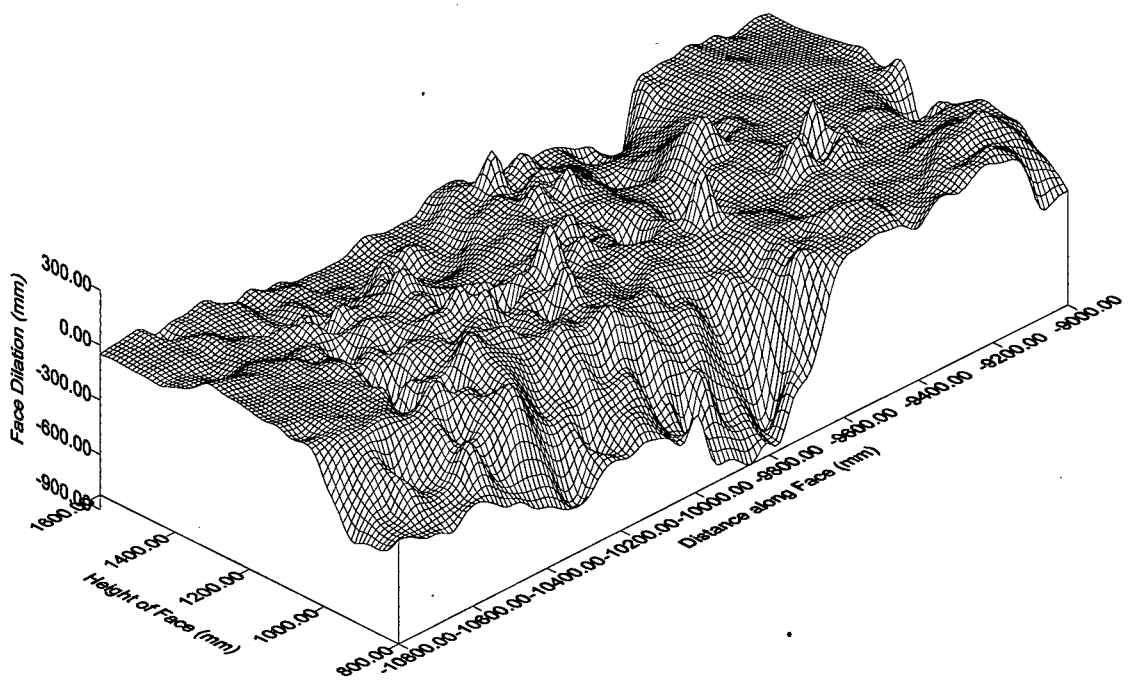

Figure 6.5 Face dilation (positive value) on a section of the face as a result of a pre-conditioning blast

Figure 6.4 shows a typical cross-section of the rock face, obtained from the digital photogrammetric data, both before and after the pre-conditioning blast. This section was taken from the central portion of the rock face measured, where the stope face has dilated by approximately 2 – 3cm. At other pre-conditioning sites, it is seen that common movements of 0.4 – 4cm occur in the plane of the rock face as a result of pre-conditioning blasts (Lightfoot *et al*, 1996). In addition to dilation, some face recession is evident. This can occur when pieces of the footwall, hangingwall and the stope face loosen and become dislodged. Such recession is particularly evident where the footwall and hangingwall join the stope face.

The three dimensional plots of the stope face before (figure 6.2) and after (figure 6.3) the pre-conditioning blast and a surface plot of the difference between the two (figure 6.5) indicate that, for this part of the face, there is a maximum face recession of 0.9m in some areas and a maximum face dilation of 0.3m in others. These results should be interpreted with care, as the data near the hangingwall and footwall tend to be

unreliable, as a result of pieces of rock becoming dislodged and either falling out or moving outwards. It is the data in the central parts of the stope face, as shown in the cross-section (figure 6.4) that provides a more realistic interpretation of the actual stope face movements.

7 ADDITIONAL TESTS AND CASE STUDIES

Further testing of the software developed, and in particular the programming of the image matching algorithm, was implemented in additional research projects undertaken at the department of Surveying and Geodetic Engineering at the University of Cape Town. The objective was to analyse the success of the software developed by mapping naturally textured surfaces. Excellent examples were provided, in the three dimensional reconstruction of the 3.6 million year old hominid footprints found at Laetoli in Tanzania and in the mapping of cheetah paw imprints for the purpose of conservation.

7.1 HOMINID FOOTPRINTS - LAETOLI (TANZANIA)

The re-excavation of the 3.6 million year old hominid track-way at Laetoli, Site G in Tanzania, provided the opportunity to accurately document the footprint record of this unique archaeological site. Professor Heinz Rüther of the Department of Surveying and Geodetic Engineering at the University of Cape Town was commissioned by the Getty Conservation Institute to provide highly accurate photogrammetric mapping of the hominid and hipparion trails, involving photogrammetric documentation of the individual footprints and the track-way surface to an accuracy of 0.5mm or better.

Photography was conducted using three different cameras: a metric Zeiss UMK with 5x7in. glass plates, a Kodak DCS420 digital camera and a Hasselblad 2.25x2.25in. camera. For the purpose of this thesis only the digital photogrammetric process will be described.

7.1.1 OBJECTIVE

It was the objective of the field campaign to obtain a complete photogrammetric coverage of the individual hominid footprints and extensive coverage of the surrounding tuff surface. The photography was to be executed with digital and conventional film cameras. Each of the images had to contain sufficient control points of sub-millimetre accuracy to enable the generation of digital terrain models with contour intervals of 5mm and 1mm for the track-way and footprints respectively. Accuracies of individual points had to be in the order of 0.5mm.

Photogrammetric processing of the individual footprints was done using digital photogrammetric processing, the track-way being processed by means of UMK imagery mounted in an analytical plotter, with one image pair being processed digitally to provide confirmation of the analytical process. Only the generation of digital terrain models for the individual footprints will be described in this document.

7.1.2 PHOTOGRAMMETRIC DATA ACQUISITION

Each hominid footprint was surveyed individually to obtain a detailed map of the imprints. This required the footprints to be photographed within a co-ordinate reference control frame, placed over each footprint in turn and surveyed into the overall co-ordinate system prior to photography. The survey of the frame, or rather three points on it, made it possible to transform the positions of the control points contained on the frame into the overall Laetoli site co-ordinate system. This is necessary in order to obtain the co-ordinates of the footprint digital terrain models in relation to the track-way.

7.1.2.1 Reference Control Point Frame

The reference control frame consisted of 70 retro-reflective targets placed on a rectangular steel frame, as seen in figure 7.1 below.

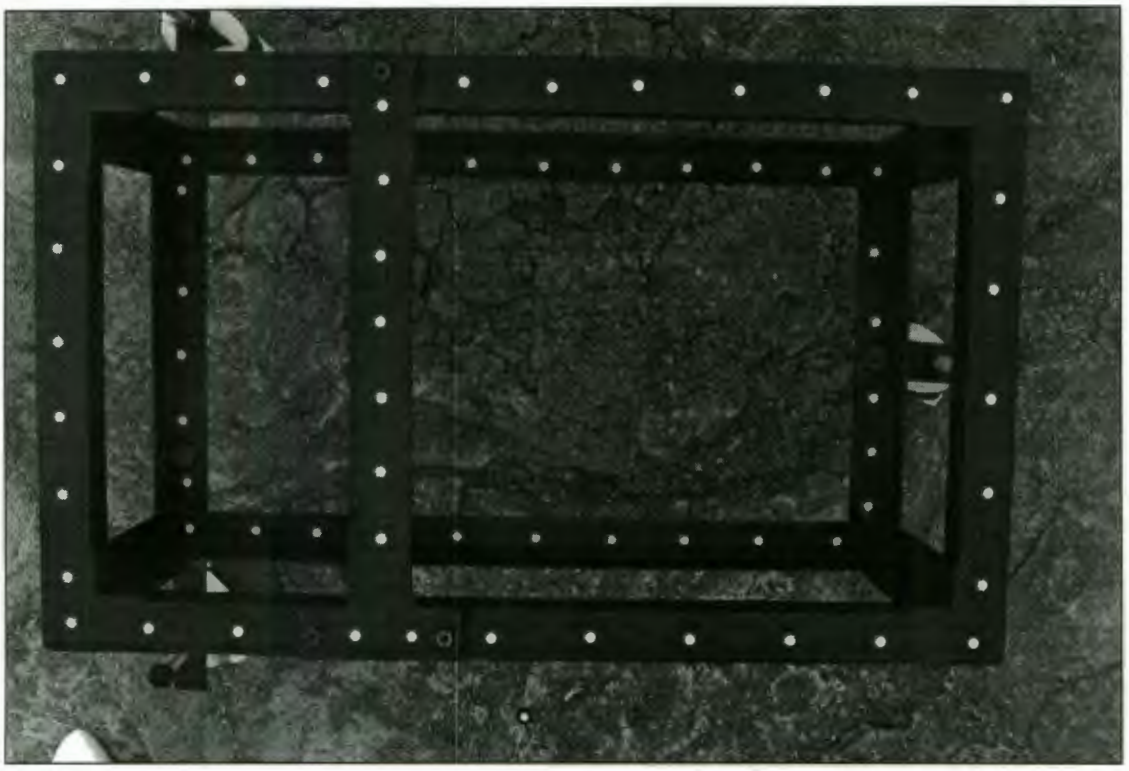

Figure 7.1 Reference control point frame

The co-ordinates of the 70 control targets on the frame were determined prior to the fieldwork using 18 images in a bundle adjustment calculation, the RMS standard deviations of the object space co-ordinate accuracies, as shown in table 7.1, all being below 0.1mm.

RMS σX (mm)	RMS σY (mm)	RMS σZ (mm)
0.02	0.02	0.07

Table 7.1 Control point accuracies

7.1.2.2 DCS420 Digital Camera Photography

Six black and white images of the footprint were captured with the control frame placed over each of the imprints in turn. The camera used was the Kodak DCS420m digital still camera. Images were captured at the six, approximately symmetrical positions, shown in figure 7.2.

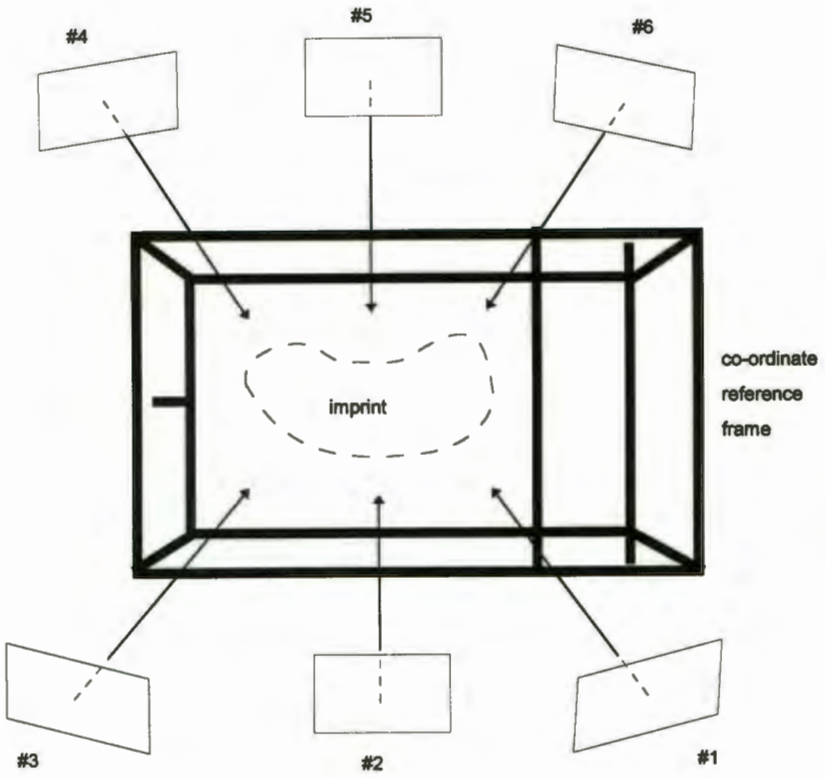

Figure 7.2 Image geometry for the digital photography of individual footprints

Image capture was done hand-held at an elevation of approximately 0.8m. A 14mm lens was used and the focusing ring was secured at a fixed (and taped down) focal length. All images were captured with the top of the image frame being oriented approximately towards the same point; i.e. there was minimal rotation about the Z-axis (κ).

7.1.3 PHOTOGRAMMETRIC DATA PROCESSING

As previously described, the first step in the digital photogrammetric data processing is the determination of the exterior orientation parameters of the camera locations in the overall track co-ordinate system. In this first step, the image positions of the 70 control frame targets were located in each of the six images, using the target location and centring routine previously described.

These target centres were then used in a bundle adjustment to provide the exterior orientation parameters of the six exposure stations. The interior orientations were calculated as a self-calibration process, independently for each footprint, in a simultaneous adjustment with the exterior orientation determination. Accuracies of the bundle adjustment can be gauged from the residuals of the image co-ordinates after the adjustment; average accuracies being in the order of:

Vx (mm)	Vy (mm)
0.003	0.002

Table 7.2 Example of bundle adjustment accuracies

These reflect the agreement between independent data sets of the frame co-ordinates determined earlier in object space and the images co-ordinates of the frame points in the digital images.

Once the interior and exterior orientation have been determined, it remains to find points of interest to represent the surface to be mapped and to match these points with corresponding points in the remaining conjugate images.

Points of interest, representing changes in texture in the images of the tuff surface containing the footprints, are located by means of interest operators as described in chapter 5.4, with sub-pixel location being calculated by the method of preservation of moments. Multi-image matching with imposed geometric constraints, in the form of

the collinearity equations, as explained in chapter 5.5, followed. The resultant list of three dimensional (XYZ) co-ordinates in the Laetoli site system represent a dense distribution of points which represent the footprint being mapped. Typical image co-ordinate precisions of 2μm were achieved, again confirming the high overall accuracies of the digital photogrammetric process used. Table 7.3 shows the average object space accuracies achieved, with match success rates exceeding 95%.

RMS σX (mm)	RMS σY (mm)	RMS σZ (mm)
0.02	0.05	0.23

Table 7.3 Example of object space accuracies achieved for interest points

Digital elevation models were generated from the dense point cloud of matched points by means of commercial surface generation software, with output being provided in numerical and graphical formats. Figure 7.3 and 7.4 below show examples the graphical output of the digital photogrammetric process used to re-construct of the hominid footprints.

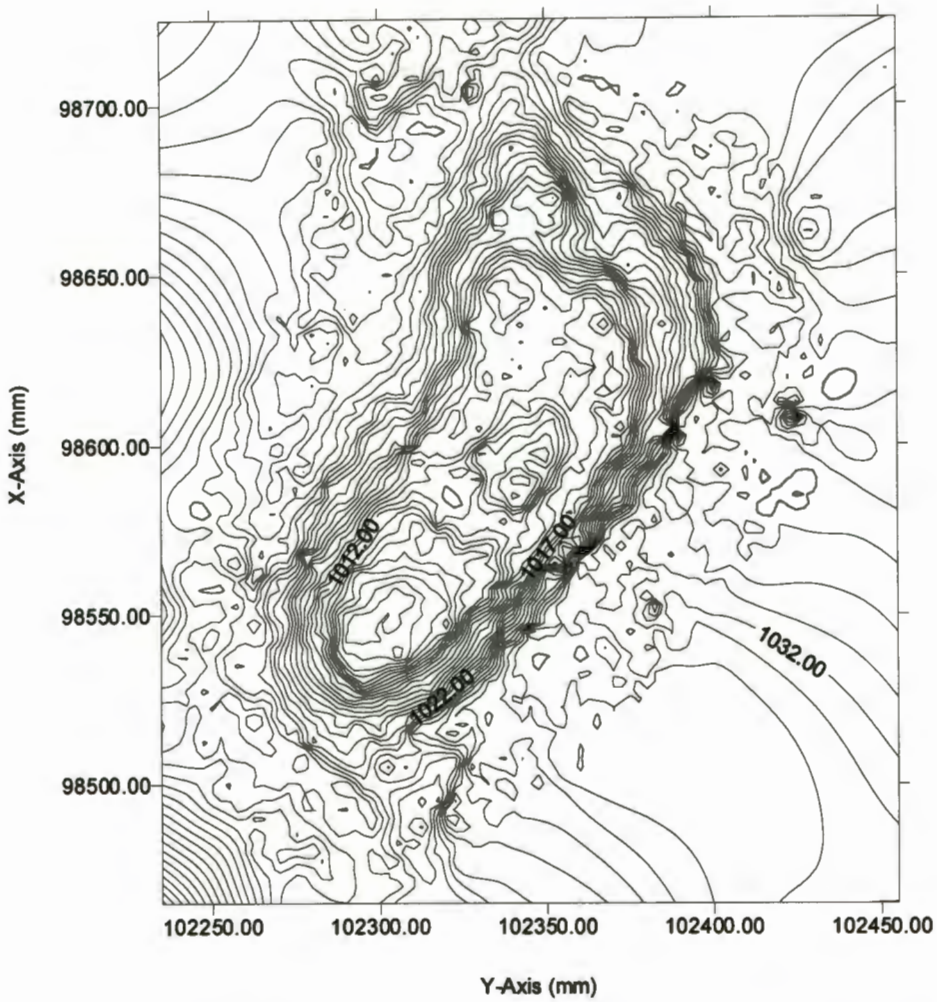

Figure 7.3 Contour plot of an individual hominid footprint

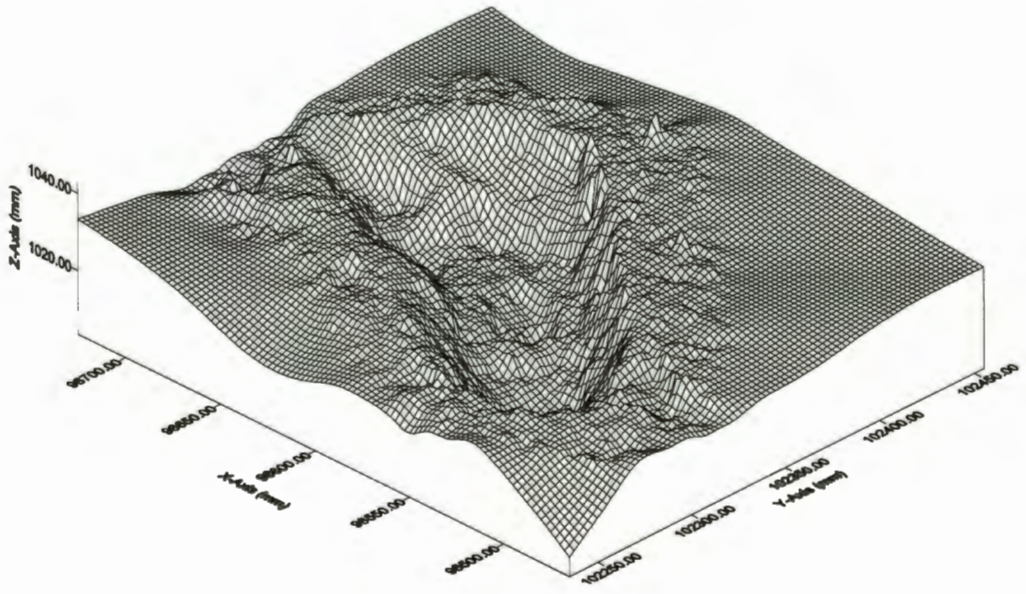

Figure 7.4 Wire mesh perspective plot of an individual hominid footprint

Further processing of the DTM's produced for the hominind footprints, allowed for more interpretative analysis. These visualisations included the production of digital ortho-images, draping of the grey-level images over the DTM's and manipulating the lighting and view perspective.

7.2 ANIMAL TRACKING

During the course of this research, two projects were initiated in an effort to track individuals in a known population of animals, for the purpose of anti-poaching operations, behaviour studies and conservation. Both these projects involved the mapping of the animal footprint, in order to build up a database of distinguishing characteristics of individuals in the particular group of animals investigated. The first project, that of the identification of individual cheetahs in a known pride, was initiated by a German zoology student, Heiko Thies. Secondly, the ongoing research into the identification of rhinoceros, initiated by conservationist Louis Liebenberg, is aimed at aiding conservation officials in tracking and monitoring of this endangered species.

7.2.1 CHEETAH PAW IMPRINTS

"It has become a responsibility of our generation to maintain the diversity of life on the planet. This can only take place with the needs of a growing mankind, hence the development of conservation techniques must take this into account. To be able to create viable techniques, it is vital to know as much as possible about the diverse life we intend to conserve" (Thies, 1996).

Such a research effort was undertaken by Heiko Thies, a German zoology student, in his diploma thesis. The project was aimed at gaining knowledge of the habits of cheetah, and in particular their use of "play trees" in their social interaction. To this

end, the identification of individual cheetahs at the trees was required; paw imprint analysis by means of digital photogrammetry formed part of this research.

7.2.1.1 Objective

One method of identifying an individual cheetah in a pride, is to view the imprint left in the surface. This method, similar to fingerprint identification of human prints, relies on distinctive characteristics on the cheetahs paw, such as size, pad distribution, claw position, imprint depth and scarring, to identify the individual. Thus, a three dimensional map of the paw imprint is useful in the identification and tracking process.

Digital photogrammetry provides an ideal tool in aiding conservation work, enabling the acquisition of a database of identifying characteristics of individual cheetahs in a pride.

7.2.1.2 Reference Control Frame

In order to obtain an accurate representation of the paw imprint, the use of a co-ordinated control frame was required to provide high accuracy co-ordinate control for the images captured. Figure 7.5 below shows the construction of the control frame used for the initial tests.

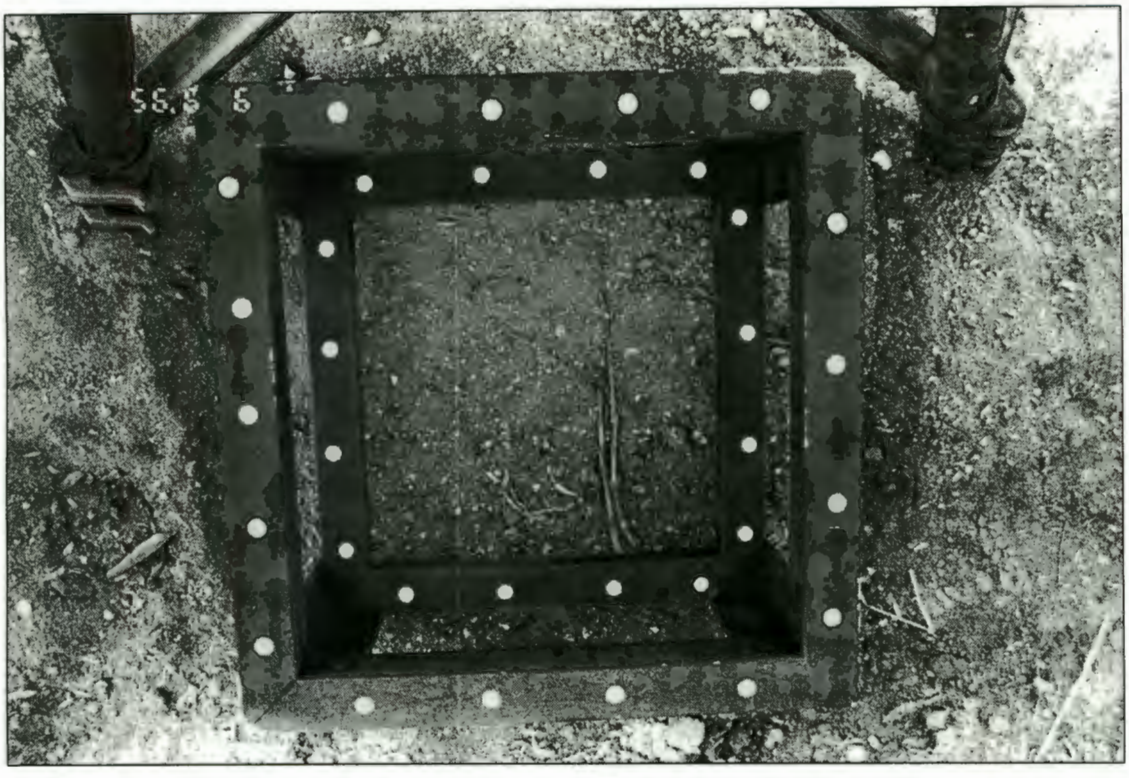

Figure 7.5 Cheetah paw imprint reference control frame

In order to attain the necessary sub-millimetre accuracy required for accurate analysis of the paw imprint, the positions of the control points located on the reference frame must be determined to a high degree of accuracy. Table 7.4 below shows the co-ordinate accuracy obtained for the control point positions, with all reference point positions being determined to less than 0.05mm in object space.

RMS σX (mm)	RMS σY (mm)	RMS σZ (mm)
0.01	0.01	0.03

Table 7.4 Reference frame control point accuracy

7.2.1.3 Image Acquisition

In order to maintain low costs and portability, image capture was done with a conventional 35mm film camera, fitted with a wide angle 28mm lens. Four images of the paw imprint, surrounded by the control frame, are taken from different perspectives. In order to prevent numerical inaccuracies in the affine transformation used in the image matching algorithm, care must be taken to ensure that no large deviations between κ rotations (about the Z-axis) for the various images occur, as large rotations are not allowed for in the existing software. Figure 7.6 shows the recommended image positions about the control frame; note the image orientations.

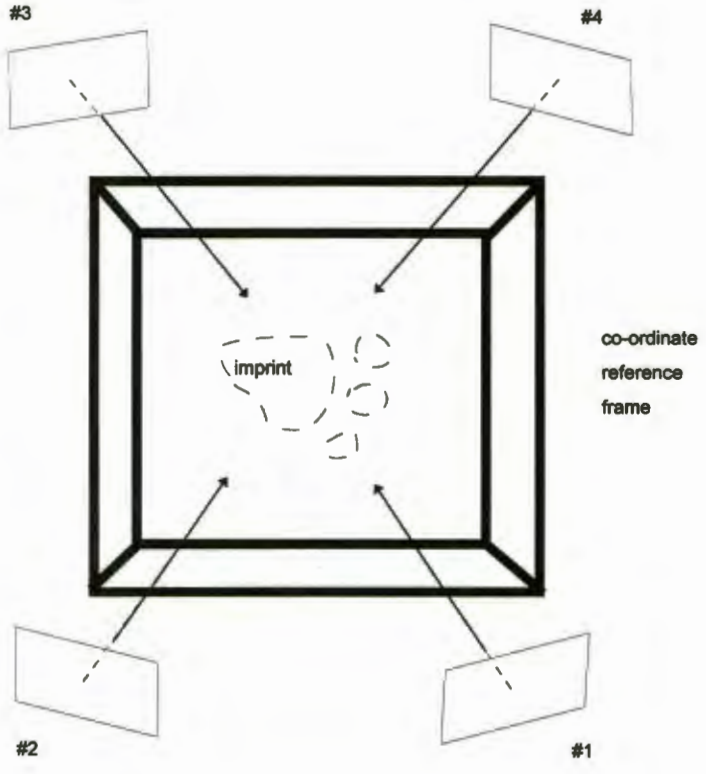

Figure 7.6 Recommended camera positions for image capture

As a result of the extended field campaigns that are typically undertaken, with imprint analysis being only one aspect of the field work undertaken, it is advised that camera calibration be undertaken at the same time as exterior orientation, i.e. self-calibration. This is recommended as it would be impossible to maintain one camera calibration for the duration of the field work, with the camera being required for other relevant

photography as well. Thus, for each imprint, the camera must be focused and the focusing ring taped into position before image capture takes place.

The effect of shadows in the images, as a result of the control frame, is significant in the image processing stage and thus must be addressed while capturing images. It is recommended that the imprint be shaded during image capture. This can be easily achieved by use of a common umbrella. Thus, the negative influence of shadow can be removed from the images, ensuring constant light conditions for the four images captured of the imprint.

7.2.1.4 Data processing

Before the digital image processing takes place, the film images must be converted into digital format. To this end, the film was developed and scanned onto a Kodak Photo-CD, providing various image resolutions, in a TIFF format. It was decided to use to 1536 x 1014 pixel size image, with a calculated pixel size of 21.815μm x 21.815μm.

As previously described, the image processing as shown in figure 5.1, provided a dense point cloud of three dimensional co-ordinates representing the cheetah paw imprint.

For the purpose of convenient testing, it was decided to use leopard paw imprints as a sample case. Point accuracies achieved for image matching and space intersections are shown in table 7.5 below; revealing the necessary sub-millimetre point positioning that is required for subsequent analysis.

RMS σX (mm)	RMS σY (mm)	RMS σZ (mm)
0.03	0.02	0.22

Table 7.5 Point accuracies for leopard paw imprint

These co-ordinates are then used to form a regular grid, or digital terrain model of the imprint, from which contour and perspective plots may be generated for visualisation, as seen in figures 7.7 and 7.8 below.

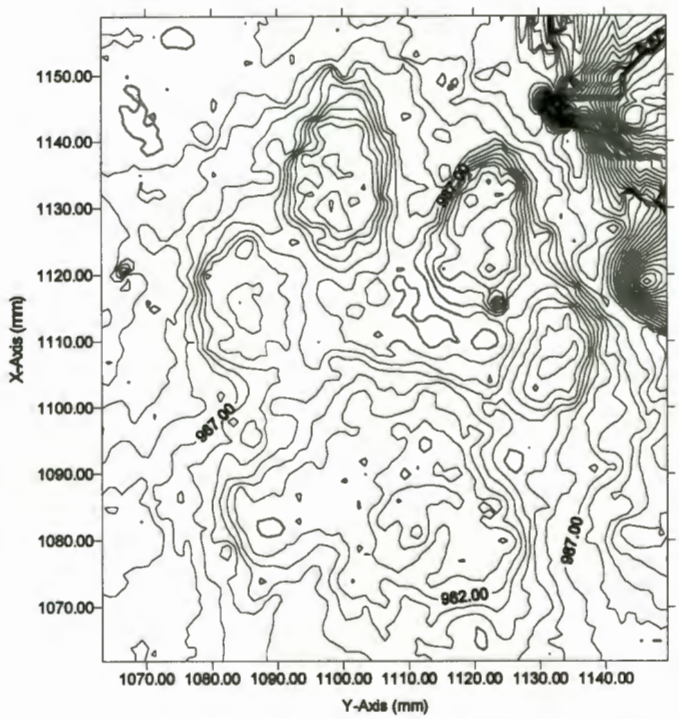

Figure 7.7 Leopard paw imprint contour map

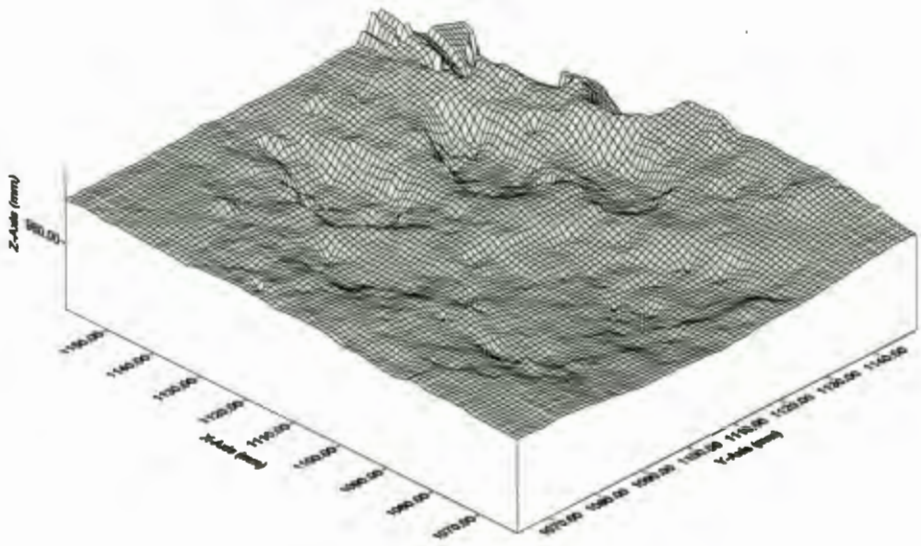

Figure 7.8 Leopard paw wire mesh perspective plot

The imprint visualisation can then be analysed by conservationists to distinguish distinctive characteristics of the individuals' imprint, and store this information in a database on the pride under investigation.

7.2.2 RHINOCEROS IMPRINTS

The black rhinoceros (*Diceros bicornis*) is an animal rarely observed, due to its diminished numbers and shy nature. Its footprint, however, is more regularly seen and identification of individuals is easily done by trained trackers in the field. For this reason, it is desired to use conventional principles of animal tracking in conjunction with computer technology, to develop a method to effectively automate the identification of individual animals (Sell, 1996).

For conservation purposes, with this highly endangered species, an effective means of identifying individual rhino's could make the management and conservation of the black rhinoceros more effective.

7.2.2.1 Objective

This research project, undertaken by surveying student Wilco Sell, as an undergraduate research project under the supervision of Professor Heinz Rüther at the University of Cape Town. The objective was to find a reliable and readily repeatable method to monitor the number of rhinoceros in their habitat, by means of footprint identification. One of the approaches investigated to achieve this was the three dimensional mapping of the footprint, by means of digital photogrammetry, in an effort to ascertain distinguishing features of the imprint, such as cracks and ridges, in three dimensional space.

The eventual aim is to allow trackers to capture images of the footprint and process them, with hand-held computers, in the field. These re-constructions will to be used to assist the tracker with identification and monitoring of individual rhinoceros. This will also enable the development of an easily maintained database relating relevant conservation information, such as movement patterns and eating habits, linked to tracking information, including the imprint analysis.

The generation of these representations of the rhinoceros imprints was approached using digital photogrammetry and followed the same procedures outlined in the hominid footprint mapping as described in chapter 7.1 above. Digital image capture, using the Kodak DCS420 digital camera provided suitable image quality of the imprints to be measured, as is seen in figure 7.9 below.

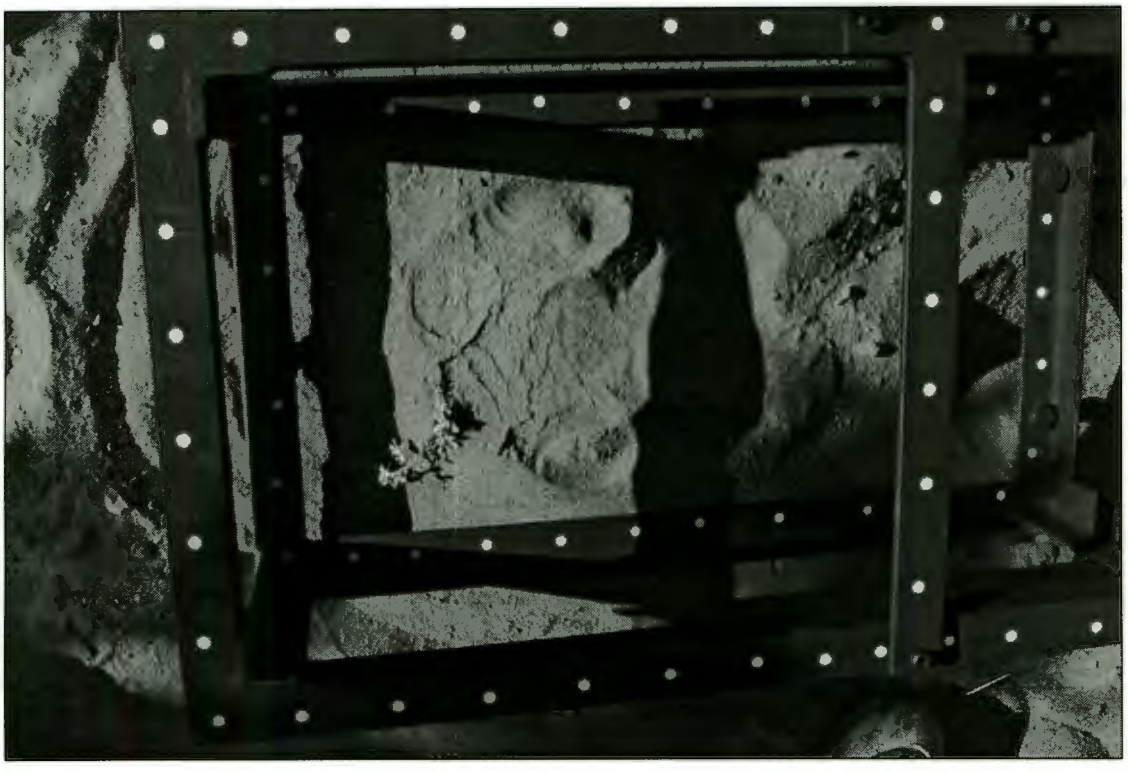

Figure 7.9 Example of rhinoceros imprint image

After digital image processing, a highly accurate three dimensional point cloud representing the imprint was produced. Examples of the accuracies achieved are presented in table 7.6 below. The root-mean-squared standard deviations of the point positions being in the order of 0.1mm in depth and 0.02mm in the plane lateral to the imprint.

RMS σX (mm)	RMS σY (mm)	RMS σZ (mm)
0.02	0.02	0.11

Table 7.6 Rhinoceros imprint point accuracies

The suitability of digital photogrammetry as a tool in the identification of rhinoceros and the viability of assisting field trackers with hand-held computers, is currently being investigated. In addition, alternative means of using the three dimensional re-constructions of the imprints, such as edge analysis on a height class image, are being examined.

8 RECOMMENDATIONS AND PROPOSED APPLICATION

8.1 RECOMMENDATIONS

From experience gained in underground mine testing, the following set of recommendations are made to provide possible solutions to the problems experienced during image capture and data processing:

- It is crucial to the photogrammetric analysis of the rock face that sufficient stereo overlap be maintained between conjugate images. At least 60% lateral overlap is required in order to transfer the co-ordinate system, via the tie points, from one image model to the next. The use of across wall images, as depicted in figure 8.1 assists in strengthening the network and increasing redundancies. Such images can play an important role in the co-ordination of the tie points.

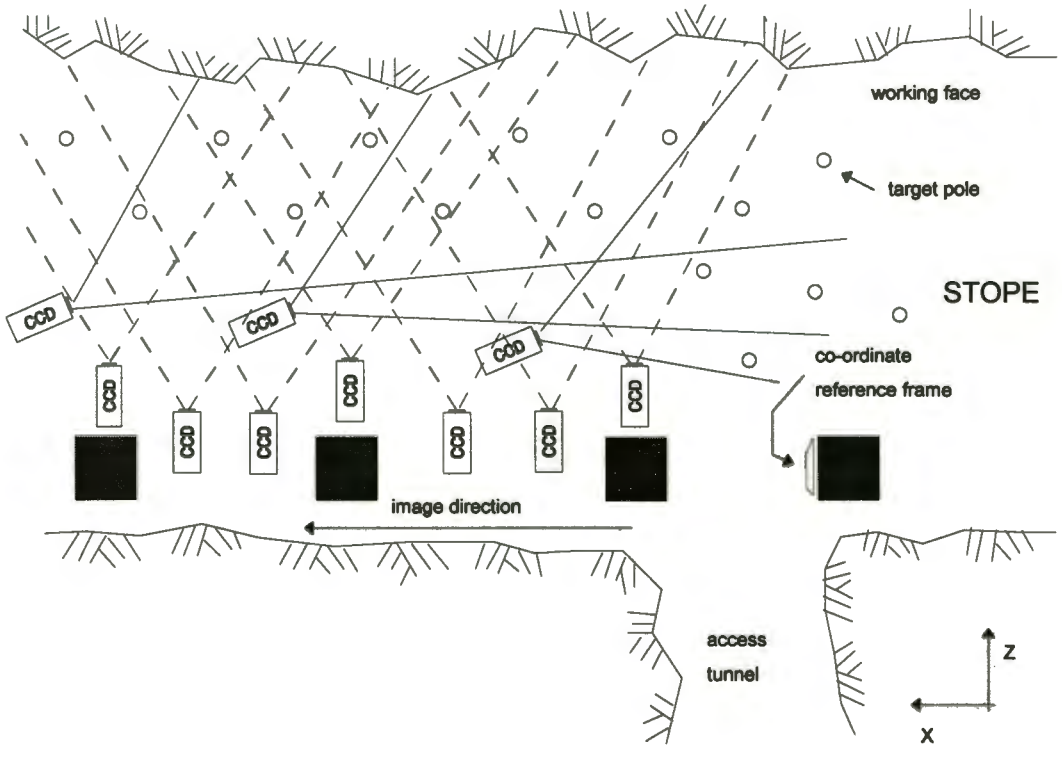

Figure 8.1 Across wall images

- It is important to ensure that the target points attached to the rock face are placed in positions where they will remain flat and free from distortion. This is because the control point centre calculation uses a weighted centre-of-gravity algorithm to determine the target centre, hence distortion in the shape of the target will lead to incorrect target centres which will have a negative effect on the achievable exterior orientation accuracies.

- An important factor to consider when working in the mine is that of control point identification. This has proved to be a problem in testing and poor target marking results in difficulties when identifying the target points in the images. It is suggested that the tie points on the target poles be arranged in patterns so that they are easily distinguished from one another. Target points on the rock face should be marked with spray paint patterns so as to provide a good measure of differentiation between targets. As mono-images are used, these patterns cannot rely on the use of colour for identification and must display distinguishing characteristics for recognition.

8.2 PROPOSED APPLICATIONS

In addition to those applications discussed, the use of the developed digital photogrammetric measurement system is in principle possible for a textured surface. It is in particular the modification of this system for use in other areas of the underground mining industry and in archaeological documentation that is proposed.

8.2.1 MINING INDUSTRY

As a result of e-mail correspondence with rock engineers, at the Mining Technology Division of the Council for Scientific and Industrial Research (CSIR) in Johannesburg, modifications to the developed digital photogrammetric measurement

system are proposed for use in alternative applications in the deep-level underground mining industry. In addition to monitoring deformation in the rock face in the stope, the development of algorithms capable of efficient fracture pattern analysis (including fracture density, orientation and pattern) will assist rock engineers in better modelling the rock mechanics of the rock face in the stope. This information should also be used in time-dependent studies, for modelling time-dependent rock behaviour during normal stope conditions.

The extension of the existing software is also suggested for monitoring borer excavations and tunnelling progress rates, as well as particle size analysis of excavated rock in the stope.

8.2.2 ARCHAEOLOGICAL DOCUMENTATION

In mid-1996, the discovery of a ship wreck off the Cape coast, exposed by winter storms, prompted the archaeological investigation of the remains, by Dr Bruno Wertz of the Archaeology department at the University of Cape Town. Due to the time limitations for work on the site, as the wreck is located within the storm tide range, excavation and documentation of the ship remains had to be done as quickly as possible.

The department of Surveying and Geodetic Engineering at the University of Cape Town was approached to carry out a detailed photogrammetric survey of the wreck, thereby enabling analysis of the data at a later stage. In the interest of containing costs and expediting the survey procedures, it was decided to carry out the image acquisition by means of a hand-held digital video recorder. This novel approach in image capture for archaeological documentation, enables the acquisition of appropriate imagery after image capture, allowing for any desired stereo overlap with a continuous image coverage.

The processing of the data, using software developed for this research, is being carried out in the same manner as that of the underground mine data, with co-ordinate reference control points at the beginning and end of the object being surveyed. Co-ordinate control is extended along the ship wreck with the use of tie points, in the form of targets attached to the wreck. This research forms part of the postgraduate studies of survey graduate Siddique Motala at the University of Cape Town.

The successful development of this dynamic video-based technique in archaeological documentation could have major implications on the traditional survey methods currently used. This would not only have the effect of reducing the time required on site, but will also ensure that minimum contact, with often delicate archaeological artefacts, is maintained. It would also provide a point density previously impossible with traditional survey methods.

9 CONCLUSIONS

The principal objective of this research was the development of a measurement system for use in the mensuration of the working rock face in the stope of a deep-level gold mine. By mapping the rock surface before and after a pre-conditioning blast, the deformations resulting from blast can be determined. This information is required by rock engineers to assist them in optimising the pre-conditioning blasting process.

The deformations are often small in extent, and the determination of the three dimensional co-ordinates of the surface, represented by densely spaced individual points, is required with sub-millimetre accuracy. Measurement of the rock face should also not interfere with normal production mining operations.

As no comparable measurement systems were found, digital photogrammetry was investigated as a possible solution to this mapping problem. The successful development of a novel digital photogrammetric measurement system, for use in this geometrically constrained and physically demanding production environment, demonstrated the measurement capability of photogrammetric techniques. The developed system not only produces highly accurate surface point measurements, but provides a permanent photographic record of present mine conditions, allowing for further analysis of the rock face. The relative speed of the process and the convenient size of the equipment makes the technology particularly suited to the underground mining environment, with minimal influence on production mining operations.

Semi-automated processing of the digital images required the development and coding of suitable algorithms, including:

- target location and centring,
- target identification,
- camera calibration,
- exterior orientation through DLT and bundle adjustment calculation,

- interest point location,
- image matching and space intersection.

Difficulties, which arose from the size, shape and environment of the object, were overcome by careful planning and pre-analysis which led to the incorporation of additional tie points placed on target poles in front of the object. It is in particular the development and implementation of the network of camera positions and tie point positions that led to the success of this process. The complex network configuration developed provided the required accuracy for the camera station locations, with lateral accuracy, in the plane of the rock face, being in the order of 0.5mm and depth accuracy in the order of 0.7mm.

The development of the image matching routine, used a new approach of applying epipolar geometry with cross-correlation as an automated means of finding provisional match positions in multiple conjugate images. These provisional values are then used in a multi-image, least squares, image matching algorithm, with geometric constraints in the form of the collinearity equations (Baltsavias, 1991). The resulting automated image matching process provides high accuracy point correlation in a theoretically limitless number of images. For practical purposes, image matching was limited to four images for the development of this project, providing a relative lateral accuracy, in the plane of the rock face, in the order of 0.1mm and depth accuracy in the order of 0.5mm, or 1:20000 and 1:4000 respectively.

The final analysis of the data made it apparent that digital photogrammetry is highly suitable for the determination of rock surface digital elevation models, for subsequent deformation analysis. This is further confirmed by the proposals of rock engineers, for the use of the developed system in monitoring other underground mining operations.

The extension of the developed software into other close-range applications further served to demonstrate the high accuracies that are achievable with such algorithms, when applied to the mensuration of naturally textured surfaces. In particular, the successful mapping of hominid footprints as well as cheetah and rhinoceros imprints

has demonstrated the high relative accuracies achievable with the developed digital photogrammetric measurement system under such controlled environments. In these cases, lateral accuracy, in the plane of the surface, was in the order of 0.05mm and depth accuracy in the order of 0.22mm, or approximately 1:20000 and 1:4000, as before.

It is, however, the successful implementation of this system in the demanding underground mining environment which is of particular significance. The development serves to fill a gap in the mining industry where previously no such system existed, thus enabling the cost effective and rapid acquisition of accurate data relevant to the movement in the rock face as a result of pre-conditioning blasts.

10 REFERENCE LIST

Abdel-Aziz, Y.I. and Karara, H.M., 1971. *Direct Linear Transformation from Comparator Co-ordinates into Object Space Co-ordinates in Close-Range Photogrammetry*, Proceedings of ASP/UI Symposium on Close Range Photogrammetry, Urbana, Illinois, USA., pp. 1 - 8.

Adams, L.P., 1989. Industrial *Photogrammetry* in **Non-Topographic Photogrammetry**, Karara, H.M. (ed.), Second Edition, American Society for Photogrammetry and Remote Sensing, pp. 349 – 358.

Anderson, H. and Stevens, D., 1982. *Mono Photographic Tunnel Profiling*, International Archives of Photogrammetry, 24(5/1), pp. 23 – 30.

Baltsavias, E.P., 1991. *Multiphoto Geometrically Constrained Matching*, PhD thesis, Mitteilungen Nr. 49, Institut für Geodäsie und Photogrammetrie, Zürich.

Beyer, H.A., 1990. *Calibration of CCD-Cameras for Machine Vision and Robotics*, SPIE, Vol. 1197, pp. 88 - 98.

Brown, D.C., 1958. *A Solution to the General Problem of Multiple Station Analytical Stereotriangulation*, RCA Data Reduction Technical Report No.43, Partick Air Force Base, Florida, USA.

Brown, D.C., 1966. *Decentering Distortion of Lenses*. Photogrammetric Engineering, Vol. 32, No.3, pp. 444 - 462.

Brown, D.C., 1981. *LNG Tank Inventory Measurement by Photogrammetry*, AGA Operating Section Proceedings, American Gas Assosciation, pp. 127 – 147.

Brown, D.C., 1985. *Adaptation of the Bundle Adjustment Method for Triangulation of Observations made by Digital Theodolites*, Paper presented at the Conference of Southern African Surveyors, 1985.

Canny, J., 1986. *A Computational Approach to Edge Detection, IEEE Transactions on Pattern Analysis and Machine Intelligence*, Vol. PAMI-8, No. 6, pp. 679 - 698.

Cooper, M.A.R., 1979. *Analytical Photogrammetry in Engineering: Three Feasibility Studies*, Photogrammetric Record, 9(53), pp. 601 – 619.

Davis, M., 1988. *Target Centreing and Image Matching in a Near Real-Time Photogrammetric System*, B.Sc.(hons) thesis, University of Cape Town.

Dold, J., Reinking, J. and Warnecke, P., 1993. *The analysis of high precision photogrammetric deformation measurements on masonry walls*, Proceedings, 7th Int. FIG Symp. On Deformation Measurements, Banff, 3 – 5 May, pp. 161 – 170.

Dowman, I.J., 1996. *Fundamentals of Digital Photogrammetry* in **Close Range Photogrammetry and Machine Vision**, Atkinson, K.B. (ed.), Whittles Publishing, Caithness, Scotland, pp. 52 - 77.

Dennen, W.H., 1989. *Mineral Resources - Geology, Exploration, and Development*, Taylor and Francis, New York.

Ekstrom, M.P. (ed.), 1984. *Digital Image Processing Techniques*, Academic Press, Inc., Orlando, Florida, Vol.2.

Ethrog, U. and Shmutter, B., 1982. *Tunnel Calibration by Photogrammetry*, Photogrammetria, 38(3), pp. 103 – 113.

Förstner, W. and Gülch, E., 1987. *A Fast Operator for Detection and Precise Location of Distinct Points, Corners and Centres of Circular Features*. ISPRS Inter-commission Workshop, Interlaken, June 1987.

Franklin, J.A. and Maurice, B.D., 1991. *Rock Engineering Applications*, McGraw-Hill, Inc., New York.

Fraser, C.S., 1984. *Network design considerations for non-topographic photogrammetry*, Photogrammetric Engineering and Remote Sensing, 50(8), pp. 1115 – 1126.

Fraser, C.S., 1985. Photogrammetric Measurement of Thermal Deformation of a Large Process Compressor, Photogrammetric Engineering and Remote Sensing, 51(10), pp. 1569 – 1575.

Fraser, C.S., 1986. *Microwave Antennae Measurement*. Photogrammetric Engineering and Remote Sensing, 52(10), pp. 1627 – 1635.

Fraser, C.S., 1989. *Precise alignment and verification by photogrammetry*, Proceedings, 11th ESTEC Workshop on Antennae Measurement, ESA Publication WPP-001, Gothenberg, 20 – 22 June, pp. 109 – 114.

Fraser, C.S., 1992a. *Photogrammetric Camera Component Calibration - A Review of Analytical Techniques*, Presented at the workshop on Calibration and Orientation of Cameras in Computer Vision (TU-1), XVII Congress, ISPRS, Washington D.C..

Fraser, C.S., 1992b. *Photogrammetric measurement to one part in a million*, Photogrammetric Engineering and Remote Sensing, 58(3), pp. 305 – 310.

Fraser, C.S. and Gustafsen, P.C., 1986. *Industrial Photogrammetry Applied to Deformation Measurement*, International Archives of Photogrammetry and Remote Sensing, 26(5), pp. 199 – 208.

Fraser, C.S., 1995. *Deformation Measurement of a Large Coal Dredger by Digital Photogrammetry*, Proceedings, Int. FIG Symp. On Deformation Analysis and Engineering Surveying, Cape Town, 7 – 10 Feb., pp. 67 – 75.

Fraser, C.S., 1996a. *Network Design* in **Close Range Photogrammetry and Machine Vision**, Atkinson, K.B. (ed.), Whittles Publishing, Caithness, Scotland, pp. 256 – 281.

Fraser, C.S., 1996b. Industrial Measurement Applications in **Close Range Photogrammetry and Machine Vision**, Atkinson, K.B. (ed.), Whittles Publishing, Caithness, Scotland, pp. 329 - 361.

Fraser, C.S. and Mallison, J.A., 1992. *Dimensional characterization of a large aircraft structure by photogrammetry*, Photogrammetric Engineering and Remote Sensing, 58(5), pp. 539 – 543.

Fraser, C.S. and Shortis, M.R., 1995. *Metric Exploitation of Still Video Imagery, Photogrammetric Record*, Vol.15, No. 85, pp. 107 - 122.

Fryer, J.G., 1986. *Distortion in a Zoom Lens*, Aust.J.Geod.Photogram.Surv., No. 44, pp. 49 - 59.

Fryer, J., 1988. *Lens Distortion and Film Flattening: Their Effect on Small Format Photography*, International Archives of Photogrammetry and Remote Sensing, 27(5), pp. 194 – 202.

Fryer, J.G., 1996. *Introduction* in **Close Range Photogrammetry and Machine Vision**, Atkinson, K.B. (ed.), Whittles Publishing, Caithness, Scotland, pp. 1 – 7.

Fryer, J.G. and Brown, D.C., 1986. *Lens Distortion for Close-Range Photogrammetry*, Photogrammetric Engineering and Remote Sensing, Vol. 52, No. 1, pp. 51 - 58.

Glen, H.W. (ed.), 1989. *The Metals and Minerals Industry in Southern Africa - Part I*, Supplement to the South African Institute of Mining and Metallurgy Journal, Johannesburg.

Gonzalez, R.C. and Wintz, P., 1987. *Digital Image Processing*, Addison-Wesley Publishing Company, Reading, Massachusetts, Second Edition.

Gruen, A.W. and Baltsavias, E.P., 1988. *Geometrically Constrained Multiphoto Matching*, Photogrammetric Engineering and Remote Sensing, Vol. 54, No. 5, pp. 633 - 641.

Gruen, A., Maas, H. and Keller, A., 1995. *Kodak DCS200 - a camera for high accuracy measurement?*, SPIE Proceedings, Vol. 2598, pp. 52 - 59.

Gruen, A., 1996. *Least squares matching: a fundamental measurement algorithm* in **Close Range Photogrammetry and Machine Vision**, Atkinson, K.B. (ed.), Whittles Publishing, Caithness, Scotland, pp. 256 – 281.

Gustafsen, P.C., 1990. *Photogrammetric surveys of the mirror support cell of the Keck optical telescope*, International Archives of Photogrammetry and Remote Sensing, 28(5/1), pp. 417 – 424.

Haggrén, H., 1993. *Industrial Metrology Applications of Photogrammetric Stations*, Proceedings, 7th Int. FIG Symp. On Deformation Measurements, Banff, 3 – 5 May, pp. 250 – 257.

Karara, H.M., 1989. *An Introduction to Non-Topographic Photogrammetry* in **Non-Topographic Photogrammetry**, Karara, H.M. (ed.), Second Edition, American Society for Photogrammetry and Remote Sensing, pp. 1 – 5.

Lightfoot, N., Goldbach, O.D., Kullmann, D.H. and Toper, A.Z., 1996. *Rockburst control in the South African deep level gold mining industry*, In: **Rock Mechanics**, Aubertin, Hassini and Mitri (eds), Balkema, Rotterdam, pp. 295 – 303.

Marr, D. and Hildreth, E., 1980. *Theory of edge detection*, Proceedings of the Royal Society of London, B 207, pp. 187 - 217.

Mason, S.O., 1994. *Expert System-Based Design of Photogrammetric Networks*, PhD thesis, Mitteilungen Nr. 53, Institut für Geodäsie und Photogrammetrie, Zürich.

Mason, S.O., 1995a. *Automatic Sensor Placement for Accurate Dimensional Inspection*, Computer Vision and Image Understanding, 61(3), pp. 454 – 467.

Mason, S.O. 1995b. *Conceptual Model of the Convergent Multistation Network Configuration Task*, Photogrammetric Record, 15(86), pp. 277 – 299.

McGlone, J.C., 1989. Analytical Data-Reduction Schemes in *Non-Topographic Photogrammetry* in **Non-Topographic Photogrammetry**, Karara, H.M. (ed.), Second Edition, American Society for Photogrammetry and Remote Sensing, pp. 37 – 57.

Meyer, R., 1973. *The Present State in Industrial Photogrammetry*, Surveying News, No. 17.

Mikhail, E.M., 1989. *Introduction to Metrology Concepts* in **Non-Topographic Photogrammetry**, Karara, H.M. (ed.), Second Edition, American Society for Photogrammetry and Remote Sensing, pp. 7 – 14.

Papo, H., 1985. *Deformation Analysis by Close-Range Photogrammetry*, Photogrammetric Engineering and Remote Sensing, 51(10), pp. 1561 – 1567.

Powell, G.E., 1984. *The Use of Photogrammetry in the Manufacture of High Performance Aircraft*, International Archives of Photogrammetry and Remote Sensing, 25(A5), pp. 622 – 626.

Rüther, H., 1982. *Relative Orientation with Limited Control in Close Range Photogrammetry*, PhD thesis, University of Cape Town.

Schwartz, D.S., 1982. *Close-Range Photogrammetry for Aircraft Quality Control*, Proceedings of the American Society of Photogrammetry Annual Meeting, Denver, pp. 353 – 360.

Sell, W., 1986. *An Investigation into Determining a Method for the Identification of Individual Rhinoceros from Digital Images of their Respective Footprints*, Unpublished undergraduate thesis, Department of Surveying and Geodetic Engineering, University of Cape Town.

Smit, J.L. and Rüther, H., 1996. *The 3D Mapping of a Textured using Digital Photogrammetric Techniques*, ISPRS, Vol. XXXI (B4), pp. 728 - 733..

Smit, J.L., Mason, S.O., Rüther, H. and Dingle, M.R., 1997. *3D Reconstruction of an Automobile Exterior Using Digital Photogrammetric Techniques*, Proceedings, CONSAS '97, Durban, 24 – 28 August.

Stewart, P.A.E., 1975. *Engine Testing Using Advanced Techniques*, Aeronautical Journal, 79(776), pp. 331 – 343.

Stewart, P.A.E., 1979. *X-Ray Photogrammetry of Gas Turbine Engines at Rolls-Royse, Photogrammetric Record*, 9(54), pp. 813 – 821.

Stewart, P.A.E., 1986. *The Non-Invasive Measurement of Void Fraction and Velocity in Two Phase Flow Using High Speed Photography and Videophotogrammetry*, Photogrammetric Record, 12(67), pp. 5 – 24.

Tabatabai, A.J. and Mitchell, O.R., 1984. *Edge Location to Subpixel Values in Digital Imagery*, IEEE Transactions on Pattern Analysis and Machine Intelligence, Vol. PAMI-6, No. 2, pp. 188 - 201.

Thies, H., 1996. "Voruntersuchungen und Methodikentwicklung zur Frage der "Spielbäume" bei Geparden (*Acinonyx jubatus jubatus*) im namibianischen Farmland", unpublished undergraduate thesis, Institut fü Zoologie, Friedrich-Alexander-Universität, Erlangen-Nürnberg.

Trinder, J.C., 1989. *Precision of Digital Target Location*, Photogrammetric Engineering and Remote Sensing, Vol. 55, No. 6, pp. 883 - 886.

Van der Merwe, N, 1995. *Development of an Image Matching Scheme Using Feature - and Area Based Matching Techniques*, PhD thesis, University of Cape Town.

Van der Vlugt, G., 1995. *Algorithms and Design Aspects of an Automated Vision Based 3-D Surface Measurement System*, PhD thesis, University of Cape Town.

Wong, K.W., 1984. *Photogrammetric Measurement of Movements in Tunnel Model Testing*, International Archives of Photogrammetry and Remote Sensing, 25(A5), pp. 779 – 788.

Wong, K.W. and Ho, W.H., 1986. *Close-Range Mapping with a Solid State Camera*, Photogrammetric Engineering and Remote Sensing, Vol. 52, No. 1, pp. 67 - 74.

Xue, R.G., 1992. *The Image Processing for the Target Centre Detection in Digital Image*, M.Sc. thesis, University of Cape Town.

11 BIBLIOGRAPHY

Abdel-Aziz, Y.I. and Karara, H.M., 1971. *Direct Linear Transformation from Comparator Co-ordinates into Object Space Co-ordinates in Close-Range Photogrammetry*, Proceedings of ASP/UI Symposium on Close Range Photogrammetry, Urbana, Illinois, USA., pp. 1 - 8.

Ackermann, F. and Hahn, M., 1991. *Image Pyramids for Digital Photogrammery*, Proceedings of the 43rd Photogrammetric Week, Heff 15, Stuttgart.

Adams, L.P., 1989. Industrial *Photogrammetry* in **Non-Topographic Photogrammetry**, Karara, H.M. (ed.), Second Edition, American Society for Photogrammetry and Remote Sensing, pp. 349 – 358.

Amir, I., 1990. *Algorithm for Finding the Centre of Circular Fiducials*, Computer Vision, Graphics, and Image Processing, Vol. 49, pp. 398 - 406.

Anderson, H. and Stevens, D., 1982. *Mono Photographic Tunnel Profiling*, International Archives of Photogrammetry, 24(5/1), pp. 23 – 30.

Ballard, D.H., 1981. *Generalizing the Hough Transform to Detect Arbitrary Shapes*, Pattern Recognition, Vol. 13, No. 2, pp. 111 - 122.

Baltsavias, E.P., 1991. *Multiphoto Geometrically Constrained Matching*, PhD thesis, Mitteilungen Nr. 49, Institut für Geodäsie und Photogrammetrie, Zürich.

Bammeke, A.A., 1993. *Development of Mathematical Formulae for Predicting Accuracies of Multistation Networks*, Photogrammetric Record, Vol. 14, No. 82, pp. 613 - 625.

Barnard, S.T. and Thompson, W.B., 1980. *Disparity Analysis of Images*, IEEE Transactions on Pattern Analysis and Machine Intelligence, Vol. PAMI-2, No. 4, pp. 333 - 340.

Benard, M., 1984. *Automatic Stereophotogrammetry: A Method Based on Feature Detection and Dynamic Programming*, Photogrammetria, No. 39, pp. 169 - 181.

Beyer, H.A., 1990. *Calibration of CCD-Cameras for Machine Vision and Robotics*, SPIE, Vol. 1197, pp. 88 - 98.

Beyer, H.A., 1992. *Advances in Characterisation and Calibration of Digital Imaging Systems*, ISPRS, Vol. XXIX (B5), pp. 545 - 555.

Bopp, H. and Krauss, H., 1978. *An Orientation and Calibration Method for Non-Topographic Applications*, Photogrammetric Engineering and Remote Sensing, Vol. 44, No. 9, pp. 1191 - 1196.

Brown, D.C., 1958. *A Solution to the General Problem of Multiple Station Analytical Stereotriangulation*, RCA Data Reduction Technical Report No.43, Partick Air Force Base, Florida, USA.

Brown, D.C., 1966. *Decentering Distortion of Lenses*. Photogrammetric Engineering, Vol. 32, No.3, pp. 444 - 462.

Brown, D.C., 1981. *LNG Tank Inventory Measurement by Photogrammetry*, AGA Operating Section Proceedings, American Gas Assosciation, pp. 127 – 147.

Brown, D.C., 1985. *Adaptation of the Bundle Adjustment Method for Triangulation of Observations made by Digital Theodolites*, Paper presented at the Conference of Southern African Surveyors, 1985.

Canny, J., 1986. *A Computational Approach to Edge Detection, IEEE Transactions on Pattern Analysis and Machine Intelligence*, Vol. PAMI-8, No. 6, pp. 679 - 698.

Cho, W., Schenk, T. and Madani, M., 1992. *Resampling Digital Imagery to Epipolar Geometry*, In Research Activities in Digital Photogrammetry at the Ohio State University, Schenk, T. (ed), Report No. 418, Department of Geodetic Science and Surveying, Ohio State University, Ohio.

Cooper, M.A.R., 1979. *Analytical Photogrammetry in Engineering: Three Feasibility Studies*, Photogrammetric Record, 9(53), pp. 601 – 619.

Davis, M., 1988. *Target Centreing and Image Matching in a Near Real-Time Photogrammetric System*, B.Sc.(hons) thesis, University of Cape Town.

Dennen, W.H., 1989. *Mineral Resources - Geology, Exploration, and Development*, Taylor and Francis, New York.

Dold, J., Reinking, J. and Warnecke, P., 1993. *The analysis of high precision photogrammetric deformation measurements on masonry walls*, Proceedings, 7th Int. FIG Symp. On Deformation Measurements, Banff, 3 – 5 May, pp. 161 – 170.

Dold, J., 1994. *A Strategy for Photogrammetric Multiple Camera Calibration Without Additional Object Information*, ISPRS, Vol. XXX (5), pp. 61 - 64.

Dold, J. and Maas, H., 1994. *An application of epipolar line intersection in a hybrid close range photogrammetric system*, ISPRS, Vol. XXX (5), pp. 65 - 70.

Dowman, I.J., 1996. *Fundamentals of Digital Photogrammetry* in **Close Range Photogrammetry and Machine Vision**, Atkinson, K.B. (ed.), Whittles Publishing, Caithness, Scotland, pp. 52 - 77.

Ehlen, J., Hevenor, R.A., Kemeny, J.M. and Girdner, K., 1995. *Fracture recognition in digital imagery. In Rock Mechanics*, Proceedings of the 35th U.S. Symposium on Rock Mechanics, Daemen and Schultz (eds), Balkerna, Rotterdam.

Ekstrom, M.P. (ed.), 1984. *Digital Image Processing Techniques*, Vol.2, Academic Press, Inc., Orlando, Florida.

El-Hakim, S.F., 1986. *Real-Time Image Metrology with CCD Cameras*, Photogrammetric Engineering and Remote Sensing, Vol. 52, No. 11, pp. 1757 - 1766.

El-Hakim, S.F., 1989. *A Hierarchical Approach to Stereo Vision*, Photogrammetric Engineering and Remote Sensing, Vol. 55, No. 4, pp. 443 - 448.

El-Hakim, S.F. (ed.), 1995. *Videometrics IV*, Proceedings: SPIE, Vol. 2598, Philadelphia, Pennsylvania

Ethrog, U. and Shmutter, B., 1982. *Tunnel Calibration by Photogrammetry*, Photogrammetria, 38(3), pp. 103 – 113.

Fellbaum, M, 1995. *Robust Image Orientation with Balanced Observations in Close-Range Photogrammetry*, IAPRS, Vol. 30, Part 5X1, pp. 151 - 156, ISPRS Intercommission Workshop "From Pixels to Sequences", Zurich, March 1995.

Förstner, W. and Gülch, E., 1987. *A Fast Operator for Detection and Precise Location of Distinct Points, Corners and Centres of Circular Features*. ISPRS Inter-commission Workshop, Interlaken, June 1987.

Föstner, W., 1993. *Feature Extraction in Digital Photogrammetry. Photogrammetric Record*, Vol. 14, No. 82, pp. 595 - 611.

Franklin, J.A. and Maurice, B.D., 1991. *Rock Engineering Applications*, McGraw-Hill, Inc., New York.

Fraser, C.S., 1984. *Network design considerations for non-topographic photogrammetry*, Photogrammetric Engineering and Remote Sensing, 50(8), pp. 1115 – 1126.

Fraser, C.S., 1985. Photogrammetric Measurement of Thermal Deformation of a Large Process Compressor, Photogrammetric Engineering and Remote Sensing, 51(10), pp. 1569 – 1575.

Fraser, C.S., 1986. *Microwave Antennae Measurement*. Photogrammetric Engineering and Remote Sensing, 52(10), pp. 1627 – 1635.

Fraser, C.S., 1989. *Precise alignment and verification by photogrammetry*, Proceedings, 11th ESTEC Workshop on Antennae Measurement, ESA Publication WPP-001, Gothenberg, 20 – 22 June, pp. 109 – 114.

Fraser, C.S., 1992a. *Photogrammetric Camera Component Calibration - A Review of Analytical Techniques*, Presented at the workshop on Calibration and Orientation of Cameras in Computer Vision (TU-1), XVII Congress, ISPRS, Washington D.C..

Fraser, C.S., 1992b. *Photogrammetric measurement to one part in a million*, Photogrammetric Engineering and Remote Sensing, 58(3), pp. 305 – 310.

Fraser, C.S. and Gustafsen, P.C., 1986. *Industrial Photogrammetry Applied to Deformation Measurement*, International Archives of Photogrammetry and Remote Sensing, 26(5), pp. 199 – 208.

Fraser, C.S., 1995. *Deformation Measurement of a Large Coal Dredger by Digital Photogrammetry*, Proceedings, Int. FIG Symp. On Deformation Analysis and Engineering Surveying, Cape Town, 7 – 10 Feb., pp. 67 – 75.

Fraser, C.S., 1996a. *Network Design* in **Close Range Photogrammetry and Machine Vision**, Atkinson, K.B. (ed.), Whittles Publishing, Caithness, Scotland, pp. 256 – 281.

Fraser, C.S., 1996b. Industrial Measurement Applications in **Close Range Photogrammetry and Machine Vision**, Atkinson, K.B. (ed.), Whittles Publishing, Caithness, Scotland, pp. 329 - 361.

Fraser, C.S. and Mallison, J.A., 1992. *Dimensional characterization of a large aircraft structure by photogrammetry*, Photogrammetric Engineering and Remote Sensing, 58(5), pp. 539 – 543.

Fraser, C.S. and Shortis, M.R., 1995. *Metric Exploitation of Still Video Imagery, Photogrammetric Record*, Vol.15, No. 85, pp. 107 - 122.

Fryer, J.G., 1986. *Distortion in a Zoom Lens*, Aust.J.Geod.Photogram.Surv., No. 44, pp. 49 - 59.

Fryer, J., 1988. *Lens Distortion and Film Flattening: Their Effect on Small Format Photography*, International Archives of Photogrammetry and Remote Sensing, 27(5), pp. 194 – 202.

Fryer, J.G., 1996. *Introduction* in **Close Range Photogrammetry and Machine Vision**, Atkinson, K.B. (ed.), Whittles Publishing, Caithness, Scotland, pp. 1 – 7.

Fryer, J.G. and Brown, D.C., 1986. *Lens Distortion for Close-Range Photogrammetry*, Photogrammetric Engineering and Remote Sensing, Vol. 52, No. 1, pp. 51 - 58.

Glen, H.W. (ed.), 1989. *The Metals and Minerals Industry in Southern Africa - Part I*, Supplement to the South African Institute of Mining and Metallurgy Journal, Johannesburg.

Gonzalez, R.C. and Wintz, P., 1987. *Digital Image Processing*, Addison-Wesley Publishing Company, Reading, Massachusetts, Second Edition.

Grimson, W.E.L. and Hildreth, E.C., 1985. *Comments on "Digital Step Edges from Zero Crossings of Second Directional Derivatives"*, IEEE Transactions on Pattern Analysis and Machine Intelligence, Vol. PAMI-7, No. 1, pp. 121 - 129.

Gruen, A.W., 1985. *Adaptive Least Squares Correlation - A Powerful Image Matching Technique*, Presented Paper at the ACSM-ASP Convention, Washington, D.C., March 1985.

Gruen, A.W. and Baltsavias, E.P., 1987. *High-Precision Image Matching for Digital Terrain Model Generation*, Photogrammetria, No. 42, pp. 97 - 112.

Gruen, A.W. and Baltsavias, E.P., 1988. *Geometrically Constrained Multiphoto Matching*, Photogrammetric Engineering and Remote Sensing, Vol. 54, No. 5, pp. 633 - 641.

Gruen, A., Maas, H. and Keller, A., 1995. *Kodak DCS200 - a camera for high accuracy measurement?*, SPIE Proceedings, Vol. 2598, pp. 52 - 59.

Gruen, A., 1996. *Least squares matching: a fundamental measurement algorithm* in **Close Range Photogrammetry and Machine Vision**, Atkinson, K.B. (ed.), Whittles Publishing, Caithness, Scotland, pp. 256 – 281.

Gustafsen, P.C., 1990. *Photogrammetric surveys of the mirror support cell of the Keck optical telescope*, International Archives of Photogrammetry and Remote Sensing, 28(5/1), pp. 417 – 424.

Haggrén, H., 1993. *Industrial Metrology Applications of Photogrammetric Stations*, Proceedings, 7th Int. FIG Symp. On Deformation Measurements, Banff, 3 – 5 May, pp. 250 – 257.

Haralick, R.M., 1984. *Digital Step Edges from Zero Crossing of Second Directional Derivatives*, IEEE Transactions on Pattern Analysis and Machine Intelligence, Vol. PAMI-6, No. 1, pp. 58 - 68.

Haralick, R.M. and Shapiro, L.G., 1993. *Computer and Robot Vision*, Vol. 1, Addison-Wesley Publishing Company, Reading, Massachusetts.

Heipke, C., 1992. *A Global Approach for Least-Squares Image Matching and Surface Reconstruction in Object Space*, Photogrammetric Engineering and Remote Sensing, Vol. 58, No. 3, pp. 317 - 323.

Ho, H. and Andrews, H., 1978. *Cubic Splines for Image Interpolation and Digital Filtering*, IEEE Transactions on Acoustics, Speech, and Signal Processing, Vol. ASSP-26, No. 6, pp. 508 - 517.

Horn, B.K.P., 1983. *Non-Correlation Methods for Stereo Matching*, Photogrammetric Engineering and Remote Sensing, Vol. 49, No. 4, pp. 535 - 536.

Huang, Y.D. and Harley, I., 1989. *Calibration of Close-Range Photogrammetric Stations Using a Free Network Bundle Adjustment*, In Optical 3-D Measurement Techniques: Applications in inspection, quality control and robotics, Gruen, A. and Kahmen, H. (eds), Wichmann, Karlsruhe.

Huertas, A. and Medioni, G., 1986. *Detection of Intensity Changes with Subpixel Accuracy Using Laplacian-Gaussian Masks*, IEEE Transactions on Pattern Analysis and Machine Intelligence, Vol. PAMI-8, No. 5, pp. 651 - 664.

Karara, H.M., 1989. *An Introduction to Non-Topographic Photogrammetry* in **Non-Topographic Photogrammetry**, Karara, H.M. (ed.), Second Edition, American Society for Photogrammetry and Remote Sensing, pp. 1 – 5.

Keys, R.G., 1981. *Cubic Convolution Interpolation for Digital Image Processing*, IEEE Transactions on Acoustics, Speech, and Signal Processing, Vol. ASSP-29, No. 6, pp. 1153 - 1160.

Lenz, R. And Fritsch, D., 1990. *Accuracy of Videometry with CCD Sensors*, ISPRS Journal of Photogrammetry and Remote Sensing, Vol. 45, pp. 90 - 110.

Li, J. and Schenk, 1990. *Aerial Image Matching Based on Zero-Crossings and Least-Squares Correlation*, Report No. 9, Department of Geodetic Science and Surveying, Ohio State University, Ohio.

Li, M., 1991. *Hierarchical Multipoint Matching*, Photogrammetric Engineering and Remote Sensing, Vol. 57, No. 8, pp. 1039 - 1047.

Lightfoot, N., Goldbach, O.D., Kullmann, D.H. and Toper, A.Z., 1996. *Rockburst control in the South African deep level gold mining industry*, In: **Rock Mechanics**, Aubertin, Hassini and Mitri (eds), Balkema, Rotterdam, pp. 295 – 303.

Maitre, H., 1986. *Contribution to the Prediction of Performances of the Hough Transform*, IEEE Transactions on Pattern Analysis and Machine Intelligence, Vol. PAMI-8, No. 5, pp. 669 - 674.

Marr, D. and Hildreth, E., 1980. *Theory of edge detection*, Proceedings of the Royal Society of London, B 207, pp. 187 - 217.

Mason, S.O. and Wong, K.W., 1992. *Image Alignment by Line Triples*, Photogrammetric Engineering and Remote Sensing, Vol. 58, No. 9, pp. 1329 - 1334.

Mason, S.O., 1994. *Expert System-Based Design of Photogrammetric Networks*, PhD thesis, Mitteilungen Nr. 53, Institut für Geodäsie und Photogrammetrie, Zürich.

Mason, S.O., 1995a. *Automatic Sensor Placement for Accurate Dimensional Inspection*, Computer Vision and Image Understanding, 61(3), pp. 454 – 467.

Mason, S.O. 1995b. *Conceptual Model of the Convergent Multistation Network Configuration Task*, Photogrammetric Record, 15(86), pp. 277 – 299.

McGlone, J.C., 1989. Analytical Data-Reduction Schemes in *Non-Topographic Photogrammetry* in **Non-Topographic Photogrammetry**, Karara, H.M. (ed.), Second Edition, American Society for Photogrammetry and Remote Sensing, pp. 37 – 57.

Meyer, R., 1973. *The Present State in Industrial Photogrammetry*, Surveying News, No. 17.

Mikhail, E.M., Akey, M.L. and Mitchell, O.R., 1984. *Detection and Sub-Pixel Location of Photogrammetric Targets in Digital Images*, Photogrammetria, Vol. 39, pp. 63 - 83.

Mikhail, E.M., 1989. *Introduction to Metrology Concepts* in **Non-Topographic Photogrammetry**, Karara, H.M. (ed.), Second Edition, American Society for Photogrammetry and Remote Sensing, pp. 7 – 14.

Niini, I., 1994. *Relative Orientation of Multiple Images using Projective Singular Correlation*, ISPRS, Vol. 30, Part 3/2, pp. 615 - 621.

Novak, K. and He, G., 1991. *Automatic Extraction of 3-dimensional Features from Stereo Image Sequences*, Technical Papers - ACSM-ASPRS Annual Convention, Photogrammetry and Primary Data Acquisition, Vol. 5, pp. 310 - 314.

Pan, H., 1994. *Two-level global optimization for image segmentation*, ISPRS Journal of Photogrammetry and Remote Sensing, Vol. 49, No. 2, pp. 21 - 32.

Papo, H., 1985. *Deformation Analysis by Close-Range Photogrammetry*, Photogrammetric Engineering and Remote Sensing, 51(10), pp. 1561 – 1567.

Petsa, E. and Patias, P., 1994. *Relative Orientation of Image Triples using Straight Linear Features*, ISPRS, Vol. 30, Part 3/2, pp. 663 - 669.

Powell, G.E., 1984. *The Use of Photogrammetry in the Manufacture of High Performance Aircraft*, International Archives of Photogrammetry and Remote Sensing, 25(A5), pp. 622 – 626.

Powers, P.S., Chiarle, M. and Savage, W.Z., 1996. *A Digital Photogrammetric Method for Measuring Horizontal Surficial Movements on the Slumgullion Earthflow, Hinsdale County, Colorado*, Computers & Geosciances, Vol. 22, No. 6, pp. 651 - 663.

Rubinstein, M., 1990. *Assessing Target Centring Algorithms for use in Near-Real-Time-Photogrammetry*, Masters thesis, University of Cape Town.

Rüther, H., 1982. *Relative Orientation with Limited Control in Close Range Photogrammetry*, PhD thesis, University of Cape Town.

Rüther, H., 1991. *Digital Photogrammetry - Introduction to a New Tool for the Photogrammerists*, Presented at the workshop of ISPRS V/4, Pretoria.

Sarker, S. and Boyer, K.L., 1991. *On Optimal Infinite Impulse Response Edge Detection Filters*, IEEE Transactions on Pattern Analysis and Machine Intelligence, Vol. 13, No. 11, pp. 1154 - 1171.

Schowengerdt, R.A., 1983. *Techniques for Image Processing and Classification in Remote Sensing*, Academic Press, New York.

Schwartz, D.S., 1982. *Close-Range Photogrammetry for Aircraft Quality Control*, Proceedings of the American Society of Photogrammetry Annual Meeting, Denver, pp. 353 – 360.

Sell, W., 1986. *An Investigation into Determining a Method for the Identification of Individual Rhinoceros from Digital Images of their Respective Footprints*, Unpublished undergraduate thesis, Department of Surveying and Geodetic Engineering, University of Cape Town.

Shih, T., 1994. *RLT: A Close Form Solution for Relative Orientation*, ISPRS, Vol. XXX, Part 5, pp. 357 - 363.

Smit, J.L. and Rüther, H., 1996. *The 3D Mapping of a Textured using Digital Photogrammetric Techniques*, ISPRS, Vol. XXXI (B4), pp. 728 - 733.

Smit, J.L., Mason, S.O., Rüther, H. and Dingle, M.R., 1997. *3D Reconstruction of an Automobile Exterior Using Digital Photogrammetric Techniques*, Proceedings, CONSAS '97, Durban, 24 – 28 August.

Smith, A.D.N., 1965. *The Explicit Solution of the Single Picture Resection Problem, with a Least Squares Adjustment to Redundant Control*, The Photogrammetric Record, Vol. V, No. 26, pp. 113 - 121.

Stephenson, G. and Radmore, P.M., 1990. *Advanced mathematical methods for engineering and science students*, Cambridbe University Press, Cambridge.

Stewart, P.A.E., 1975. *Engine Testing Using Advanced Techniques*, Aeronautical Journal, 79(776), pp. 331 – 343.

Stewart, P.A.E., 1979. *X-Ray Photogrammetry of Gas Turbine Engines at Rolls-Royse, Photogrammetric Record*, 9(54), pp. 813 – 821.

Stewart, P.A.E., 1986. *The Non-Invasive Measurement of Void Fraction and Velocity in Two Phase Flow Using High Speed Photography and Videophotogrammetry*, Photogrammetric Record, 12(67), pp. 5 – 24.

Sun, G.X., Reddish, D.J. and Whittaker, B.N., 1992. *Image analysis technique for rock fracture pattern studies around longwall excavations*, Transactions of the Institute of Mining and Metallurgy., Vol. 101, pp. 159 - 165.

Tabatabai, A.J. and Mitchell, O.R., 1984. *Edge Location to Subpixel Values in Digital Imagery*, IEEE Transactions on Pattern Analysis and Machine Intelligence, Vol. PAMI-6, No. 2, pp. 188 - 201.

Thies, H., 1996. "Voruntersuchungen und Methodikentwicklung zur Frage der "Spielbäume" bei Geparden (*Acinonyx jubatus jubatus*) im namibianischen Farmland", unpublished undergraduate thesis, Institut fü Zoologie, Friedrich-Alexander-Universität, Erlangen-Nürnberg.

Thomas, P.R., Mills, J.P. and Newton, I., 1995. *An Investigation into the use of Kodak Photo CD for Digital Photogrammetry*, Photogrammetric Record, Vol. 15, No. 86, pp. 301 - 314.

Torre, V. and Poggio, T.A., 1986. *On Edge Detection*, IEEE Transactions on Pattern Analysis and Machine Intelligence, Vol. PAMI-8, No. 2, pp. 147 - 163.

Trinder, J.C., 1989. *Precision of Digital Target Location*, Photogrammetric Engineering and Remote Sensing, Vol. 55, No. 6, pp. 883 - 886.

Tsai, W., 1985. *Moment-Preserving Thresholding: A New Approach*, Computer Vision, Graphics, and Image Processing, No. 29, pp. 377 - 393.

Van der Merwe, N. and Rüther, H., 1994. *Image Matching Through a Combination of Feature- and Area Based Matching*, Presented Paper, ISPRS Commission V, Working Group V/III, Melbourne, March 1994.

Van der Merwe, N, 1995. *Development of an Image Matching Scheme Using Feature - and Area Based Matching Techniques*, PhD thesis, University of Cape Town.

Van der Vlugt, G., 1995. *Algorithms and Design Aspects of an Automated Vision Based 3-D Surface Measurement System*, PhD thesis, University of Cape Town.

Ward, J. and Cok, D.R., 1989. *Resampling Algorithms for Image Resizing and Rotation*, SPIE, Vol. 1075, pp. 260 - 269

Wong, K.W., 1984. *Photogrammetric Measurement of Movements in Tunnel Model Testing*, International Archives of Photogrammetry and Remote Sensing, 25(A5), pp. 779 – 788.

Wong, K.W. and Ho, W.H., 1986. *Close-Range Mapping with a Solid State Camera*, Photogrammetric Engineering and Remote Sensing, Vol. 52, No. 1, pp. 67 - 74.

Wright, D.E., Cox, D.E. and Cheffins, O.W., 1969. *Photogrammetric Measurement of Rock Surfaces in a Power Tunnel*, Water Power, London.

Xue, R.G., 1992. *The Image Processing for the Target Centre Detection in Digital Image*, M.Sc. thesis, University of Cape Town.